A MESS OF ROTTEN EGGS FROM THE TWO MEDICINE FORMATION, MONTANA

by

Katherine Lydia Tucker

A thesis submitted in partial fulfillment
of the requirements for the degree

of

Masters of Science

in

Earth Sciences

MONTANA STATE UNIVERSITY
Bozeman, Montana

May 2024

ACKNOWLEDGEMENTS

First, I would like to thank my committee members Dr. Devon Orme, Dr. Collin Shaw, and Dr. David Varricchio for all of their help with the research and writing of this thesis. Thank you for your patience with me dropping in to your offices at inconvenient times. Thank you, Dr. Devon Orme, for pointing out things that I am missing. Thank you, Dr. Collin Shaw, for all the assistance with the analyses and EBSD. Thank you Dr. David Varricchio for guiding me through this entire process. I would also like to thank several other people including Dr. Seung Choi who helped get me started on this project, Eric Przybyszewski who helped with both editing and fossil preparation, my parents, and all of my fellow graduate students.

I would like to thank the Museum of the Rockies for access to the specimen and the site. Thank you to Dr. Sarah Maccagnano-Zacher and the Imaging and Chemical Analysis Laboratory (ICAL), part of the Montana Nanotechnology Facility and a member of NNCI, which is supported by the National Science Foundation (Grant# ECCS-2025391). I would also like to thank Gary Wyss and the Center for Advanced Materials Processing (CAMP) at Montana Technical University. Finally funding for this research was provided by the Paleontological Society through a student research grant.

TABLE OF CONTENTS

TABLE OF CONTENTS CONTINUED

LIST OF TABLES

Table Page

LIST OF FIGURES

Figure Page

LIST OF FIGURES CONTINUED

Figure Page

LIST OF FIGURES CONTINUED

Figure Page

LIST OF FIGURES CONTINUED

Figure Page

LIST OF FIGURES CONTINUED

Figure Page

LIST OF FIGURES CONTINUED

Figure Page

ABSTRACT

The Two Medicine Formation of Montana is known for producing many dinosaur eggs in varying states of preservation. An unusual clutch of eggs MOR 11881 was recently found in the formation that exhibits some distinctive preservation features. The purpose of this research is to describe this clutch using multiple techniques to identify and better understand its taphonomic history. To do this the clutch was prepared by removing sediment from around the eggs, then examined using light microscopy, scanning electron microscopy (SEM), cathodoluminescence (CL), energy dispersive x-ray spectroscopy (EDX), and electron backscatter diffraction analysis (EBSD).

Preparation uncovered eleven partially compressed ellipsoidal eggs in the clutch. Microscopy of the eggshell revealed that it is made of two structurally distinct layers. The lower layer at the base of the eggshell is here referred to as the blocky layer based on the blocky texture of the crystals in SEM images. This layer is sometimes interrupted by a phosphatic dark region. The second layer is the lobed layer found along the outer surface of the eggshell. It is characterized by lobes of blocky crystals surrounded by smaller radiating crystals. In addition to the eggshell the eggs also preserve a phosphatized eggshell membrane, two distinct types of pellets, large masses of collophane crystals and hyphae like structures. Unaltered eggshell is found in the sediment surrounding the clutch.

The eggshell of the MOR 11881 clutch does not match any described ootaxon but is similar to eggshell found at the Egg Mountain quarry which was never identified. The unusual structure of the eggshell could be the result of multiple stages of alteration. Several structures in the eggshell including the lobes and the dark region are most likely the result of alteration. The presence of unaltered eggshell near the eggs indicates that the source of alteration was the decay of the eggs as recorded by their contents. This decay also produced the conditions necessary for the exceptional preservation of the eggshell membrane.

CHAPTER ONE

INTRODUCTION AND BACKGOUND

Introduction

Fossil eggs, nests and neonates contain a wealth of information about extinct dinosaur's reproduction, ontogeny, and ecology (Carpenter, 1999). Despite the importance of fossil eggs, our understanding of their taphonomy is incomplete. Most studies of fossil eggs listed below have focused on either whole nest structure, eggshell with recognizable structure, or have examined single alteration factors. There is a lack of studies examining the outcomes of multiple processes affecting eggs as they decay. This research focuses on describing an unusual clutch of fossil eggs which contain multiple features that potentially result from their decay.

Two papers have examined the process of egg decay. Hayward et al. (1997) examined the fate of eggs in marine environments, including the decay process of submerged eggs, but did not examine the eggshell structure afterward in detail. Similarly, Bravo et al. (2003) experimentally determined that eggs mummify under both desiccating and acidic conditions around a pH of 4.5 to 5 but only ran his experiments for eight months. In addition to these two studies other research has examined eggshell alteration of isolated processes. These studies include those that look at eggshell transport such as Oser and Jackson (2014), which examined the abrasion patterns of experimentally abraded eggshell for comparison to isolated eggshell fragments found in many eggshell baring formations. Imai et al. (2015) used flume experiments to differentiate between transported and in situ eggshell assemblages based off of the proportions of concave up

to concave down eggshell. Clayburn et al. (2004) did experiments examining the effects of pH and temperature on eggshell separately.

There are several whole nest and colonial nesting site studies focused on modern examples to better understand what nesting sites look like in the fossil record. Ferguson et al., (2020) examined and compared modern bird nests with both precocial and altricial young to determine if there were differences in the sedimentary signatures between the two that could be used to determine hatchling mobility in the fossil record. Ferguson (2016) examined alligator and caiman nests for comparison to dinosaurs as many dinosaur eggs are inferred, based on gas conductance, to have been buried. Hayward et al. (2000) examined a gull nesting colony to determine if signs of predation could be distinguished from signs of hatching and compared it to a dinosaur nesting site. Jackson et al. (2015b) examined both sea turtle and tortoise nests as another buried nest proxy for dinosaurs. The fate of eggs in marine environments has also been examined including the recruitment of eggs into marine environments, and transport of eggs by floating (Hayward et al., 1997). In addition there has been one long running case study examining the fate of eggs buried by the eruption of Mt. Saint Helens. These eggs did not preserve embryos, but did preserve eggshell for several years before the calcite started to dissolve due to the acidity of the volcanic ash (Hayward et al., 1989, 1991; Janssen et al., 2011).

On the microscopic level several studies have been conducted looking at taphonomic changes in eggshell structure with the goal of differentiating between taphonomic structures and pathologic eggshell. Jackson and Schmitt (2008) examined multilayered dinosaur and turtle eggshell from several sites using light microscopy and scanning electron microscopy (SEM). They generated a list of criteria for recognizing multi-layered eggshell that is more likely to be

pathological based off of the characteristics of the contact between the two layers or the material separating the layers. Grellet-Tinner et al. (2010) reexamined several pieces of eggshell thought to be pathological under light microscopy, SEM, and cathodoluminescence (CL), which revealed that the abnormal crystal growths in the shell were taphonomic in nature. Moreno-Azanza et al. (2016) used light microscopy, SEM, CL, and electron backscatter diffraction analysis to find and identify secondary crystal growth within eggshell. Most of the eggshell studied in these experiments have at least some recognizable eggshell structures in them and focused on determining the difference between original and secondary structures that look very similar; they did not focus on highly altered eggshell that no longer resembles the original structure.

Other studies have looked at elemental and isotopic composition changes in eggshell to determine if they can be used for environmental reconstruction. Graf et al. (2018) compared eggshell oxygen isotope values to soil carbonate values both from the Gobi Desert and found that none of the eggshell was unaltered enough for paleoenvironmental reconstructions. They also examined eggshell samples with light microscopy and CL to divide the eggshell into groups based off of how much of the original crystal structure was preserved. He et al. (2021) focused on eggs from a single formation in China, examining both their isotopic composition and their elemental composition in addition to examining them under CL. Again, most of these studies have focused on eggs that have some recognizable remaining microstructure making it difficult to use them to compare to eggs without recognizable structure.

There is a lack of actualistic and case study publications on the decay process of eggs with most papers focusing on pathology or taking a more macroscopic approach. This research is a case study describing a new clutch of eggs from the Two Medicine Formation of Montana

using light microcopy, SEM, CL, energy dispersive x-ray spectroscopy (EDX) and electron backscatter diffraction analysis (EBSD) with the goal of understanding their taphonomic history. The clutch exhibits highly unusual eggshell, semi-three-dimensional preservation of the eggs, and a range of other structures associated with the clutch.

Geologic Setting

The new clutch of eggs, given the Museum of The Rockies (MOR) accession number MOR 11881 from site TM-1600, was found west of the town of Choteau, Montana, in the Willow Creek Anticline of the Two Medicine Formation. The Two Medicine Formation's type section is located along the Two Medicine River, north western Montana, where it is 575m thick (Lorenz, 1981; Lorenz and Gavin, 1984). However, near Choteau the formation is estimated to be approximately 660m thick when the separate exposures are reconstructed as a continuous sequence (Lorenz and Gavin, 1984).

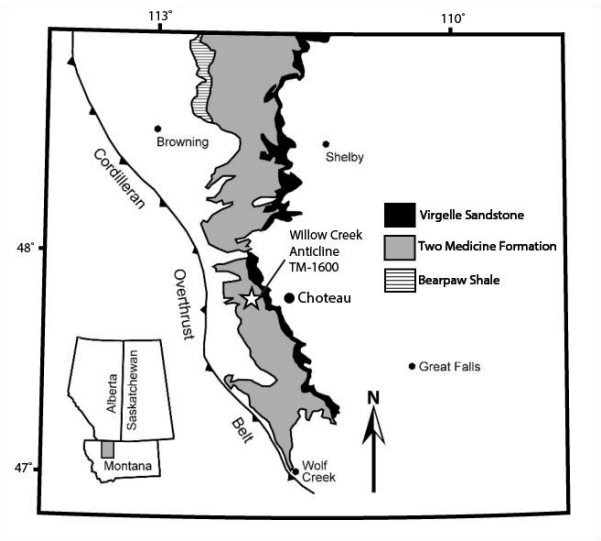

Figure 1: Map of the Two Medicine Formation, modified from (Rogers et al., 2010) showing the location of site TM-1600.

Sediments in the Two Medicine Formation are derived from volcanic material from the elkhorn volcanics and older foreland basin deposits (Fuentes et al., 2011). The formation has been dated using U-Pb dating on volcanic zircons from bentonite beds which yielded dates of 82.419±0.074 Ma at 15.5m above the formation's base and 75.259±0.027 Ma from 40m below the top of the formation in the type section (Ramezani et al., 2022). In the area surrounding the Willow Creek Anticline a bentonite approximately 30m top of the formation yields a date of 74.430 ± 0.015 Ma (Rogers et al., in press). These dates place the formation as being deposited during the Campanian in the late Cretaceous.

The Two Medicine Formation formed in upland fluvial and lacustrine environments of the North American Cordilleran foreland basin system during the Campanian (Fuentes et al., 2011). Rogers et al. (In press) divide the Two Medicine Formation into four members listed from the base of the formation to the top of the formation as the Cut Bank Creek Member, Sheilds Crossing Member, Hagans Crossing Member, and the Flag Butte Member. The Willow Creek Anticline that MOR 11881 was found in spans the uppermost two members of the formation the Hagans Crossing Member and the Flag Butte Member (Rogers et al., In Press).

Based on the correlations done by Shelton (2007) MOR 11881 is located above the Egg Mountain Quarry. In the new subdivision of the formation the Egg Mountain Quarry is located in the lacustrine interval at the base of the Flag Butte Member, placing MOR 11881 above the lacustrine interval in the same member (Rogers et al., In Press). Above the lacustrine interval is a return to fluvial facies characterized by massive grey, grey green, red-brown and purple mudstone interbedded with tabular siltstones and sandstones (Rogers et al., In Press). This region above the lacustrine deposits is interpreted as being deposited in a fluvial environment by an

anastomosing stream (Lorenz and Gavin, 1984; Shelton, 2007). The lacustrine interval in the Willow Creek Anticline is tentatively correlated with a similar interval in the type section where a dated bentonite bed located 9m above the interval yields a date of 76.247 ± 0.087 Ma (Rogers et al., In Press).

Paleoecology

The Two Medicine Formation represents an upland fluvial environment. Initially the environment was interpreted as being semi-arid due to the presence of caliche nodules in the formation which are similar to those found on the semi-arid Indogangetic plain (Lorenz and Gavin, 1984). However, these deposits also form in wetter environments that have a pronounced dry season suggesting that the environment could be significantly wetter (Nadon, 1993). Isotope studies of the vertebrate, invertebrate and soil carbonates show gradients in isotopic concentrations between upland and lowland environments that are consistent with a monsoonal environment (Foreman et al., 2011). Furthermore, in the lower Two Medicine Formation periodic interruptions in tree growth are seen in fossil wood that are similar to those found in seasonal megathermal climates where temperatures remain high year around with high seasonal rainfall such as those found in East Africa (Falcon-Lang, 2003). The warm, seasonally wet environment of the Two Medicine Formation hosted a diverse fauna.

The Two Medicine Formation contains a rich fossil record of bones, tracks, coprolites, and eggs. In the Willow Creek Anticline and surrounding area fossilized bones of many individuals of the dinosaurs *Maiasaura*, *Orodromeus*, and *Troodon* have been found (Horner and Makela, 1979; Horner, 1982; Horner and Weishampel, 1988; Horner and Weishampel, 1996; Varricchio et al., 1997). Scattered tyrannosaurid teeth are also fairly common in the anticline

(Dalman et al., 2018). In addition to dinosaurs, a mammal *Filikomys primaevus* (Weaver et al. 2021), an Azhdarchid pterosaur and squamate bones belonging to a lizard have been found (Padian and Smith, 1992; Montellano et al., 2000; DeMar et al., 2014). Trace fossils found in the formation include wasp pupation chambers, hadrosaur coprolites, regurgitaliths and nests complete with eggs (Chin, 2007; Jackson et al., 2015a; Freimuth and Varricchio, 2019; Freimuth, 2020).

Fossil eggs and eggshell are extremely common throughout the Two Medicine Formation and the Willow Creek Anticline. Eggs were first reported in the formation in 1979 with the discovery of a clutch of perinatal bones and eggshell fragments which was followed by more nests including complete and crushed eggs (Horner and Makela, 1979; Horner, 1982, 1999; Horner and Weishampel, 1988). The first eggs reported from the formation belonged to *Maiasaura peeblsorum* and were identified by the perinatal bones that were found with the eggshell (Horner and Makela, 1979). In addition to the *Maiasaura* eggs, both whole eggs and eggshell fragments from many other animals have been found in the formation. Originally identified as belonging to *Orodromeus*, *Troodon* eggs are also found in the formation (Horner and Weishampel, 1988; Horner and Weishampel, 1996). Unlike the *Maiasaura* eggs the *Troodon* eggs are preserved three dimensional in the formation due to the rapid deposition of calcareous mudstone that they were found in, unhatched state of the nest and caliche formation after their burial (Hirsch and Quinn, 1990; Varricchio et al., 1997, 1999, 2002). Eggshell not associated with embryonic or perinatal bone found in the formation include *Montanoolithus strongorum*, *Spheroolithus choteauensis*, *Triprismatoolithus stephensi*, *Prismatoolithus hirschi*, *Tubercuoolithus tetonensis*, *Continuoolithus canadensis*, and *Krokolithes sp*. (Zelenitsky and

Therrien, 2008; Jackson and Varricchio, 2010). Avian and geckonoid eggshell have also been found in the Lower Two Medicine formation (Hirsch and Quinn, 1990).

CHAPTER TWO

METHODS

Collection

Collection began in the fall of 2020 with several pieces of eggshell in float from locality TM-1600 for initial examinations and a few petrographic thin sections. The bulk of the material was left in the ground due to time constraints imposed by COVID-19 protocols. Only isolated pieces of float that were separate from any clumps of material were collected to keep any pieces of intact eggs together.

The remaining eggs at TM-1600 were collected in the summer of 2021 by a crew of three people over three days. Pictures of the site were taken before and during the collection of the nest. Collection started with clearing the surface of caliche and other debris. With the debris removed, we determined if chunks of eggs on the surface were in situ, based on if they were partially buried or arranged with other fragments. Moved egg fragments were collected from the surface and labeled as float.

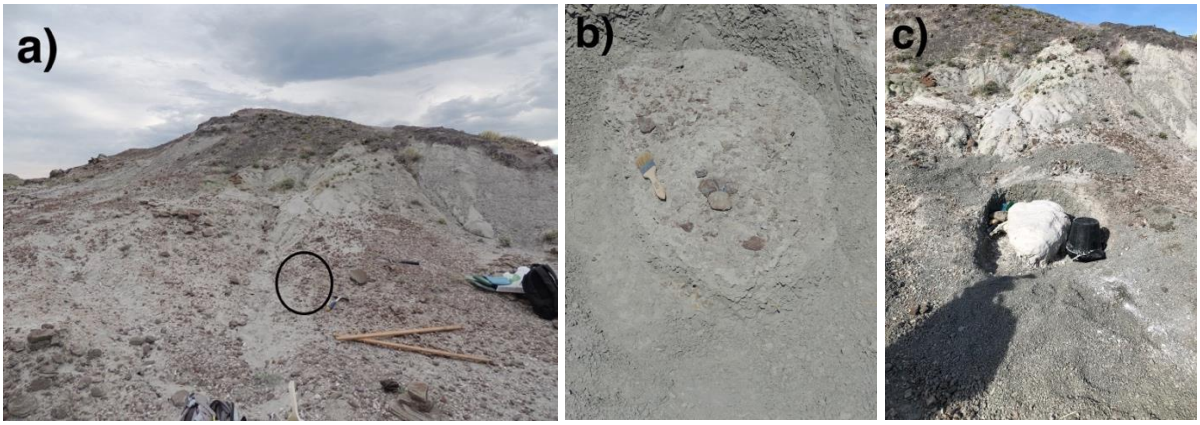

Figure 2: a) TM-1600 before collection of the clutch and cleaning of the site with the exposed egg circled. Hammer for scale. b) Close up view of the cleaned clutch. Brush is 18.5 cm long. c) TM-1600 with the clutch jacketed and ready for removal.

The egg fragments determined to be float were placed in bags labeled according to their general orientation to the rest of the nest. Fig. 3 shows the general areas of each bag of float and its relation to the jacket. The initial two bags were the upper and lower float bags. The additional bags of float were added as concentrations of shell were found that were not in place. The trench float bag was separated from the wash bag because its contents was from the trench rather than the surface. In addition to the egg float material, non-egg float material from the site was placed in a separate bag and consisted of a single pupa case and a fragment of bone. After collection of the jacket, further inspection of the area yielded a few more fragments of egg that were classified as float and were collected in another bag labeled post collection float.

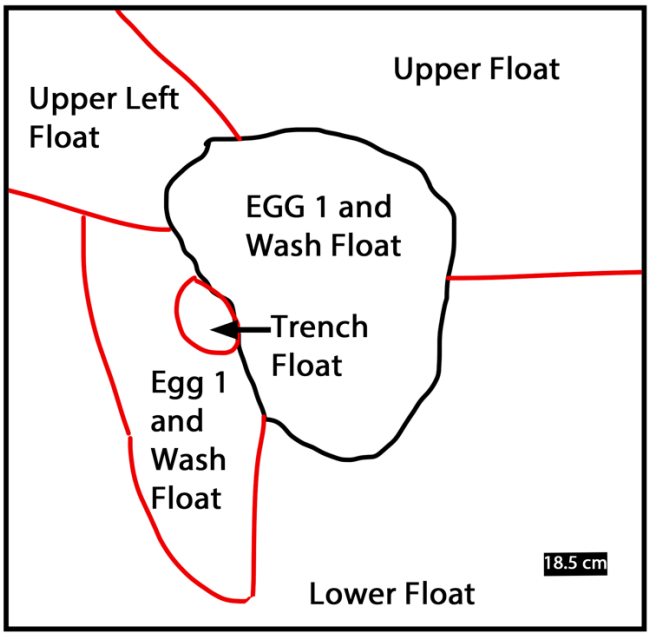

Figure 3: Schematic of each region of float that was collected into a separate bag. Black outline marks the edge of the jacket and red outlines the boundaries for each bag. The egg 1 and wash float bag contained both float material from directly around the jacket and the wash next to it which is why it is labeled both inside and outside of the jacket. Scale bar is 18.5cm.

After the surface was cleaned, the edges of the nest were determined by slowly removing sediment from the edges and top to determine the extent of the cluster of eggs. The nest was roughly sketched and then jacketed for transport back to Bozeman. The jacket was assigned the field number 6-5-21-1 and stored at Montana State University while it was prepared. All the material from site TM-1600 is assigned the accession number MOR 11881.

The site was revisited in the summer of 2022 to record more detailed geologic information about the site. A stratigraphic column of the sedimentary layers immediately above and below the nest was made to compare with existing columns of the area. Layers at the site were also tracked back to measured sections from Shelton (2007). Finally, several rock samples were collected from surrounding layers and pictures those layers were taken.

Jacket Preparation

Jacket 6-5-21-1 accessioned MOR 11881 containing the cluster of eggs was prepared at Montana State University in the Varricchio Paleontology lab using hand tools and an airscribe. The clutch was prepped from the bottom up according to convention. Eggs were assigned numbers in the order that they were revealed inside the jacket as it was prepared. Pictures were taken of the jacket throughout the process using a Nikon COOLPIX P510 to document the process. The siltstone was wetted with water to make it easier to remove with dental picks and brushes. Harder areas of siltstone were removed using an airscribe with and without water. Thin polyvinyl acetate was used to stabilize the eggshell and glue fragments back in place. Approximately one five-gallon bucket of removed siltstone was sieved during the first three months of preparation to look for small bones and shell fragments which were missed during the removal of the sediment. The sieving produced hundreds of eggshell fragments under 2mm long, a few pellet sized coprolites but no bones. After the initial five-gallon bucket was sieved, the remaining sediment was not sieved.

After preparation the clutch and eggs were measured using a tape measure. The depth of several eggs was also measured from the top of the egg to where they contacted the jacket. The depth measurements were possible for the eggs because the tops of the eggs were partially exposed during the jacketing process to determine the edges of the nest. Egg measurements were only taken of eggs that had eggshell on most sides. Volume of the eggs was calculated using $V = K_e LWD$ where V is volume, K_e is the coefficient for ellipsoid eggs 0.5236, L is the length and W is the width and D is the depth modified from Douglas (1990) to account for the compression of the eggs. Egg mass was calculated using the equation $M = K_e\, LWD$ where M is mass in grams,

K_e is the average mass coefficient of 0.548 for multiple types of eggs, L is the length of the egg, W is the width of the egg and D is the depth of the egg modified from Hoyt (1979). Egg seven was excluded from the averages for depth, volume, and mass due to it being impossible to get a depth measurement for it. The average mass of the eggs from MOR 11881 was then added to the data set from Legendre et al. (2022) for comparison to other eggs.

Slides

Of the initial specimens collected in the fall of 2020, one piece of float with eggshell and sediment adhering to the underside of the eggshell was chosen for petrographic thin sectioning. After the collection of the nest and preparation of the jacket began, further fragments of float and sediments from within the jacket were sampled for thin sectioning. Thin sections were also made from six shell fragments retrieved through sieving the sediment removed from the jacket. Eggshell fragments from eggs one, five, six, eight, and nine were also removed during preparation for thin sectioning. The full list of slides numbers, their origin and preparation are given by appendix 1.

Professionally prepared thin sections were made of both egg material and sediments collected from the inside of the jacket. They were prepared by Spectrum Petrographic. These thin sections were given ES numbers and are numbered ES-579 through ES-584. All other eggshell thin sections were made at Montana State University and assigned KE numbers based off the informal name of the site Katies Klutch. The KE thin sections were made using the following procedures: the eggshell was embedded in allied-145 epoxy using both a vacuum and positive pressure step for added clarity and adhesion to small pores. Thin sections were made using a Hillquist thin section machine and finished using increasingly fine-grained metallurgic sandpaper

on an Allied High Tech MetPrep 3 Grinder/Polisher. Thin sections used for electron backscatter diffraction analysis (EBSD) were further polished using 3μm diamond paste and 1μm diamond paste finishing with a colloidal silica bath. After the colloidal silica bath, the slides were rinsed in water to remove any residue from the silica.

The thin sections were viewed using both plain and crossed polarized light using a Leica DM 750 P polarizing microscope. The same microscope was used to take pictures of the thin sections using a Leica EC 3 camera attachment and the Leica application suite LAS EZ version 3.3.0. Pictures taken with this microscope were processed using the same Leica software and Adobe Illustrator version 28.2. Measurements taken using light microscopy were taken using Adobe Illustrator's line tool.

Scanning Electron Microscopy

Several pieces of float comprised of both eggshell and egg contents were selected for scanning electron microscopy. The pieces were cleaned by hand, and several were broken to give fresh surfaces before being coated. In addition to float pieces, a fragment of eggshell with membrane from egg 10 was selected and broken for pictures of both membrane fibers and the shell. Table 1 lists all of the eggshell fragments used in SEM, their locations in relation to the clutch and coating along with hand samples used for images or measurements.

All fragments and slides were coated in carbon with only KS-4 being coated in iridium. Both the coating and scanning electron microscopy (SEM) were carried out at Montana State University's Imaging and Chemical Analysis Laboratory (ICAL). For the carbon coating each piece was sputter coated with 12nm to 13nm of carbon using a Pella 108 carbon coater before

imaging. KS-4 was sputter coated with 10nm of iridium using a Emitech K575X peltier cooled metal coater.

Table 1: SEM and hand samples

Chunk samples	Location	Coating	Associated Slides
KS-1	Upper Float	Carbon	
KS-2	Upper Float	Carbon	ES-581
KS-3	Upper Float	Carbon	
KS-4	Upper Float	Iridium	
KS-5	egg 2	Carbon	
KS-6	egg 10	Carbon	
KS-7	Jacket coprolites	none	
KS-8	Cut through bag	polyvinyl acetate	

Images were taken with a Zeiss SUPRA 55VP field emission (FE) SEM under the high vacuum setting. Accelerating voltage (EHT) was set between 1kV and 10kV. Electron backscatter diffraction analysis (EBSD) and energy-dispersive x-ray spectroscopy (EDX) were conducted on the same instrument using uncoated slides under the variable pressure setting.

Cathodoluminescence

Initial cathodoluminescence images were taken at Montana Technological University in Butte using a Tescan MIRA 3 GMU – TIMA X field emission scanning electron microscope using a Tescan panchromatic cathodoluminescence detector. For these images accelerating voltage (EHT) was set to 20kV Additional Cl images were taken at ICAL using the same FE SEM used for the rest of the SEM imaging. The ICAL images were obtained using coated slides under high vacuum using the variable pressure sensor. EHT was set to 20kV and the aperture was

60μm. To get more clear images, the exposure times were set at 20 minutes for the Tescan and 21.6 minutes for the Zeiss.

Energy-Dispersive X-ray Spectroscopy
and Electron Backscatter Diffraction

Mapping for both energy-dispersive x-ray spectroscopy (EDX) and Electron Backscatter diffraction analysis (EBSD) were carried out using Aztec 6.1 software on ICAL's Zeiss SUPRA 55VP. EDX was performed on both coated and uncoated slides with the carbon maps disregarded if the slides had been previously carbon coated. When only mapping EDX data the maps were run between five and twenty minutes until map detail stopped increasing. Several EDX maps were recorded concurrent with EBSD and were thus run for the duration of the EDX mapping. Elements that were automatically mapped were sometimes removed when their absence made the expected spectrum fit the observed spectrum better. EDX maps were made of both freshly broken eggshell and polished slides. EDX maps did not undergo any post processing but were combined and compared using photoshop. Weight percentages for isolated regions of the maps were calculated in AZtec.

EBSD mapping was preformed using variable pressure on uncoated polished slides. The step size for the EBSD maps ranged from 1.5 to 5.37μm based on the resolution desired for the eggshell. A higher resolution test map with a 1μm step size was made; however, it did not increase the resolution or decrease the size of the blank spaces where there was no data. Due to the lack of improvement seen in the test map and lack of patterns seen in these areas no higher resolution maps were made. The phases mapped were calcite, dolomite, and aragonite.

Post processing of the EBSD maps was performed in AZtecCrystal version 3.1. The raw maps were cleaned by wild spike removal followed by neighbor extrapolation using six to eight neighbors (Moreno-Azana et al., 2013). Grain boundary maps and inverse pole diagrams were also made using this software. Inverse pole diagrams were made for both the entire map and specific regions of the eggshell based off changes in crystal size and orientation to better quantify the changes.

CHAPTER THREE

RESULTS

Location

MOR 11881 is an assemblage of eggs and associated float material collected from locality TM-1600 in Teton County, Montana. This locality is in the upper Two Medicine Formation near the Egg Mountain quarry. The specimen was found in the middle of a massive light grey siltstone bounded by a mottled mudstone beneath and a massive sandstone above.

Beneath the mottled mudstone is a thick bentonite layer that can be traced back to the Nest in the Wall section measured by Shelton (2007), where it is found in the upper portion of the section and stratigraphically above the Nest in the Wall site. Shelton's correlations between sections place this new site approximately 13.5m above the top of the Egg Mountain stratigraphic section (Shelton, 2007).

MOR 11881 was found isolated without any other concentrations of eggshell near the site. The matrix within the jacket is a calcareous silty mudstone that is poor to moderately cemented. Preparation revealed areas within the jacket that were more thoroughly cemented and small concentrations of medium sand sized particles. The concentrations of sand sized particles were randomly distributed throughout the jacket. The more thoroughly cemented areas of the jacket are of irregular indeterminate shape. One of these regions formed a bent cylinder, which could represent a cast of a burrow, with uneven sides in the southern region of the jacket. This structure was removed during preparation though the pieces were kept. The largest of these cemented regions was located below eggs eight and seven. These better cemented regions also

range greatly in size from around a centimeter to approximately twelve centimeters for the one below eggs eight and seven. The concentrations of sand are one to three centimeters in diameter but of indeterminate shape and poorly cemented.

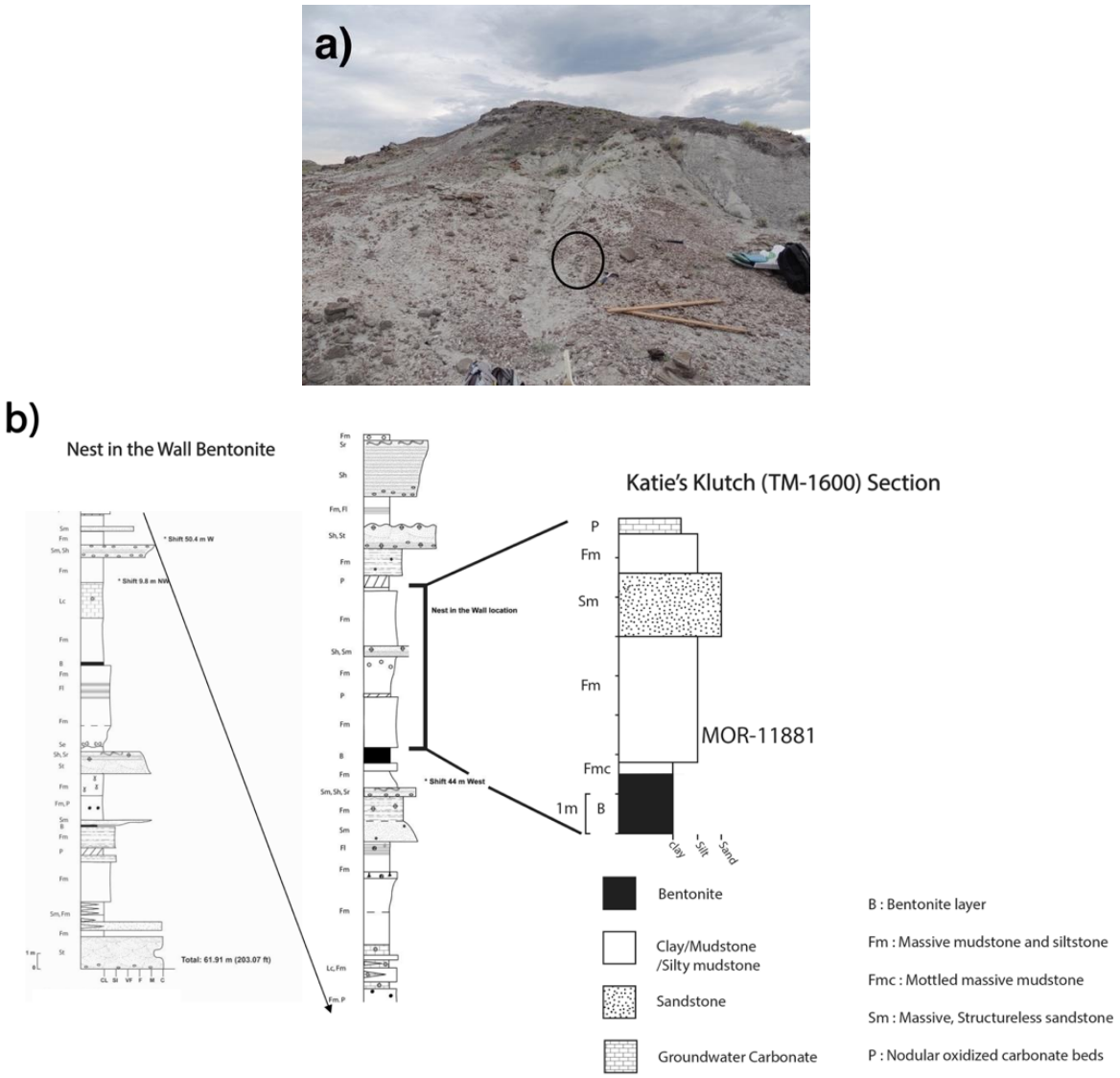

Figure 4: a) TM-1600 clutch site, with nest circled. b) Stratigraphic column of nest site and its location in the nest in the wall section modified from Shelton (2007). Full key for the Nest in the Wall section found in appendix 2 (Shelton 2007).

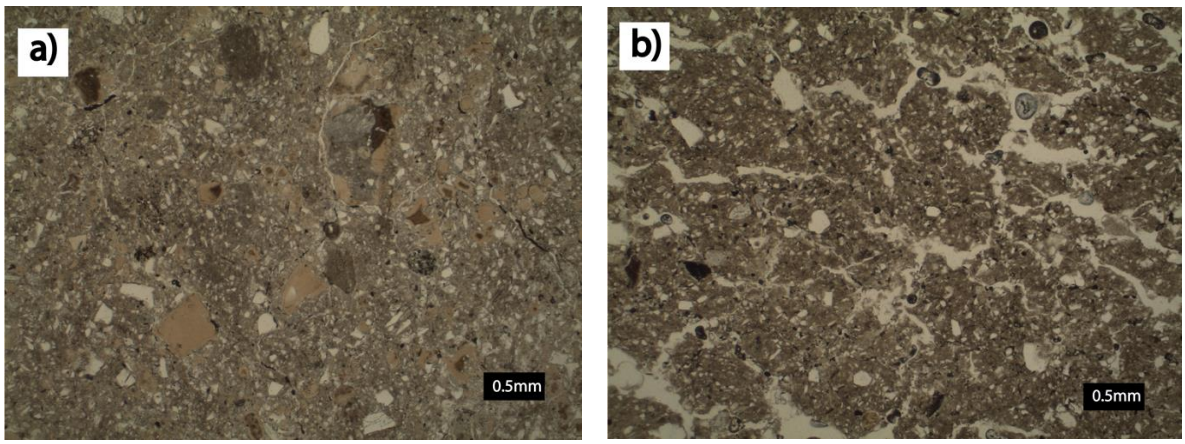

Figure 5: a) ES-579 of the more cemented mudstone and b) ES-580 of the more poorly cemented mudstone. Both in plain polarized light with scale bars of 0.5mm.

Slides were made of the two different levels of induration revealing a slight difference between them. The more well cemented mudstone has more microsparite replacing the matrix compared to the less well cemented mudstone (Fig. 5). Slide ES-579 is from the more cemented sediment and is comprised of an estimated 32% microsparite, 13% micrite, and 50% silt and 5% sand grains. The grains are 70% quartz, 10% feldspars, and 20% lithic fragments based on a point count of 100 grains. Slide ES-580 is of the more common and less cemented mudstone and is also comprised of an estimated 35% micrite, 10% microsparite, and 50% silt and 5% sand grains. The crystal size of the microsparite in ES-580 is also smaller than those seen in ES-579 and both appear muddy in plain polarized light. The sand and silt grains have approximately the same composition with 71.7% quartz, 9.1% feldspar and 20.2% lithic fragment based off a point count of 99 grains. The level of rounding of grains in both slides is the same with most grains in both slides being very angular to sub-angular.

Clutch

Description of the Eggs

MOR 11881 was collected as a single jacket and several bags of float. The bags of float primarily consist of fragments of eggshell and egg contents that were not associated with complete or partial eggs. The only piece of bone found in float is a single rib fragment approximately 2.8cm wide and 5.7 cm long which was found as surface float near the nest. The clutch itself is 81cm long by 48cm wide, measured from the edges of the two eggs furthest from each other. The widest section is measured perpendicular to the length measurement. There was a small wash to the west of the nest that could have eroded any further eggs on the western side meaning that it is unclear if the preserved eggs represent a whole or partial clutch. The state of the eggs makes it difficult to determine if any of the partial eggs were truncated by erosion or if their state is due to other factors.

The final prepared clutch consists of eleven individual eggs, isolated eggshell fragments, and clusters of pellets (Fig. 6). The presence of egg-6 and the float on top of the clutch suggests that there may have been a second layer of eggs that eroded away. The eggs are arranged with a cluster of six eggs at the northern end of the jacket and three in a staggered row extending to the southern end. With the exception of egg-6, all eggs are arranged in a single plane. Egg-6 is located stratigraphically above and is in contact with eggs-1 and egg-5. The eggs are roughly parallel to each other and the bedding plane, based off the layers above the massive mudstone.

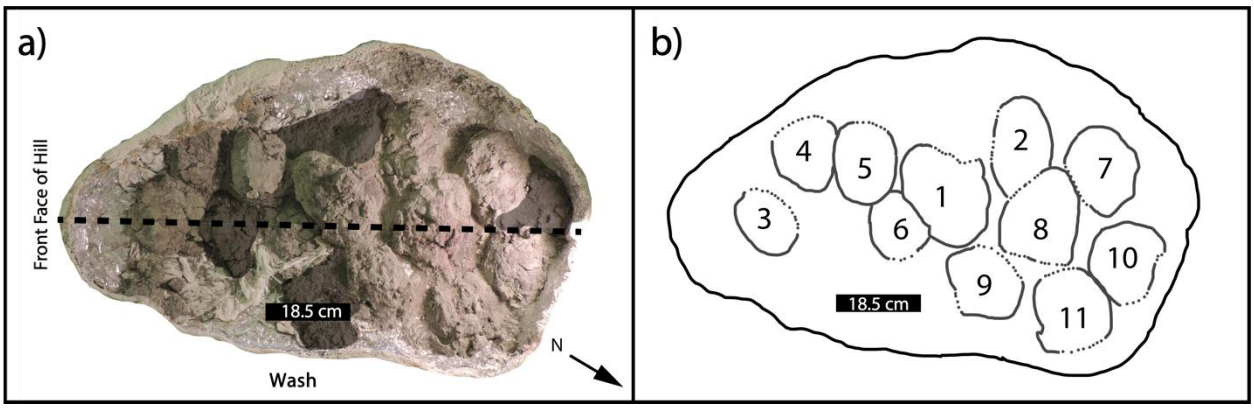

Figure 6: Prepared jacket photograph and schematic Both scale bars are 18.5cm. a) Photograph of prepared jacket with the approximate location of North labeled. Shaded areas indicate regions of the jacket still covered in sediment. Dashed line is the 0º line for angle measurements. b) Schematic of the jacket with the eggs numbered in order of discovery. Solid lines represent intact edges of eggs while dotted lines represent broken, or sediment covered edges of eggs. Where eggs cover each other the completeness of the egg on the bottom is represented.

Each egg is subspherical to ellipsoidal with one axis longer than the other. The average length of the eggs is 15.8cm while the average width is 12.9cm. The average depth of the eggs is 6.0cm. The average volume of the eggs is 641.2cm^3.

Table 2: Measurements of the eggs length, width, depth, and calculated volume.

Egg number	Length (cm)	Width (cm)	Depth (cm)	Vol (cm^3)
5	13	11.4	6.7	519.9
1	17.1	13.5	7	846.1
8	17	15.7	5.5	768.6
7	16.5	13.5		
10	15.5	10.6	5	430.1

The orientation of each egg's long axis was measured compared to the long axis of the clutch. Egg-1, egg-2, egg-4, egg-5, egg-7, egg-8 and egg-10 are between 10º to 33º from perpendicular to the long axis of the jacket. They are semi-three-dimensional retaining some thickness but having distorted shapes. Eight of the eleven eggs have distinct lateral and polar

edges with the remaining three primarily preserving the semi-flattened bottom surface of the shell which slopes toward the top of the jacket. The eggs without distinct edges are egg-3, egg-9, and egg-11. Egg-six is located stratigraphically above the other eggs and is therefore partially obscured in the jacket due to the preparation from the bottom. Before the jacket was made egg-6 was more visible and appeared to be three dimensional and almost spherical in shape.

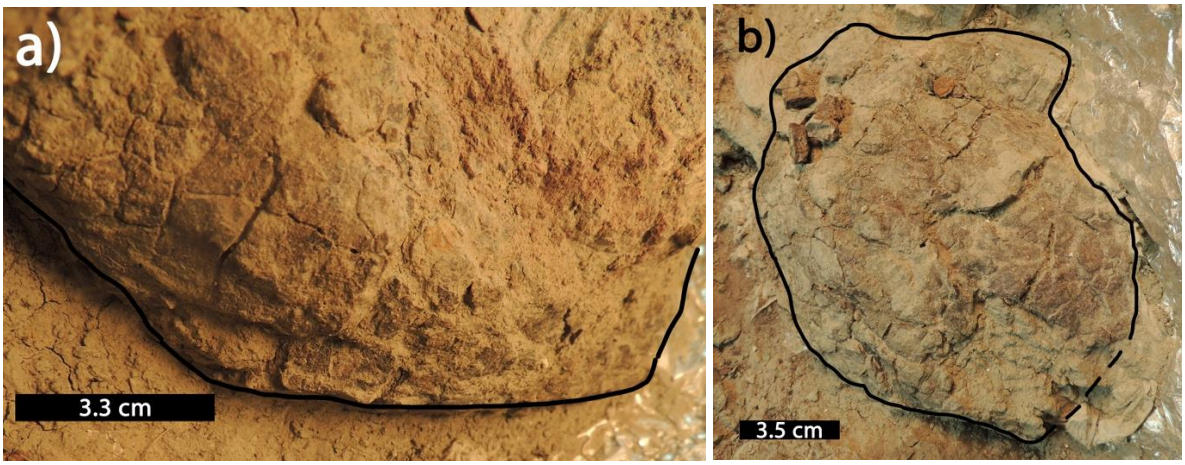

Figure 7: Detailed images of eggs showing the deformation of their shape. Black lines mark the edges of the eggshell. a) Egg two showing the folding along the sides of the eggs. Scale bar is 3.3cm. b) Egg 10 showing distortion of the bottom surface. Scale bar is 3.5cm.

Where the sides of the eggs are present, they are often folded parallel to the bedding plane as seen in figure 7 a). Egg-4 and egg-5 are the least deformed in shape, with few indents or folds. Egg-2, egg-7, egg-8, egg-10 and egg-11 all show varying degrees of folding along their sides. Egg-1 does not show much folding but does show displaced sections of eggshell in two places. One place is along a fault running through the egg and the other is a section of shell that is stratigraphically higher than the rest of the egg. This raised section of shell is located directly above where the shell in the rest of the egg stops and follows the general outline of the egg. The

bottom surfaces of the eggs are also deformed with concave and convex areas, some of which are more pronounced than others as seen in Fig. 7b.

The eggs in this study have dark brown to black eggshell that is sometimes coated in white translucent calcite as seen in Fig. 9 b). The exact color of the eggshell is variable with some exposed patches of shell being darker than others. Egg-2 and egg-10 are mostly lighter brown while the remaining eggs have darker brown shell. The inorganic calcite coating the shell is found on both the float fragments and the whole eggs of the jacket. The eggs are filled with a mixture of well cemented red colored sediment and large collophane masses. Collected float includes fragments of eggshell, eggshell with infill sediments adhering to their undersides and chunks of the red infill sediments that are not associated with eggshell.

External Eggshell Description

Each egg of the clutch can be divided into three parts: eggshell, eggshell membrane, and egg contents. In addition to these parts most of the eggs have mineral coatings of either calcite or amorphous apatite covering the eggshell on the outside. The presence of the eggshell membrane on the inside of the eggshell along with other mineral deposits both inside of the shell and outside of it makes measuring the thickness of the shell using calipers impossible. These mineral deposits also make observing the inner surface of the eggshell difficult.

The eggshell is primarily brown with irregular blocks colored black possibly due to a thin coating of collophane on the outside of the shell as seen in the eggshell in Fig. 8. These black patches are often fragile and tend to flake off when exposed and can be found on both surfaces of the eggshell.

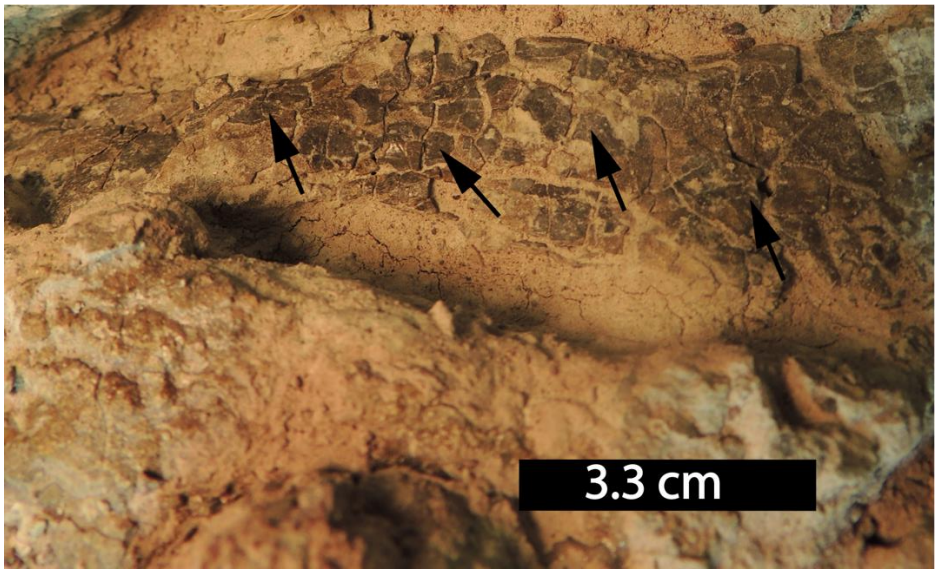

Figure 8: Detail view of the eggshell from egg eight showing black patches on brown eggshell.

Where the surface of the shell is not covered in mineral deposits, the eggshell is smooth to the naked eye. Under 10x magnification the eggs have a surface texture that resembles very tiny sagenotuberculate ornamentation of Mikhailov's (1991) variant 3. This surface texture can be observed in Fig. 9a. Even under magnification all of the eggshell of the clutch lacks visible pore openings.

A second surface texture of straight lines is observed only on egg-5 and is pictured in Fig. 9b. The straight lines appear to be perpendicular to the long axis of the egg unlike lineotuburculate ornamentation. These lines are also replicated in the layer of calcite coating the shell and are only found in areas where the calcite has been removed from the shell. They are also most visible under 10x magnification. The eggshell structure of egg-5 shows the same structures and layers found in the other eggs of the clutch. The eggshell of egg-5 is also thinner than the average thickness for the clutch, with an average thickness of 379µm.

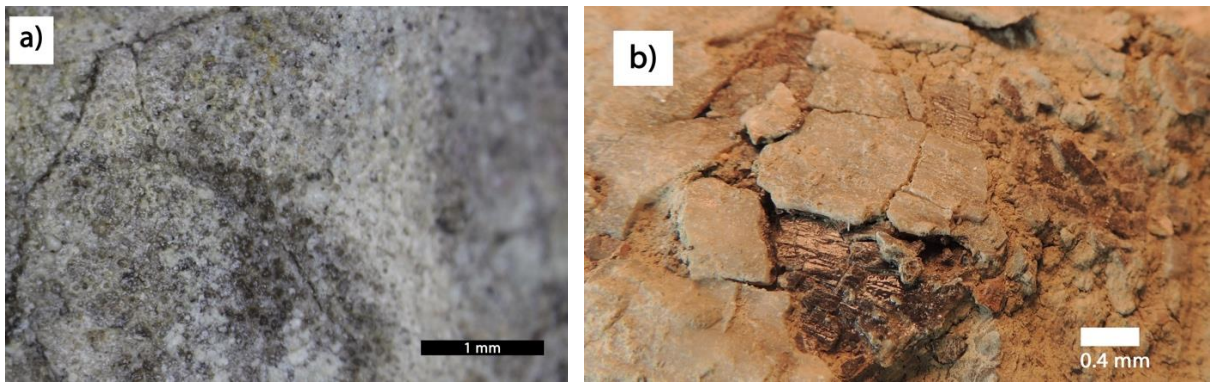

Figure 9: Eggshell surface patterns. a) Detail view of eggshell showing common surface pattern. Scale bar is 1mm. b) Linear surface pattern and covering calcite. Scale bar is 0.4mm.

When viewed under SEM the tiny compactituberculate-like pattern is comprised of clusters of blocky crystals surrounded by slightly raised acicular crystals radiating from the clumps (Fig. 10). These acicular crystals form a pattern of rosettes on the surface of the shell. The rosettes form a variety of shapes, ranging from circular to the shape of a human kidney. The more circular rosettes range in diameter from 147µm to 105µm. The more elongate rosettes can have long axes around 180µm. There is little space between the rosettes. There are also no visible, recognizable pore openings on the surface of the eggshell when it is viewed under SEM. The underside of the eggshell is not visible due to layers adhering to the underside of the eggshell.

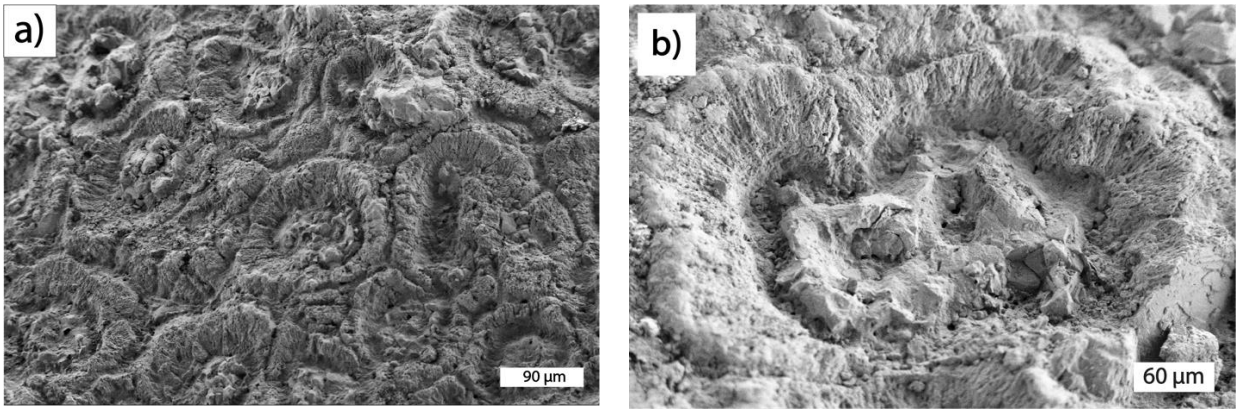

Figure 10: a) More common surface texture pattern as seen under SEM. Scale bar 90µm. b) Detail of single rosette, showing both blocky crystals in the middle and thin radiating crystals along the outside. Scale bar 30µm.

Eggshell Structure Description:

The average thickness of the eggshell is 512 µm ± 135µm. In thin sections, the eggshell from the clutch is light brown in plain polarized light and is consistent with calcite. The eggshell of the clutch can be differentiated from the inorganic calcite covering it under normal polarized light due to its brown or grey-brown color while the inorganic calcite is clear. EDX mapping of the eggshell shows that chemically the eggshell varies from the inorganic calcite in magnesium and manganese concentrations as seen in Table 3. The eggshell has over twice the magnesium and one and a half times the manganese when compared to the inorganic calcite as shown in the table below. The inorganic calcite also lacks the trace amounts of phosphorous seen in the eggshell.

Table 3: Weight percentages calculated from Slide KE-9 EDX map 1. Carbon has been removed from the table and calculations due to the slide being carbon coated.

Element	Eggshell Weight %	Inorganic Calcite Weight %
O	49.43	49.59
Ca	47.5	48.63
Mn	1.22	0.71
Si	0.7	0.57
Mg	0.64	0.19
Al	0.18	0.18
Fe	0.13	0.14
P	0.12	
S	0.05	
Cl	0.02	
W	0.01	

The eggshell can be divided into three regions based on crystal structure and composition. These regions are shown in Fig. 11a. From the inner surface of the eggshell to the outer surface they are the blocky region, dark region and lobed region. The first region is the blocky region that is located along inside surface of the eggshell. This region is characterized by large calcite crystals that have a blocky texture on broken surfaces and form large triangular to trapezoidal crystals in EBSD. Located in the upper portion of the blocky region is the dark region. It is dark brown in thin sections and does not map in EBSD. This region is not present in all eggshell fragments examined. The final region is the lobed region which is located along the outer surface of the eggshell. This region is characterized by long blocky crystals originating in the blocky region that extend up into a layer of radiating acicular crystals.

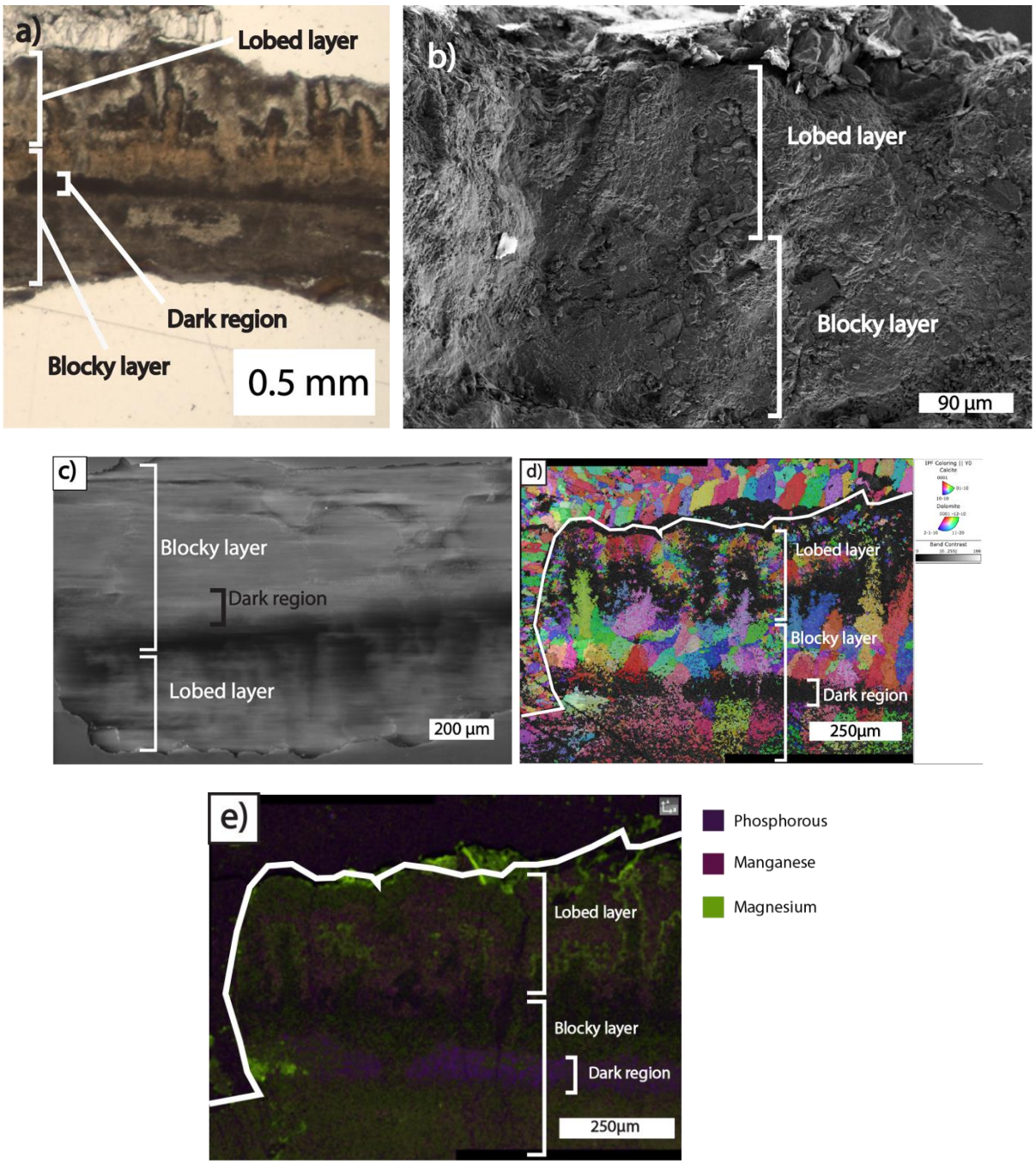

Figure 11: a) Thin section KE-9 taken from egg 6 viewed under plain polarized light. Lobed, dark and blocky regions indicated by brackets surface of the eggshell is at the top of the image. Scale bar 0.5mm b) SEM specimen KS-1 viewed in SEM with lobed and blocky regions indicated by brackets. The dark region missing from this sample. Surface of the eggshell is at the top of the image. Scale bar is 90µm. c) CL image of KE-9 with layers labeled. d) EBSD inverse pole map of the Y coordinate. d) Compound EDX map of KE-9 with colors enhanced for greater visibility.

EBSD of the eggshell gives poor hit rates with Kikuchi lines not being observed for large regions of the shell. Slides KE-9 and KE-7 were mapped using EBSD. Slide KE-7 taken from egg one lacks the dark region while it is present in slide KE-9 from egg 6. The primary phase mapped was calcite, however dolomite and aragonite were also mapped. Processing of the maps by wild spike removal removed all points mapped as aragonite but not all the mapped dolomite as seen in Fig. 12b.

Slide KE-7 taken from egg 1 had a 56.54% hit rate after the map was cleaned up sampling every 5.37μm (the step size of the map). Meaning that after wild spikes were removed and non-mapping points with up to six neighbors were filled in 56.54% of the sites sampled were giving recognizable Kikuchi patterns. Slide KE-9 taken from egg 6 had a 56.16% hit rate with a step size of 2.1749 μm. Sites that did not give recognizable patterns when checked revealed a lack of any Kikuchi patterns when the areas were randomly sampled. Decreasing the step size did not increase the hit rate or resolution of the EBSD maps of the eggshell. The inorganic calcite coating the eggshell mapped with few points giving zero solutions due to a lack of patterns detected. Most of the angles between the y axes of grain boundaries are over 20° in both the eggshell and the inorganic calcite. Low angle grain boundaries under 15° are usually short where they are present. The crystals of the eggshell have a slightly preferred orientation as seen in Fig. 12c.

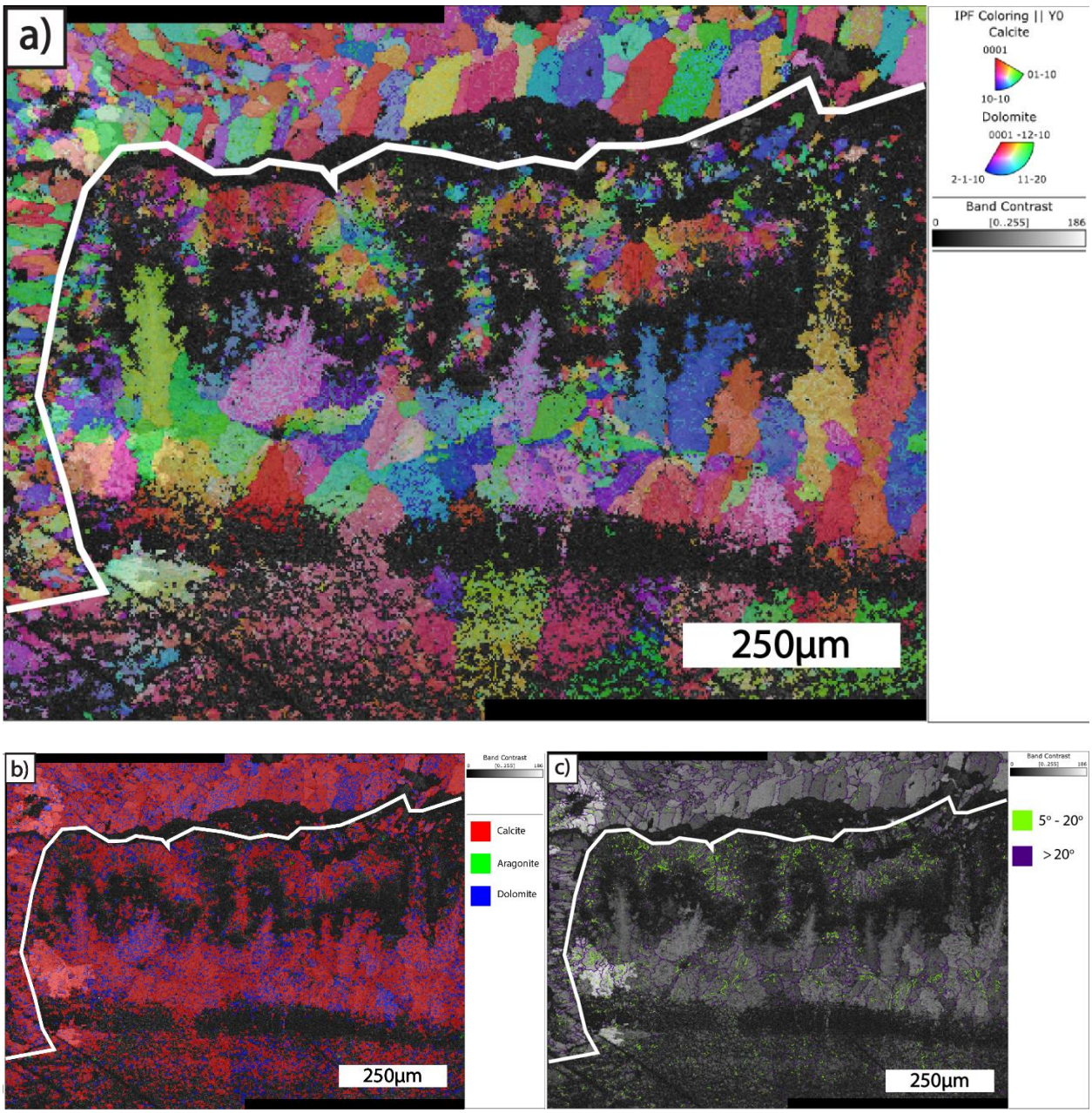

Figure 12: EBSD maps of slide KE-9 site 1. The white line marks the boundary between the inorganic and organic calcite. Background image is the band contrast image in all three. All scale bars are 250µm. The edge of the eggshell is marked by a white line. a) Inverse pole figure map of the y axis. b) Phase map showing calcite and dolomite. c) Grain boundary map.

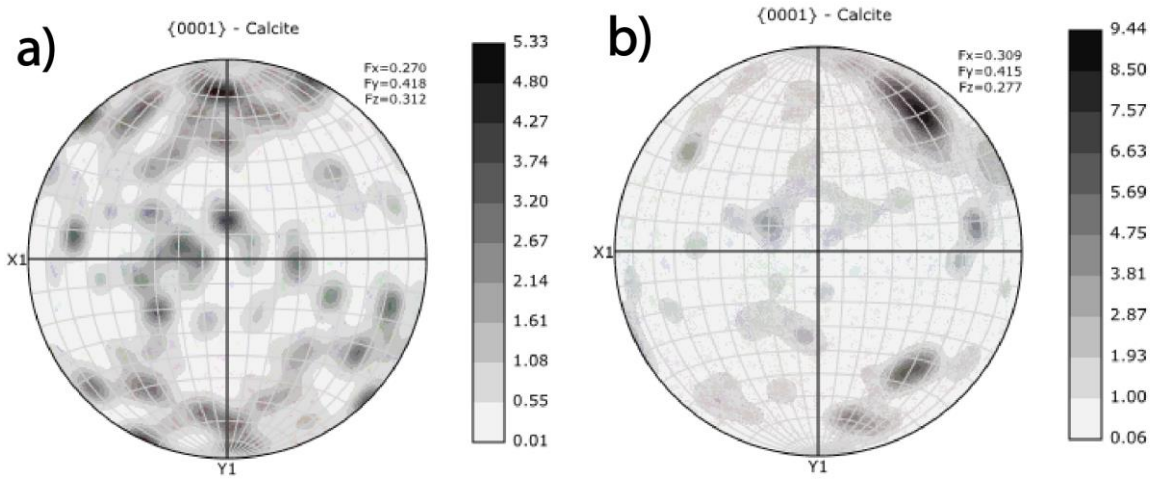

Figure 13: Pole figures of slide KE-9 site 1 map. a) Pole figure of inorganic calcite. b) Pole figure of eggshell calcite.

The blocky region is an average of 232µm ± 104µm thick. Under plain polarized light, thin sections of the blocky region of the eggshell are light brown with darker flecks dispersed throughout the region. Under crossed polarized light the crystals that comprise this layer mostly undergo extinction in a random order compared to each other. In some pieces of eggshell there are circular formations of calcite crystals in this region. In EBSD the blocky layer maps as a series of large crystals that sometimes map well and sometimes map poorly as seen in Fig. 12 a). In slides KE-9, KE-10 and ES-582 the blocky layer is divided into two areas by the dark region as seen in Fig. 11a. Under EBSD some crystals in both the upper and lower blocky regions share the same orientations as seen in Fig. 15.

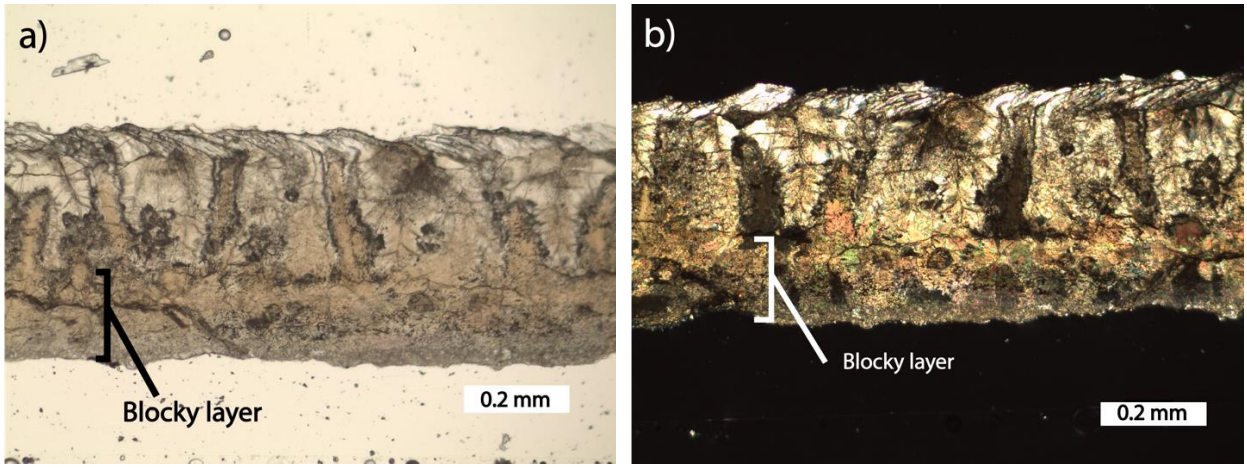

Figure 14: Eggshell that exhibits only the blocky and lobed layers. Both Scale bars are 0.2mm. a) Plain polarized light view of slide KE-8. The blocky layer is marked by a black bracket and the surface of the eggshell is at the top of the image. b) Cross polarized light view of slide KE-8. Blocky layer indicated by a white bracket and surface of the eggshell at top of image.

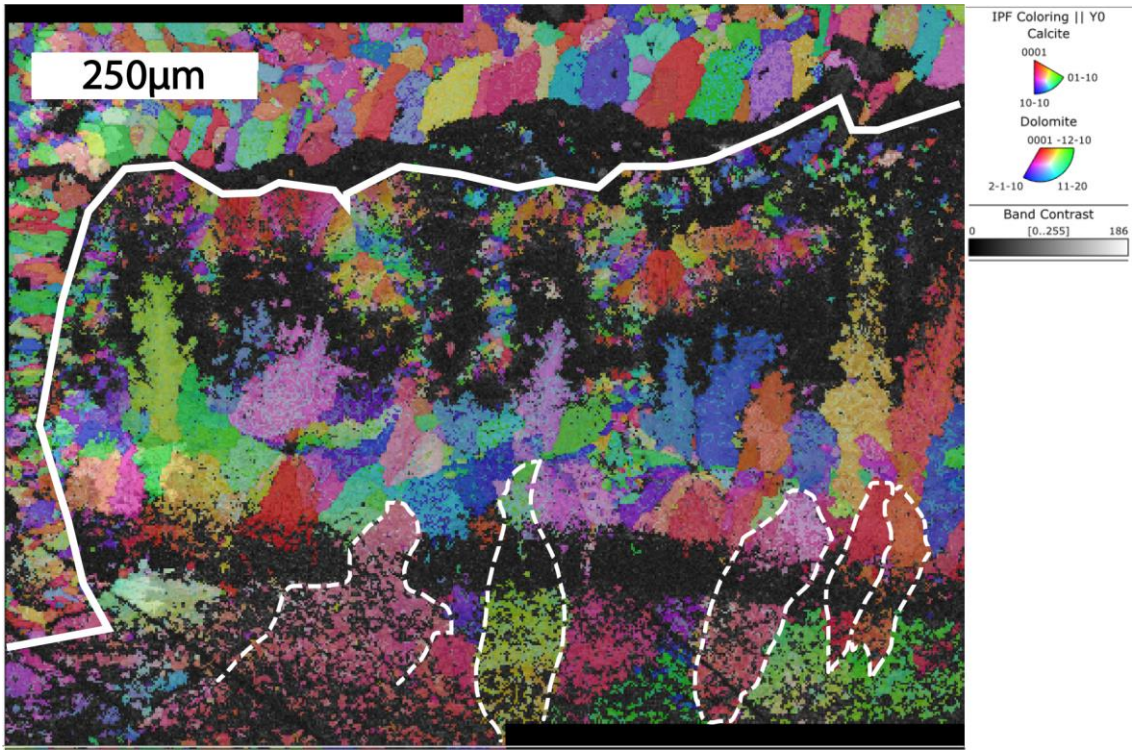

Figure 15: EBSD IPF-Y site 1 map of slide KE-9 with the surface of the shell marked by the solid white line. Crystals that can be traced across the dark layer are outlined in dashed white lines. Scale bar is 250µm.

The eggshell fluoresces on the red to orange end of the spectrum under CL which in turn causes streaking and out of focus appearance (Fig. 16) due to the long wavelength. In CL the blocky region fluoresces weakly above the dark region and brightly beneath the dark region (Fig. 16). The orange to red fluorescence usually indicates the presence of manganese in these regions and therefore alteration (Carpenter, 1999; Cazenave et al., 2003). In the EDX maps of these eggshells the lower area of the blocky region has only slightly higher levels of magnesium compared to the rest of the eggshell. Eggshells that do not possess a dark region show a less pronounced version of the same pattern with the upper area of the blocky region not fluorescing as much as the lower area near the inner surface of the shell (Fig. 16b). In these eggshells the blocky layer beneath the dark layer has less well-defined crystals that map poorly in EBSD but still retain indications of larger crystal size based on the large areas that intermittently record the same orientations in the layer (Fig. 15).

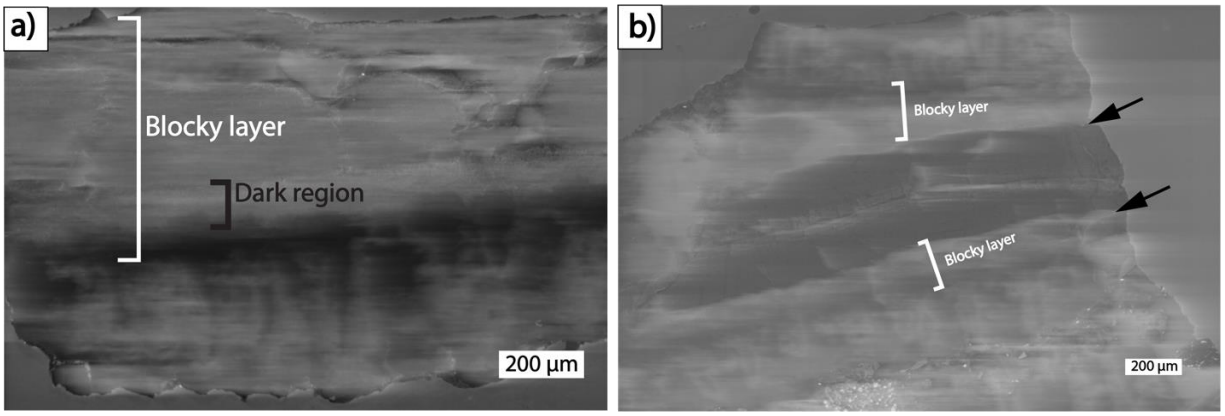

Figure 16: CL images of eggshell with and without the dark region. Both scale bars are 200µm. a) Slide KE-9 with blocky region and dark region. b) Slide KE-11 of eggshell from egg nine exhibiting multiple layers of eggshell. Black arrows indicate the bottom surfaces of the two pieces of eggshell.

The Dark region, when present, is located in the middle of the eggshell and in the upper half of the blocky region. It is an average of 97µm ± 50µm thick. The upper surface of the region

is jagged, and the lower surface is more even. Under cross-polarized light this region does not undergo extinction. EDX mapping shows that the region is highly phosphatic (Fig. 19c). The dark region does not map in EBSD and point scans of the area do not give any patterns indicating that the area is poorly crystalline.

The lobed region is the outermost region of the shell and is an average of 254µm ± 67µm thick. The base of the lobed region is the base of the crystals that surround the lobes. The crystals that the lobes are comprised of originate in the blocky layer as seen in Fig. 17.

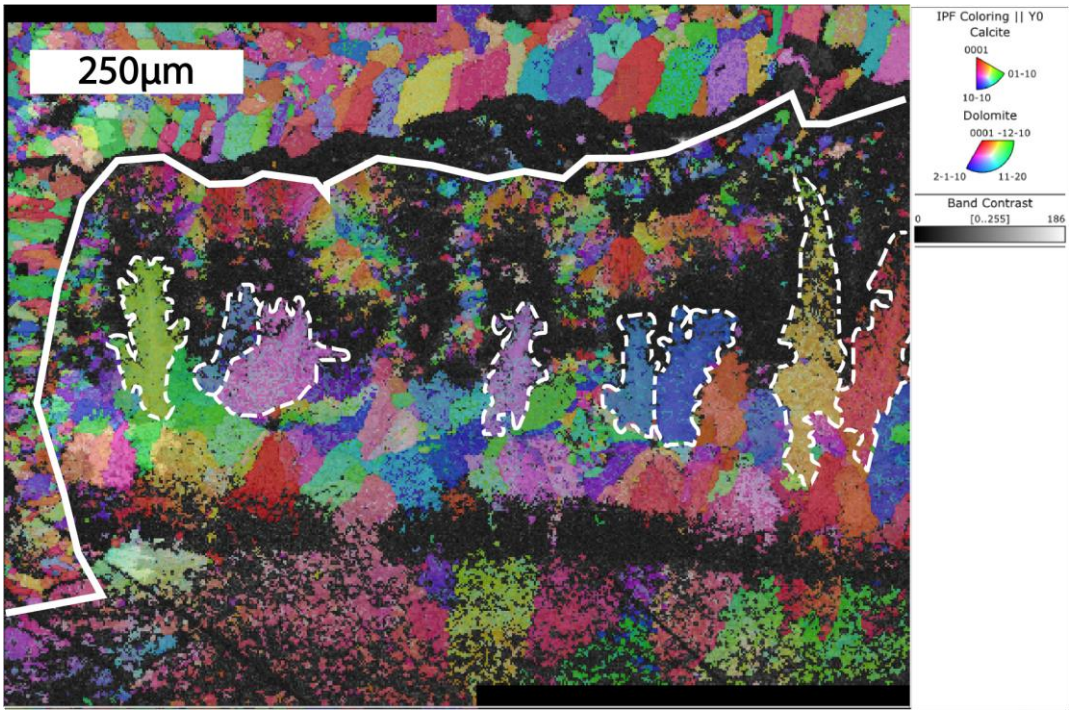

Figure 17: KE-9 EBSD area 1 map with lobe forming crystals outlined in a dashed white line. Surface of the shell is at bottom of image and the solid white line marks the boundary between inorganic calcite and eggshell. Scale bar is 250µm.

Under plain polarized light the lobes of this layer are brown and the crystals surrounding them are a lighter brown that ranges to almost clear. The lobes extend anywhere between halfway through the shell to the surface of the shell. The lobes orientation and shape are variable

also with some perpendicular to the shell but other sub perpendicular or bent. The lobe crystals undergo extinction randomly like the crystals of the blocky region beneath the lobed region, however the crystals surrounding them undergo undulating extinction that follows the edges of the lobes. The lobes do not form larger structures as seen in the tangential slide shown in Fig. 18.

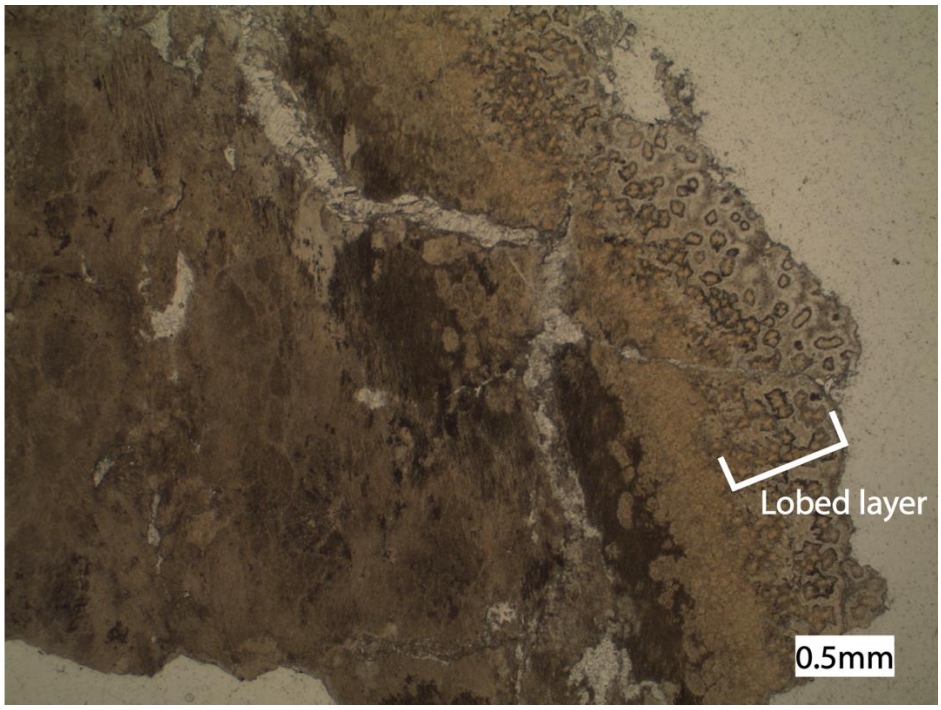

Figure 18: Tangential slide KE-12 from egg 8 under plain polarized light. Darker brown ovals are the lobes of the region surrounded by lighter crystals. Scale bar is 0.5mm.

The lobe crystals are often surrounded by a thin black outline that fluoresces brightly under Cl which is associated with magnesium. EDX maps confirm that these outlines are magnesium (Fig. 19b). The EBSD maps also reveal that the crystals that surround the lobes radiate out from the lobes as seen in Fig. 11c. The EBSD maps also show that the low angle grain boundaries are concentrated in the region of the radiating acicular crystals (Fig. 12c). In EBSD maps the region closest to the lobes maps poorly with the edges of the crystals far from

the lobe crystals map the best. In EDX maps the areas around the lobes are rich in Manganese as seen in Fig. 19 a which is probably responsible for the lack of patterns in this area.

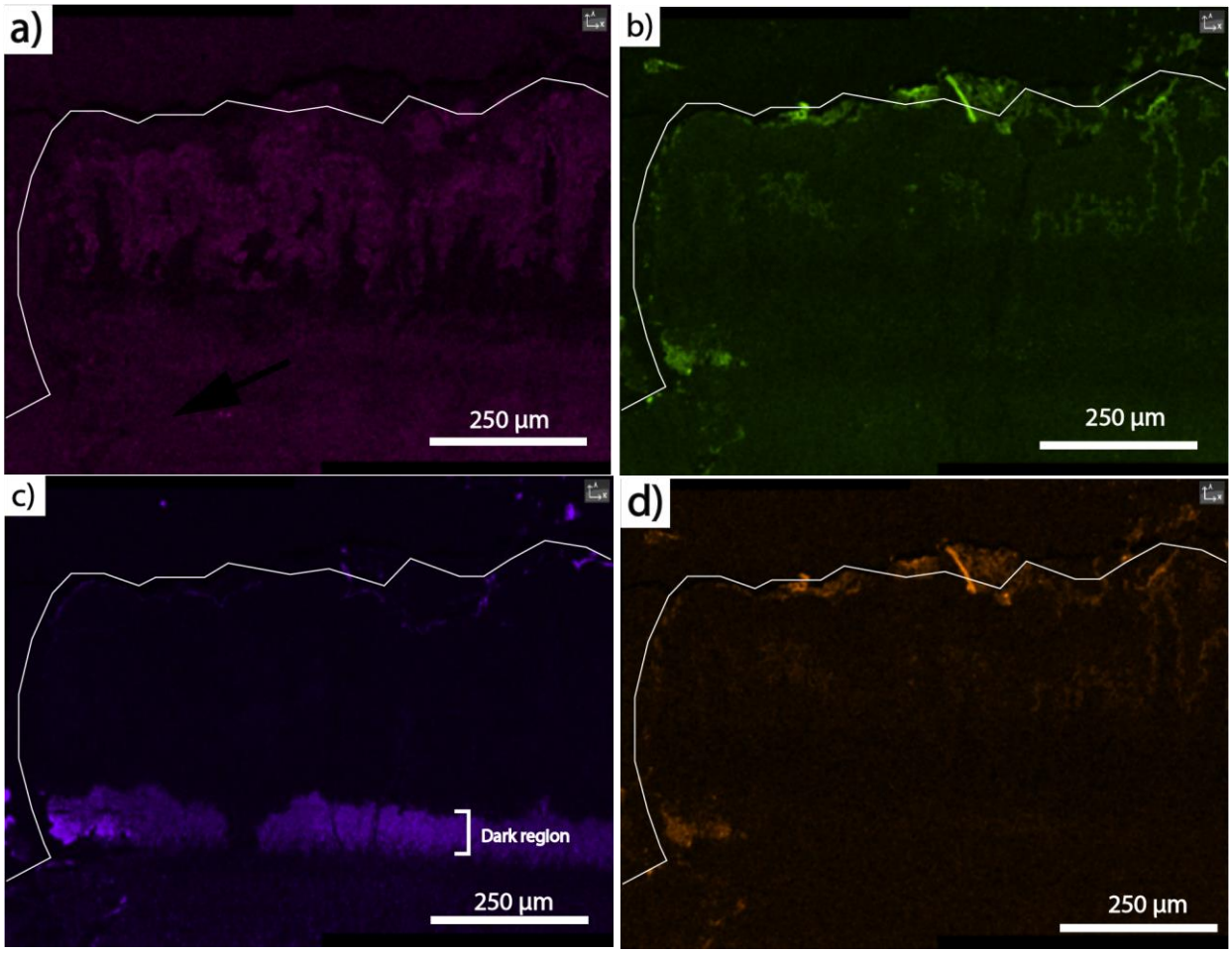

Figure 19: EDX maps of Slide KE-9. Eggshell surface is at the bottom of the image and marked by a white line. Scale bar is 250µm. a) Manganese map b) Magnesium map c) Phosphorus map d) Iron map

Eggshell Membrane

There is a layer of material located beneath the shell in six of the nine slides that is consistent with eggshell membrane found in modern and fossil eggs. Under light microscopy this layer is brown with darker brown bands parallel to the inner surface of the eggshell (Fig. 20). The bands become more prominent when viewed using crossed polarized light but are also

visible under plain polarized light. The darker bands and the lighter bands undergo extinction at different times. Under high magnification faint traces of individual fibers are visible using light microscopy.

Under SEM the fibers are distinct, and their orientations are visible, with each band being comprised of parallel fibers oriented perpendicular to the bands above and below (Fig. 22). This organization of fibers is identical to modern eggshell membrane from both crocodilians and birds which share layers of fibers in alternating orientations (Mine, 2007; Lensink et al., 2023).

The membrane is often broken in places with sharp edges indicating that it broke after fossilization (Fig. 20a). Less commonly, the membrane appears torn, leaving more jagged edges and separating the layers of fibers (Fig. 20c). The more torn appearance could be due to the membrane tearing before mineralization or the growth of calcite crystals between the layers of fibers after mineralization. Fragments of the membrane can also be found floating in the egg contents and will be discussed more later.

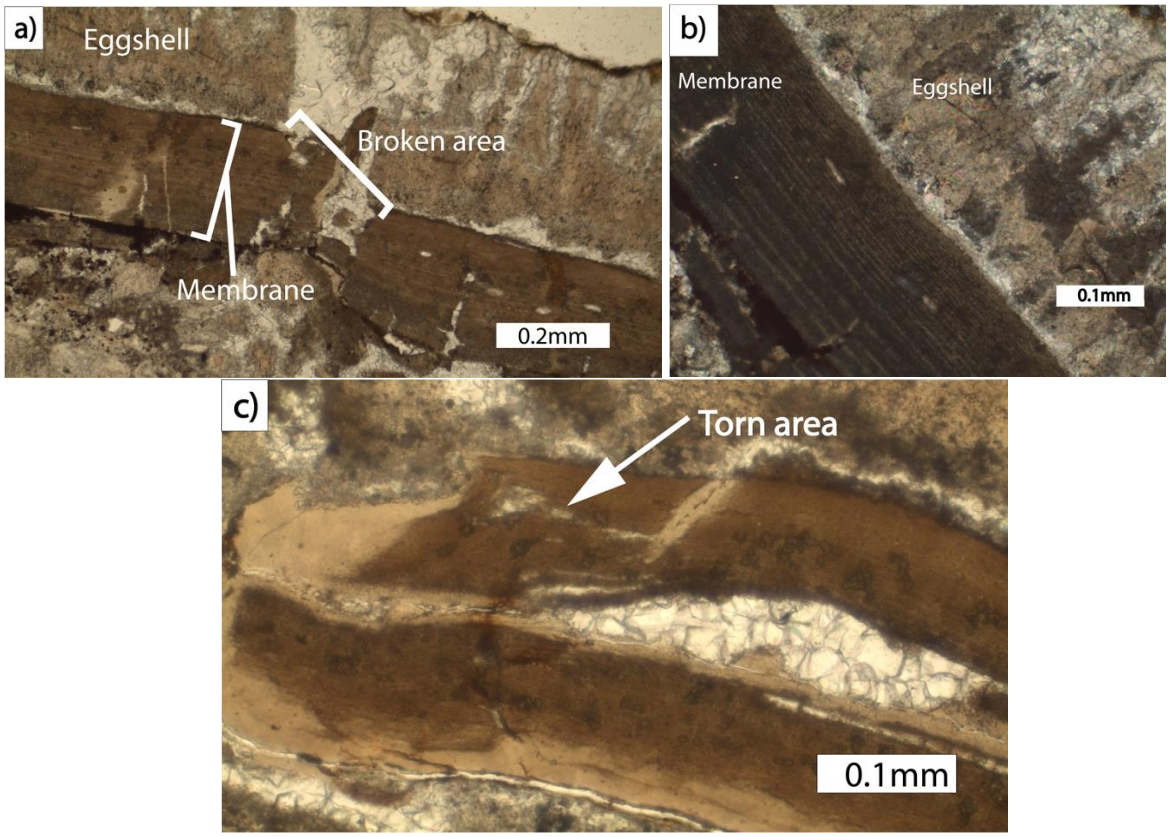

Figure 20: Eggshell membrane from slide ES-581 taken from egg 9. a) Eggshell membrane under plain polarized light showing a sharply broken area of membrane. Scale bar is 0.2mm. b) Eggshell membrane under cross polarized light showing layering of the membrane. Scale bar is 0.1mm. c) Torn section of membrane indicated by a white arrow. Scale bar is 0.1mm.

The thickness of this membrane is highly variable; however, the inner edge of the membrane is often jagged indicating that the full thickness of the membrane is rarely preserved. The sections of membrane that are in contact with the eggshell have an average thickness of 133µm ± 68µm based off ten measurements from five different slides of different eggs. The thickness of the membrane is highly variable with the thickest section of membrane measured being 220µm thick and the thinnest section measured being 48µm thick.

In freshly broken pieces of eggshell taken from egg 10, the membrane beneath the shell is visible. On the broken surfaces, long fibers are preserved and can be found imbedded in the

surrounding matrix (Fig. 21). These parallel fibers are similar to those observed in Cretaceous fossil eggs from India that also show a pattern of preserved parallel fibers (Lourembam et al., 2023). These fibers are oriented in multiple directions, but the ones oriented nearly parallel to the break are the most easily spotted and the least cryptic in shape. The parallel fibers reoccur at regular intervals throughout the membrane and correspond with the layering seen in the light microscopy images.

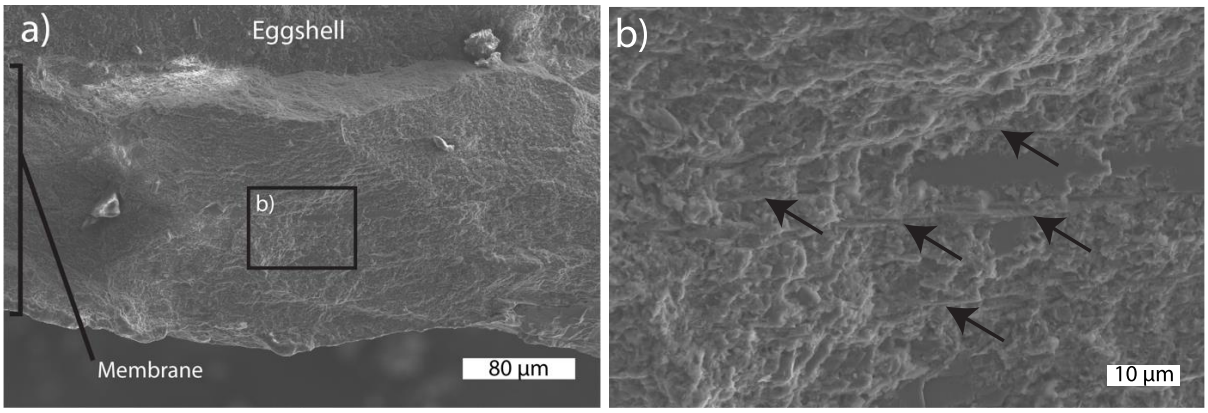

Figure 21: SEM images of membrane fibers. A) Entire thickness of membrane and contact with the bottom of the eggshell. Scale bar 80 µm. B) Close up view of the middle of the membrane with visible fibers indicated by black arrows. Scale bar 10µm.

Backscatter images of the polished slides that include eggshell membrane show lighter colored fibers surrounded by the darker ground mass (Fig. 22). Both fibers parallel to the surface of the slide and those perpendicular to it are easily visible unlike in the freshly broken sections where only parallel fibers are easily distinguished. In the polished slides parallel fibers show up as long lines while the perpendicular fibers show up as round to oval cross sections as seen in Fig. 22b.

Due to the clarity of both fiber orientations, it is easy to distinguish the different layers in the backscatter images. Individual fibers have an average diameter of 1.2 µm ± 0.4µm. The fiber

diameter increases slightly further from the base of the eggshell. The average diameter of these fibers is within the normal ranges of both avian inner eggshell membrane fibers at between 0.1μm to 3μm and outer eggshell membrane fibers which are between 1μm and 7μm (Liong et al., 1997). This average diameter is also consistent with the outermost and middle layers of modern crocodilian eggshell membranes which have average diameters of 1μm and 0.85μm respectively (Lensink et al., 2023). These measurements are not however, consistent with the innermost layer of modern crocodilian eggshell membrane with an average diameter of 0.3μm (Lensink et al., 2023).

EDX maps of the polished slides give more detailed chemical data on the composition of the fibers and the surrounding ground mass. The fibers are comprised of a calcium phosphate such as apatite, as they are rich in calcium, phosphorus and oxygen. The ground mass surrounding the fibers is rich in silicon, aluminum, iron and magnesium, in addition to calcium and oxygen suggesting that the ground mass may be comprised of aluminosilicates such as clay minerals. The different compositions of the fibers and the ground mass is illustrated by Fig. 22c.

During EBSD mapping the eggshell membrane did not map and had only occasional isolated single points referred to as wild spikes giving data. The epoxy without any crystalline structure also shows similar random data points in it. This is the expected result as apatite was not mapped, however checking random points within the membrane did not give any Kikuchi patterns indicating that the area is comprised of amorphous material. If the membrane was crystalline then some of the patterns for the area would have given Kikuchi patterns that do not match those for calcite.

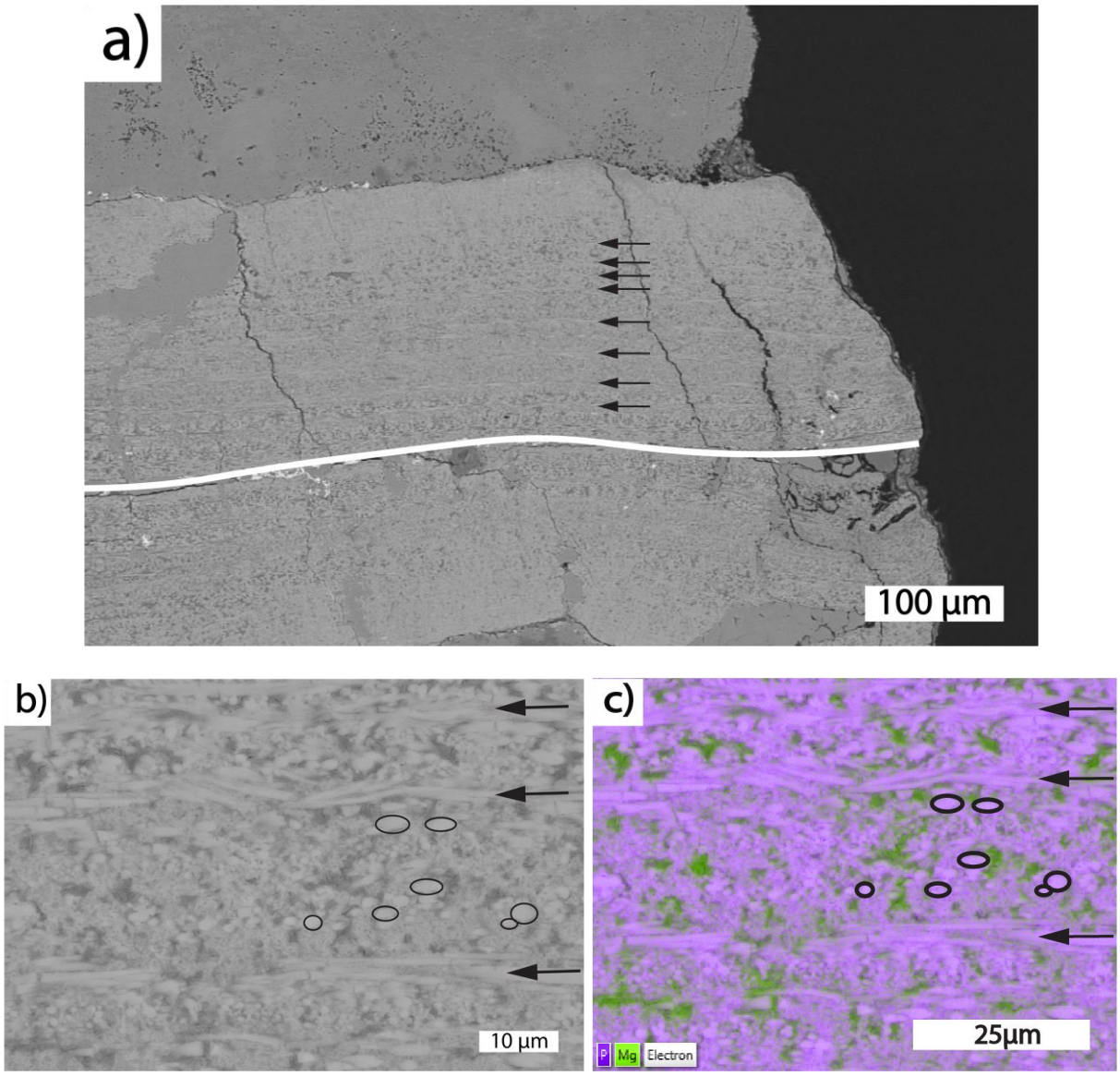

Figure 22: Backscatter images and EDX maps of the eggshell membrane. a) Backscatter image showing the entire width of membrane. White line marks the division between two layers of membrane adhering to two different pieces of eggshell. Black arrows indicate fibers parallel to surface of the slide. Scale bar is 100µm. b) Magnified view of backscatter image. Scale bar is 10µm. Several perpendicular fibers are outlined in black as examples while horizontal ones are indicated with black arrows. C) Layered EDX map of b) with phosphorus in purple and magnesium in green overlayed on top of SEM image of area. Scale bar 25µm.

Egg Contents

The material found inside of the eggs is distinct from the surrounding matrix except for a few regions closely associated with the eggs. The eggs of this study are filled with a mixture of mudstone derived from the surrounding matrix, sparry calcite, collophane crystals, small coprolites, and hematite crystals. The proportions of each of these materials differs considerably between eggs within the clutch and between different float pieces. Pieces of eggshell removed from eggs in the jacket have revealed a range of different materials inside of the eggs with some areas containing more mudstone and others more collophane.

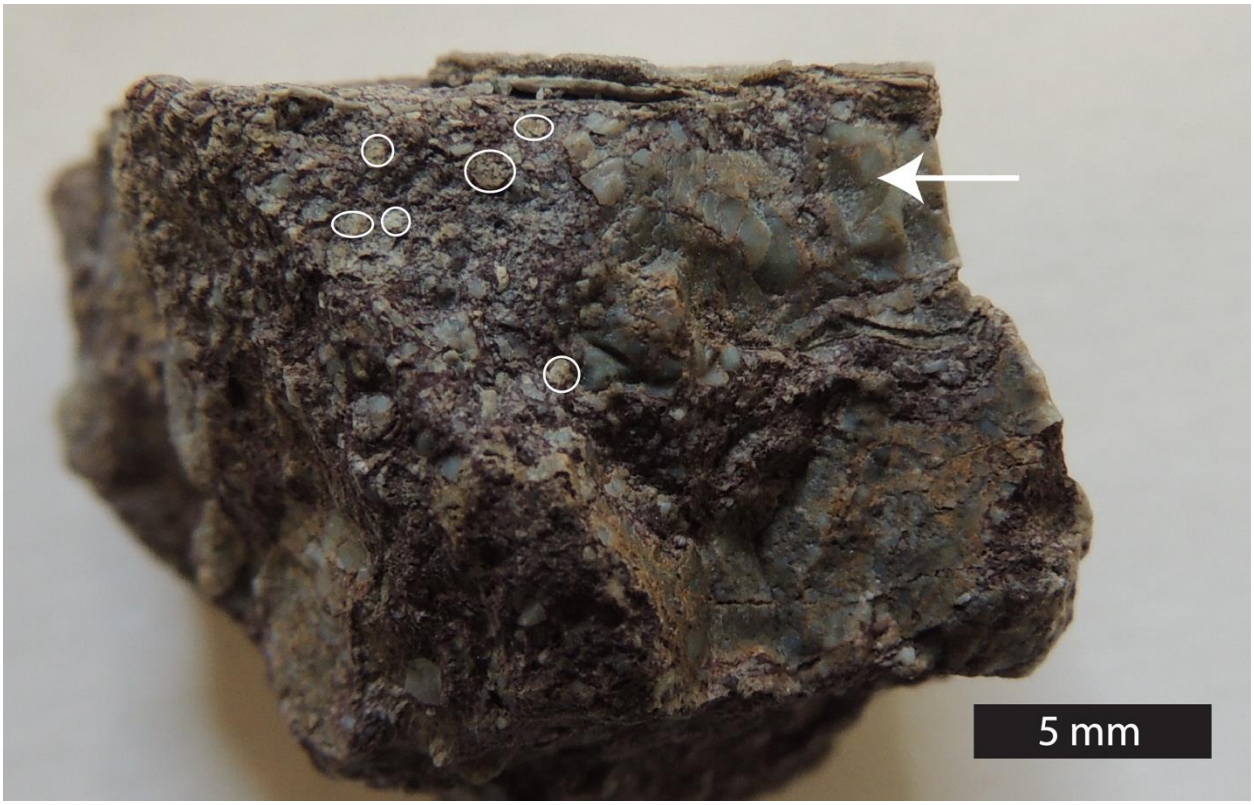

Figure 23: Piece of float with type 1 pellets (circled) and large weathered collophane crystal (white arrow). Eggshell is at the top of the image. Scale bar is 5mm.

In several areas of the jacket, outside of the eggs, there are regions in direct contact with the eggs that are rich in hematite and contain fragments of collophane as seen in Fig. 23 indicated by the white arrow. These regions are not found away from the eggs, and none were found during the excavation of the nest in the surrounding area. The position and composition of these regions suggests that they are associated with the eggs. These regions are identifiable by their pink color due to the hematite, small black collophane crystals and higher concentrations of eggshell fragments.

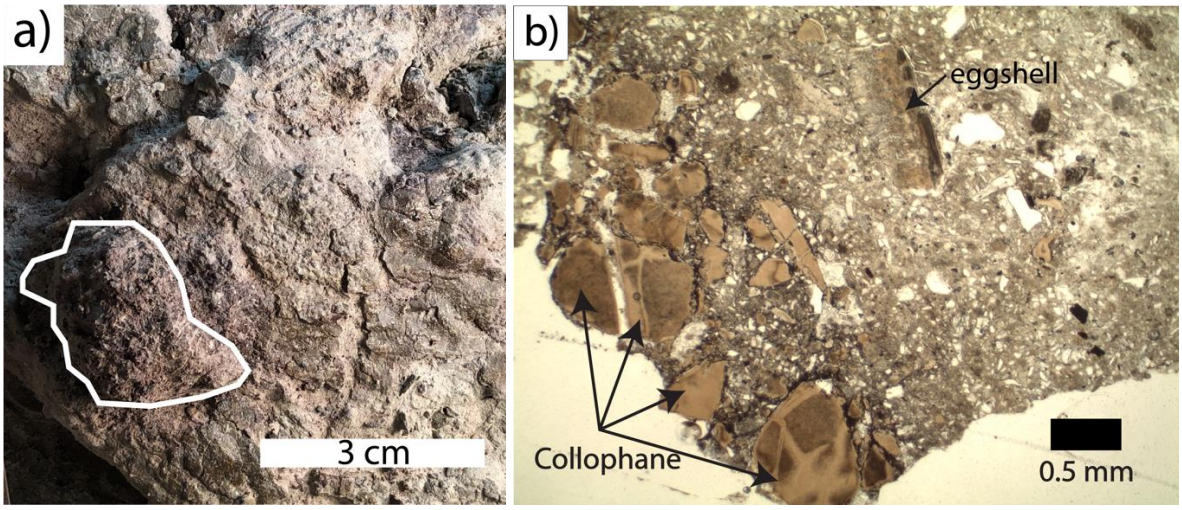

Figure 24: a) Sediment region beneath egg 8 showing compositional differences from the rest of the matrix outlined in white. Scale bar is 3cm. b) Sample from the edge of this region of sediment under plain polarized light in slide ES-584. Hematite is black rinds around grains. Scale bar is 0.5mm.

The contents of the eggs are most easily observed in the fragments of float material which usually preserve both eggshell and the internal contents of the eggs. Most float pieces display a red mix of materials with occasional coprolites and collophane crystals (Fig. 25), however several pieces only contain collophane, such as the one in slide ES-583 shown in Fig. 26. The more common mix of materials is found in ES-582, which has coprolites, collophane,

sparry calcite, hematite, silt, and clay. ES-581 with multiple shell layers has mostly silt and clay with small amounts of sparry calcite separating the layers.

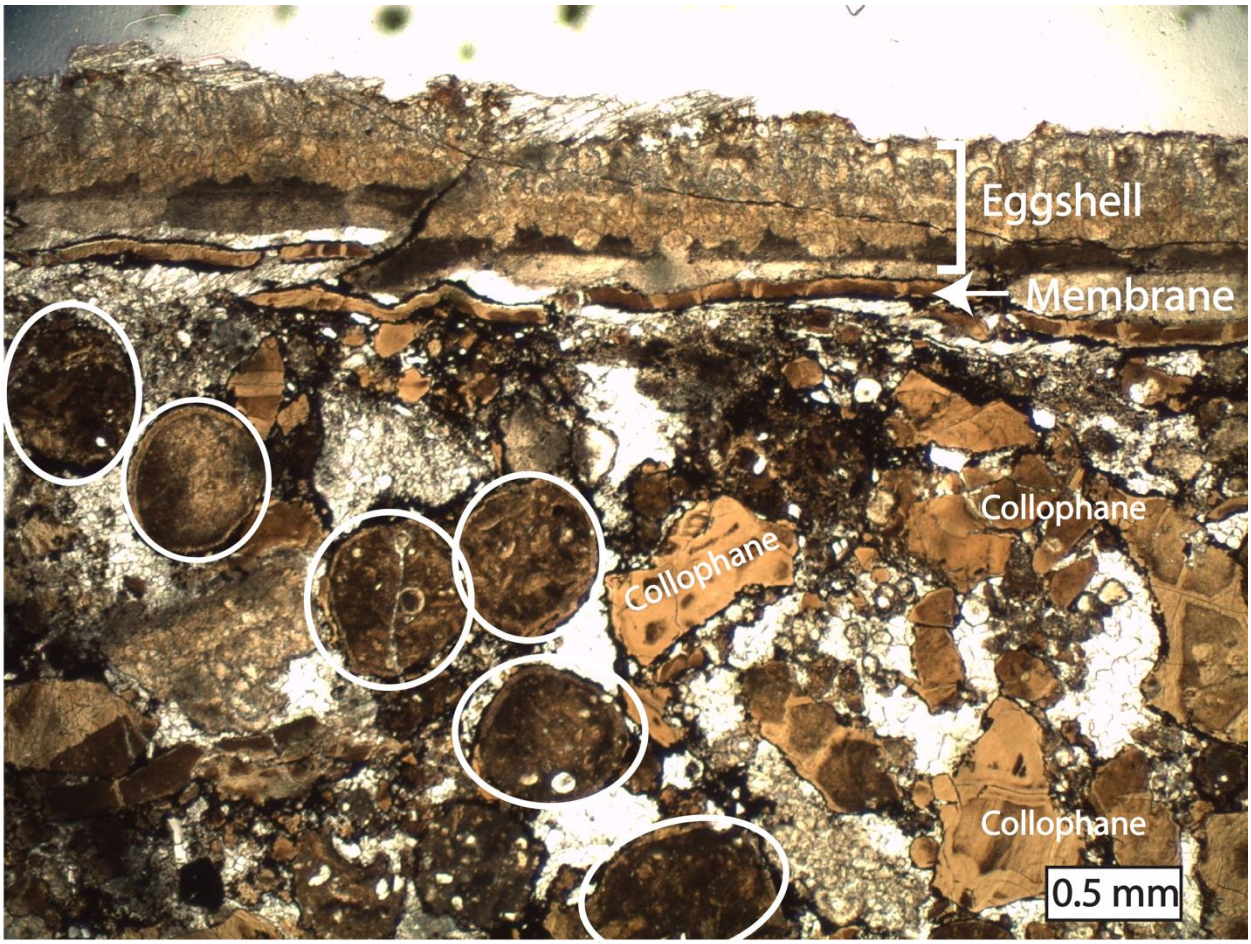

Figure 25: Egg contents in slide ES-582 comprised of coprolites, sparry calcite, collophane and hematite. Coprolites are circled in white. Scale bar is 0.5mm.

In thin sections observed through light microscopy, the ground mass of the egg contents is comprised of sparry calcite and clay minerals. The sparry calcite is comprised of euhedral crystals of mostly uniform size and fills voids between collophane masses, coprolites, mudstone and fragments of membrane. The mudstone is almost compositionally the same as the matrix surrounding the clutch but with additional hematite. The hematite can be found scattered as small

crystals throughout the sediment but is most prominent coating the surfaces of collophane masses, coprolites, and membrane fragments. The collophane masses are large fragments of collophane with no distinctions between crystals. They are inconsistent in shape and range in size from filling the most of an egg to microscopic fragments. In thin sections the collophane masses sometimes contain cracks that are discolored around the edges in a lighter brown color than the surrounding collophane as seen in Fig. 26. The membrane fragments found in the egg contents are similar to those found associated with the shell.

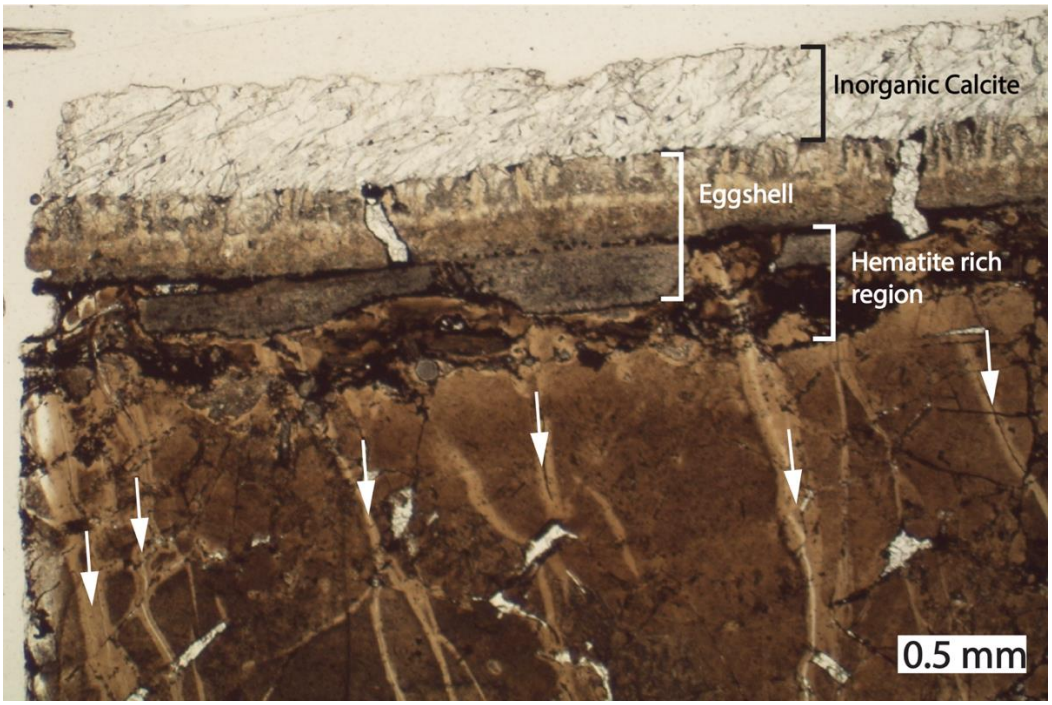

Figure 26: Egg contents of slide ES-583 comprised of primarily collophane and with some hematite beneath the shell. The lighter colored areas surrounding cracks are indicated by white arrows. Seen under normal light. Scale bar 0.5mm.

Pellets:

There are two types of pellets found in the eggs. They can be identified as coprolites based off their defined shapes and composition. Coprolites can be distinguished from pseudo-

coprolites by having defined shapes, compositions, inclusions, or external ornamentations (Francischini et al., 2016; Knaust, 2020). Type 1 pellets in MOR 11881 can be distinguished from type 2 pellets by their larger size and phosphatic composition. Type 1 pellets are elliptical with fragments of undigested material. Type 2 pellets are found in clusters, are elongate with tapering ends and are comprised of calcite. Type 1 pellets are more common than type 2.

Pellet Type 1: Type 1 pellets are small elliptical coprolites with an average diameter of 0.628 mm and an average length of 1.07mm. They are found both inside of the eggs and in clusters in the surrounding matrix near the eggs. They are also occasionally found as single isolated pellets. When found in clusters, they are distributed over a small area usually under 1cm^2 and do not take shapes reminiscent of burrows. Fig. 27a shows one of these clusters of coprolites taken from between eggs seven and ten. The clusters do not form burrow shapes and are located near the eggshell. The outsides of these coprolites are smooth and lack any surface features.

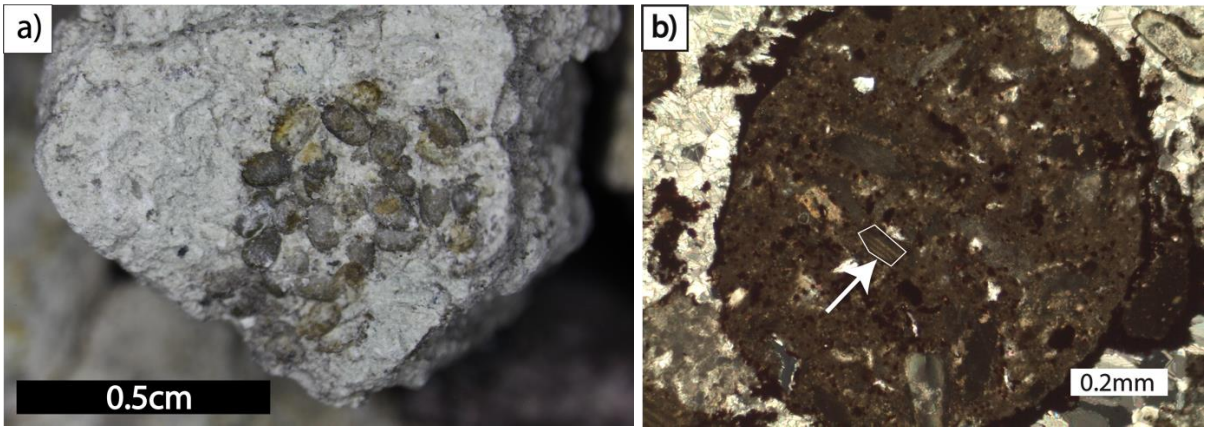

Figure 27: a) Type 1 pellet cluster removed from the sediments surrounding the eggs inside of the jacket. Scale bar 0.5cm. b) Thin Section of type 1 coprolite from ES-582 with a fragment of membrane inside of it indicated by the white arrow and outlined in white. Seen in cross polarized light. Scale bar is 0.2mm.

In thin sections they range from light grey to dark brown and sometimes contain hematite crystals (Fig. 27b). They are comprised of brown to grey matrix material and angular brown to grey grains, most of which are barely distinguishable from the surrounding matrix. However, there are a few fragments of eggshell membrane, recognizable due to their layering and quartz silt grains in a few coprolites (Fig. 27b). The grains in the coprolites do not show any preferred orientation. Some of these coprolites have lighter rinds around their edges and most have crusts of hematite surrounding their outer surfaces such as those seen in Fig. 26 and Fig. 27b.

In EDX, these larger coprolites are rich in calcium, silicon, oxygen, phosphorous and magnesium (Fig. 28). The calcium, silicon, oxygen, and phosphorous are all semi-evenly spread The silicon and aluminum are most common in the ground mass while the calcium and phosphorous are more concentrated in the grains.

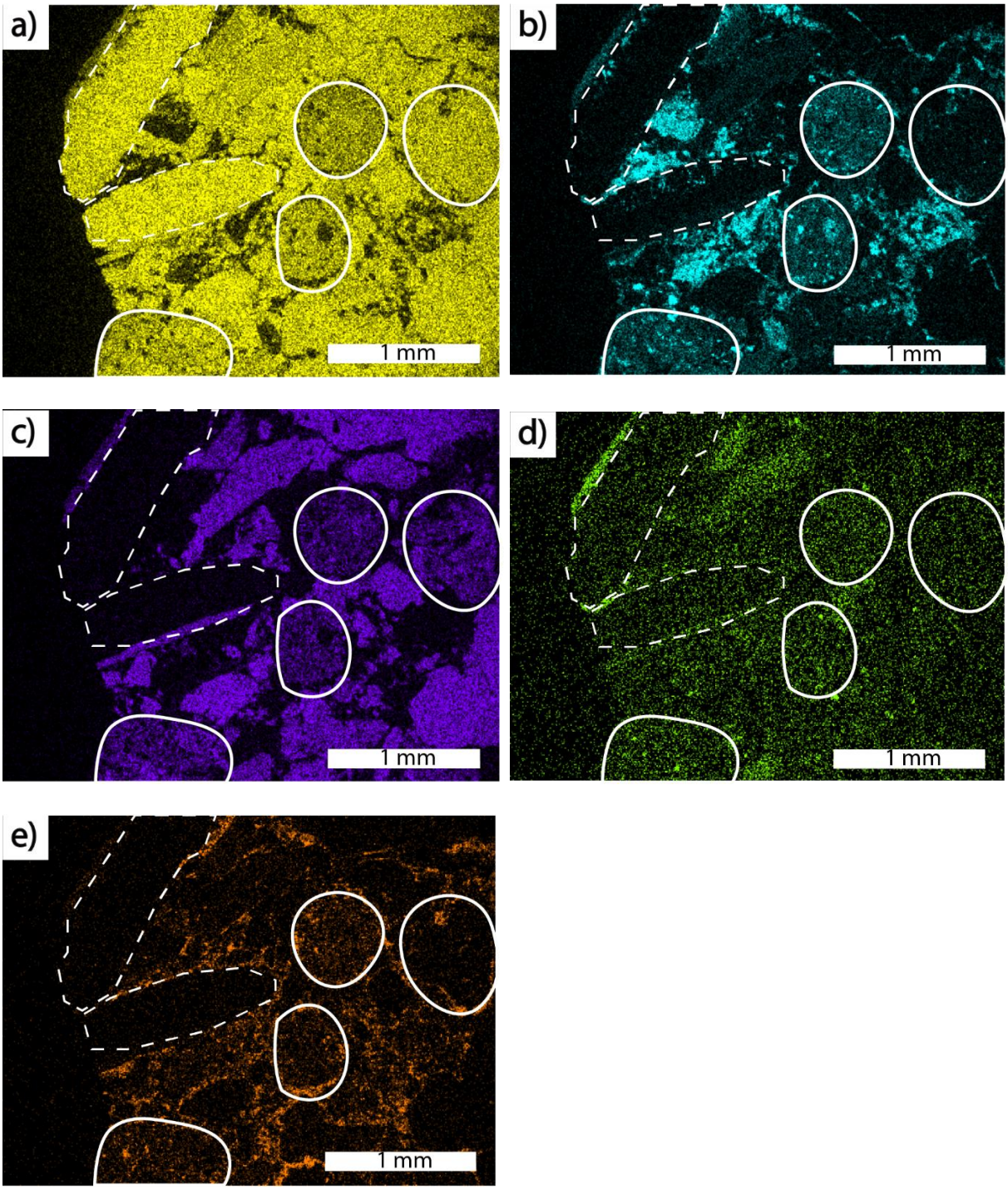

Figure 28: EDX maps of slide KE-2 with several type 1 pellets and large collophane masses. Eggshell outlined with a white dashed line. Pellets outlined in a solid white line. a) Calcium, b) Silicon, c) Phosphorous, d) Magnesium, e) Iron. All scale bars 1mm.

Pellet Type 2: The second type of pellet is smaller and found in clumps in thin section ES-583 (Fig. 29). The clumps form elongate masses found in the collophane crystals that are 2.35mm long and 0.82 mm wide. Each clump is comprised of a dozen or more randomly oriented pellets. The pellets comprising the clumps have an average diameter of 74 μm ± 12μm. The length of each pellet varies widely due to their random orientations in relation to the surface of the slide. However, most of the pellets are longer than they are wide with an average length of 240 μm ± 33μm based off the three pellets that were clearly oriented with their long axis parallel to the slide.

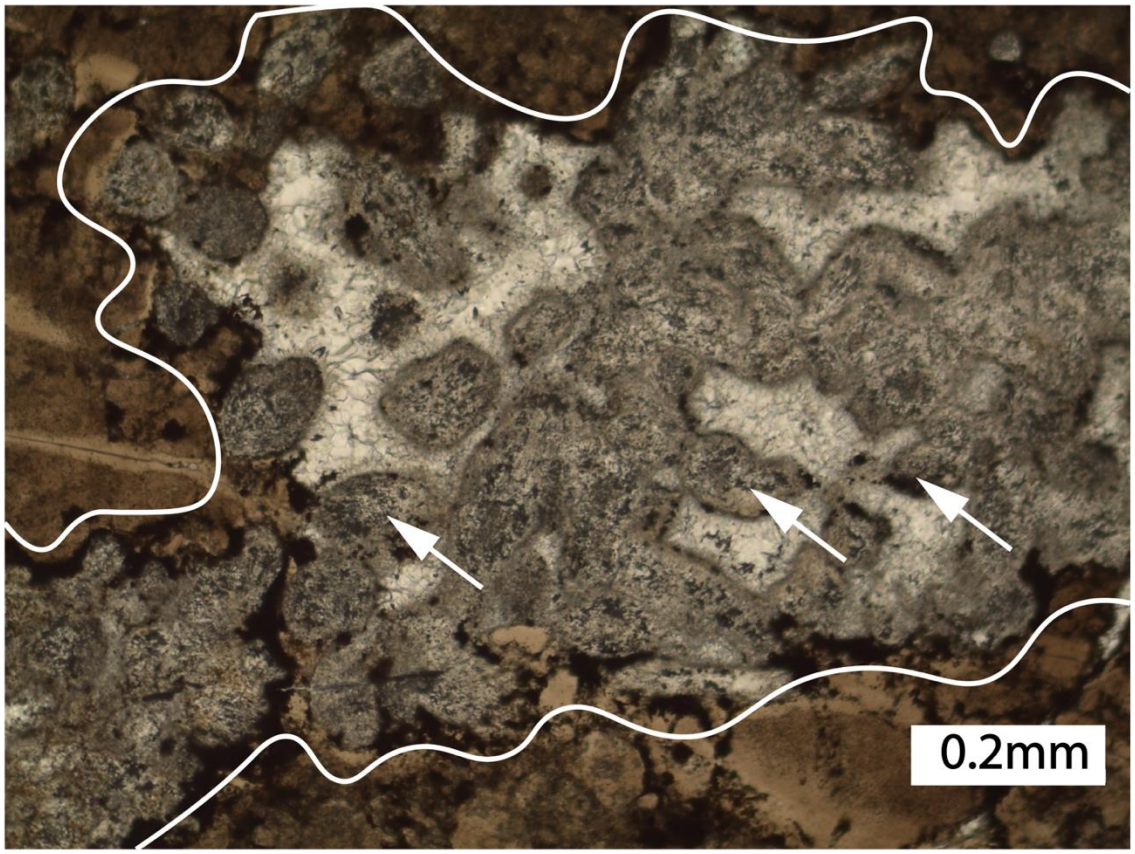

Figure 29: Type 2 pellet concentration from ES-583 under normal light surrounded by collophane and outlined in dark hematite crystals. The white line outlines the main cluster while the white arrows indicate coprolites with tapered ends. Scale bar 0.2mm.

The space between each individual pellet in the clumps is occupied by sparry calcite. The pellets themselves are elongate and are sometimes tapered at the end as seen in Fig. 29. Due to the cross-sectional nature of the slides, it is difficult to determine if the ends of the pellets are always tapered. These pellets are light grey with darker grey to black flecks under plain polarized light. Mineralogically they are comprised of calcite and undergo extinction radiating out from the center of each pellet. Under EDX these pellets are comprised of calcium, carbon, and oxygen with small amounts of silicon which trace the outlines of the individual pellets as seen in Fig. 30. Unlike the type 1 pellets, type 2 pellets lack phosphorous.

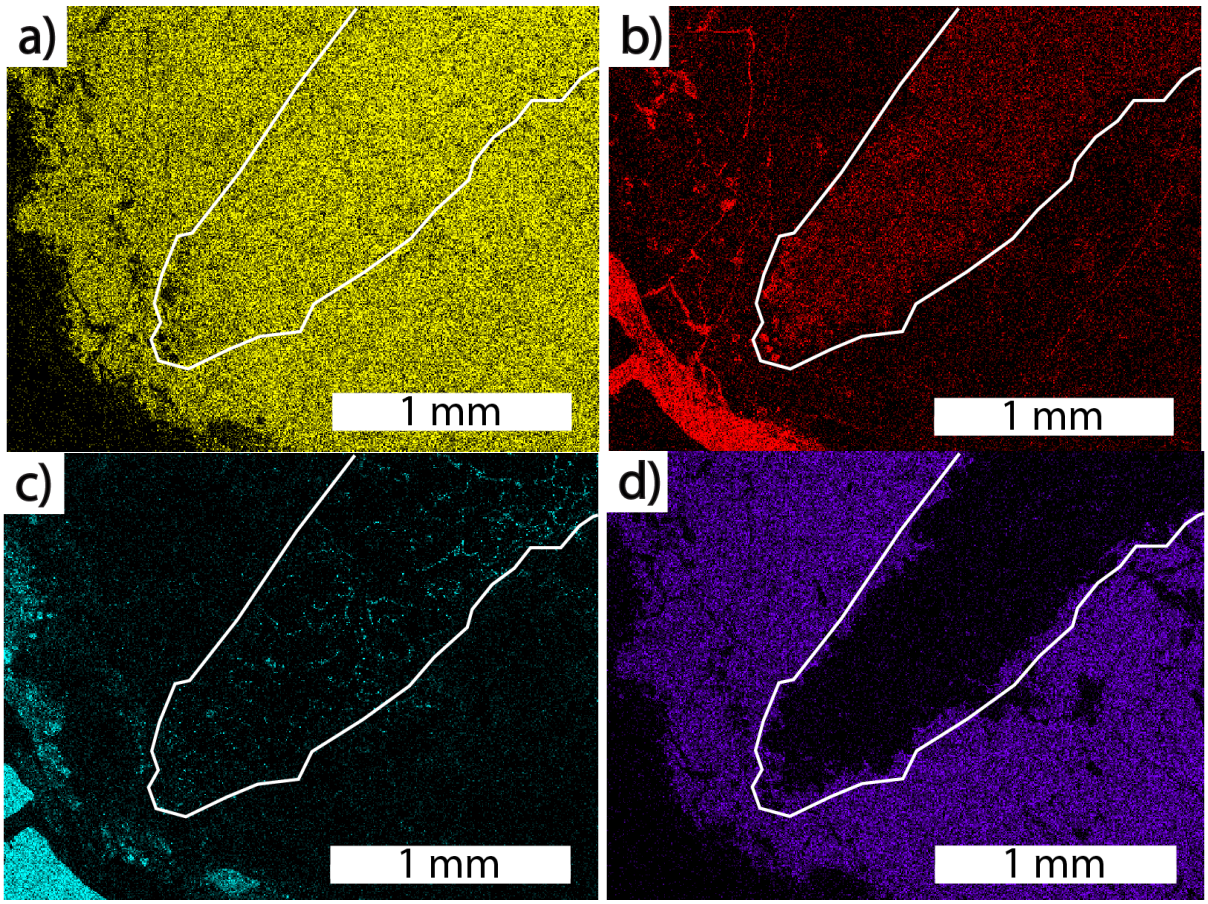

Figure 30: Type 2 pellets EDX maps of slide ES-583. Entire pellet cluster is outlined in white. a) calcite, b) carbon, c) silicon, d) phosphorous. All scale bars are 1mm.

Hyphae Like Structures: In slide ES-582 and the float slide, there are branching structures found throughout the egg contents (Fig. 31). These structures can be found permeating the collophane crystals, membrane layer and coprolites in these two slides. The regions that they affect vary in size depending on the density and spread of the branches. Approximately a quarter of Slide ES-582 is affected by the branches while KE-1 only has a few small patches. The branches themselves vary in width but have an average diameter of 8 µm ± 2 µm based off measurements taken using both light microscopy and SEM images. These structures have only been found in petrographic slides but were imaged using SEM and EDX on those slides.

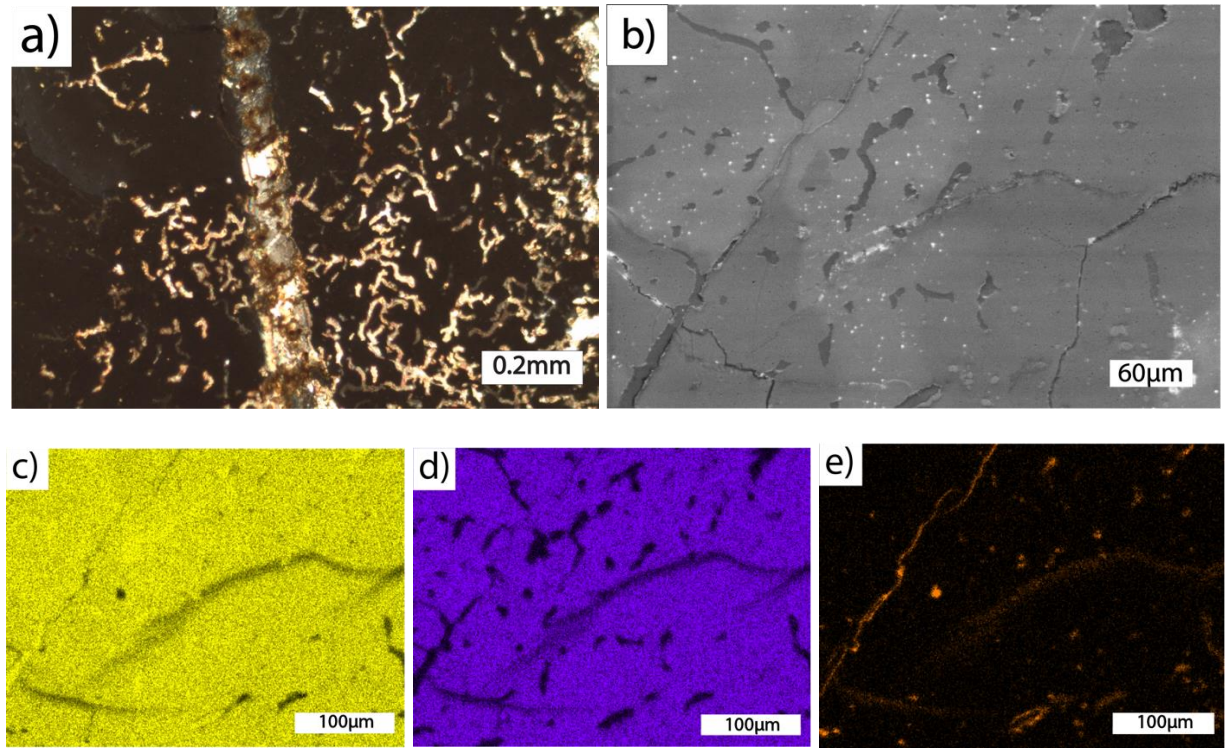

Figure 31: Branching structures found in collophane crystals from slide ES-582. a) Structure under cross-polarized light. scale bar is 0.2mm. b) Branching structure under SEM scale bar is 60µm. c) Calcium EDX map with a scale bar of 100µm. d) Phosphorous EDX map with a scale bar of 100 µm. e) Iron EDX map with a scale bar of 100 µm.

The SEM images indicate that the structures are hollow and often filled with crystals different from the surrounding collophane. EDX maps indicate that the crystals filling the tubes are calcite as seen in Fig. 31c where many of the branches seen in the phosphorus map (Fig. 31d) are not present in the calcite map. In the Calcium map the dark branches are the completely hollow areas of the branches. Combined the SEM and EDX maps indicate that these structures molds and casts of the original organic structure. In addition to being molds and casts, they also lack any clear diagnostic features beyond their branching structure and size.

Other Eggshell

The eggshells from the surrounding sediments inside of the jacket, retrieved through sieving come in three different types. Type-a sieve eggshell is the most common and matches the eggshell of the clutch. Type-a sieve eggshell is usually under 3mm long, light to dark brown in color, and lacks any surface ornamentation. Type-b and type-c sieve eggshell is black in color and differs structurally from the eggshell of the clutch. Type-b sieve eggshell can be distinguished from type-c by thickness and surface ornamentation.

Six of the fragments of eggshell from the sieved material were thin sectioned. The three brown eggshell pieces sectioned are all type-a eggshell. The three pieces of black eggshell included two pieces of type-b eggshell and one piece of type-c eggshell. Two of the type-a eggshell fragments also have attached eggshell membrane and one of them is coated in inorganic calcite. The type-b and type-c fragments did not show signs of major alteration to the original crystal structure when examined in petrographic thin sections.

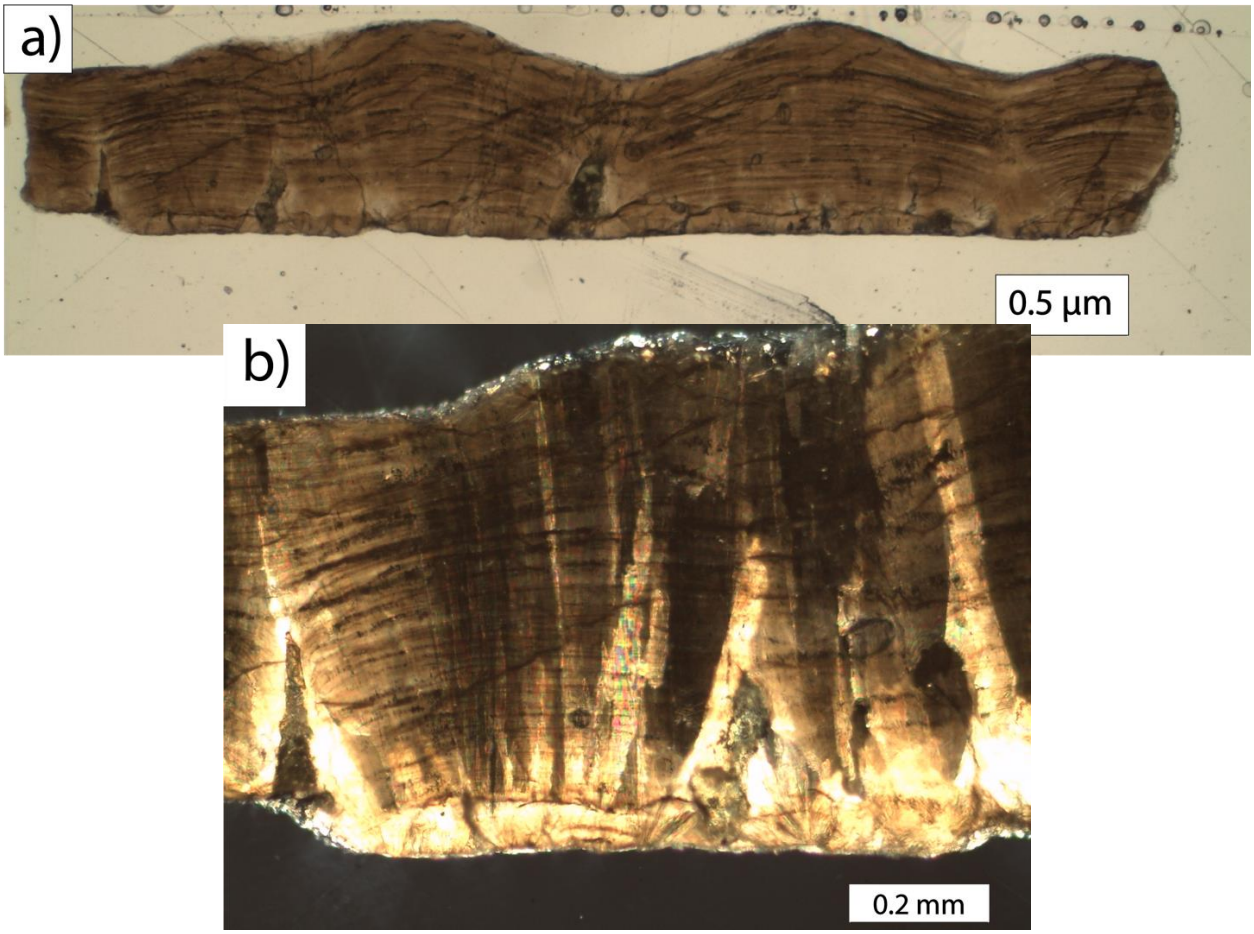

Figure 32: Type-b eggshell retrieved through sieving identified as *Spheroolithus* from sieve Slide KE-4. a) Full fragment sectioned under normal light. Pores indicated by black arrows. Scale bar 0.5mm b) Detail view of eggshell under cross polarized light. Scale bar is 0.2mm.

Type-b sieve eggshell fragments belong to the oofamily *Spheroolithus* based off of the ornamentation, thickness of the eggshell and the prolatospherulitic structure of the eggshell (Mikhailov, 1991, 1997). These eggshell fragments have Mikhailov's (1991) variant 1 sagentotuberculate ornamentation and are between 0.61mm and 0.82mm thick. This eggshell is comprised of a single layer of radiating spherulites with nucleation sites between 0.13mm and 0.28mm apart as seen in Fig. 32b. The shell units are not distinct from one another and undergo undulatory extinction under crossed polarized light. This eggshell also preserves dark growth

lines that follow the curve of the eggshell. The petrographic thin section of this eggshell has partial cross sections through three pores. These three pores are prolatocaniculate based off each cross sections of the pores having uneven thickness, and curving shapes (Mikhailov, 1997). Due to the shape of each pore they appear to truncate before reaching the surface of the shell because surface of the slide is not aligned parallel to the pores.

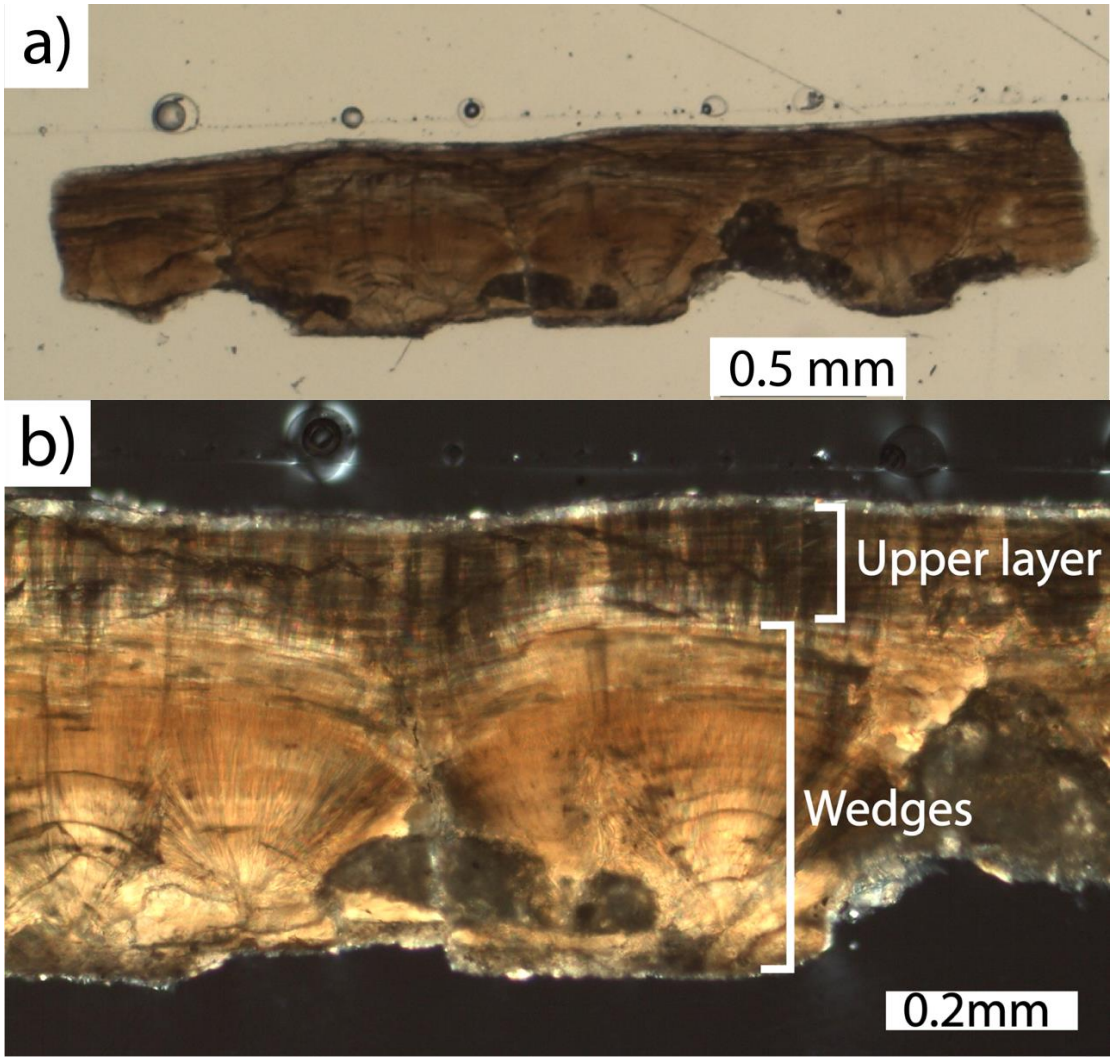

Figure 33: Type-c sieve eggshell from slide KE-4. a) Full fragment sectioned under normal light. Scale bar is 0.5mm. b) Detail view under cross polarized light. Scale bar is 0.2mm.

Type-c sieve eggshell does not have any ornamentation and is 0.46mm thick. It has two distinct shell layers; the lower layer is comprised of wedges of radiating crystals while the upper layer is comprised of more vertical crystals which contain horizontal accretion lines (Fig. 33). The wedges are around 0.2mm apart and are 0.18mm to 0.24mm high making them approximately half of the shell's thickness. These wedges are similar to those seen in crocodilian eggshell where instead of a mammillary layer the calcite crystals originate in loosely organized basal plate groups that form large wedges of radiating crystals (Mikhailov, 1991). However the wedges in crocodilian eggshell undergo blocky extinction, unlike the eggshell in MOR 11881 (Marzola et al., 2015). Between the wedges are interstices filled with either sparry calcite or sediment. No pores are seen in the petrographic thin section of this eggshell type.

The transition between the wedges and the upper portion of the shell is gradual. Under crossed polarized light the wedges undergo undulatory extinction under crossed polarized light while the top layer undergoes extinction in random order. All of the crystals of the top layer undergo extinction in quick succession, almost at the same time. The upper layer of the shell has many prominent growth lines that start at the top of the wedges and become more pronounced closer to the surface of the shell.

Type-c sieve eggshell is the most similar to crocodilian eggshell. Crocodilian eggshell is characterized by wedges of crystals and basal plate groups rather than a mammillary layer (Mikhailov, 1991). A secondary shell layer with prominent growth lines is seen in multiple types of crocodilian eggshell. However, these eggshell layers do not show different extinction patterns from the inner wedge layer (Marzola et al., 2015). Type 3 eggshell is both thinner and has closer spacing between wedges than the crocodilian eggshell found in the lower Two Medicine

Formation which was not described in thin sections (Jackson and Varricchio, 2010). The potential crocodilian eggshell from TM- 012 is more similar to type-c sieve eggshell in that it also has prominent growth lines and large wedges, however it is also almost twice as thick as the type-c eggshell (Hirsch and Quinn, 1990). This eggshell type does not match any eggshell currently described from the formation but is most likely crocodilian in origin.

Egg Mountain Eggshell

Some eggshell described in Oser (2014) from the egg mountain quarry was examined for comparison to the new clutch due to their similarities to the clutch from MOR 11881. The two egg clusters found in the egg mountain quarry are semi-three dimensional, have heavily altered eggshell and are filled with collophane (Oser, 2014). For better comparison EBSD and EDX mapping was conducted of slide ES-422 which was referenced in Oser (2014).

Slide ES-422 from the Egg Mountain quarry contains a single piece of eggshell from egg cluster one (Oser, 2014). The eggshell piece is covered on both sides with a thin brown mineral layer of collophane. In the eggshell from MOR 11881 the float slide also has a phosphatic layer covering the shell, however this layer is mostly clear in the thin section. The eggshell itself is comprised of two layers, a faint lobed layer, and a blocky layer (Fig. 34). The Egg Mountain eggshell lacks the phosphatic layer found in the eggshell of the MOR 11881 clutch. Like MOR 11881 the lobes themselves originate in the blocky layer and the lobed layer is characterized by thin needle like crystals radiating out from the lobes. In slide ES-422 the radiating crystals are often smaller than those from MOR 11881 and map in EBSD even less frequently. The lack of data on these crystals suggests that they are either comprised of completely amorphous calcite or have individual crystals too small to differentiate.

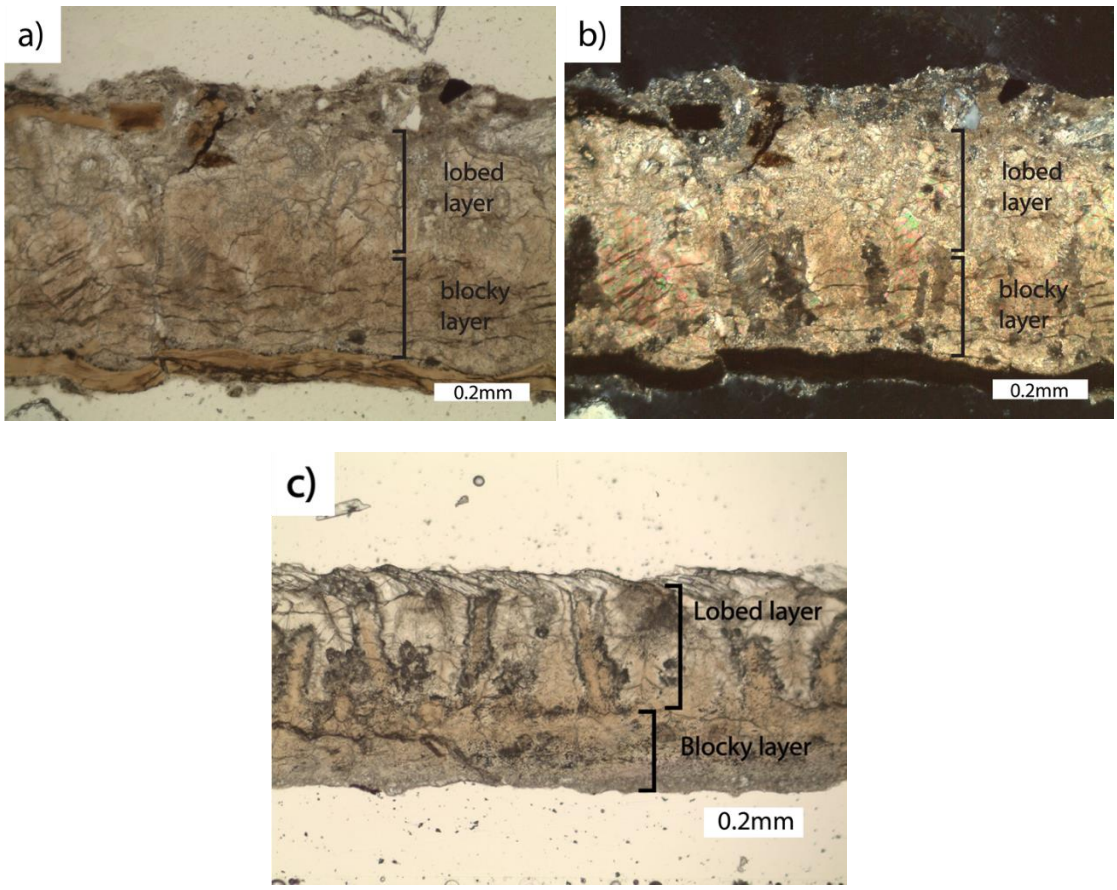

Figure 34: ES-422 Under plain a) and polarized light b). Scale bars 0.2mm. c) Slide KE-8 from egg five of MOR-11881 seen under plain polarized light. Scale bar is 0.2mm.

EBSD of ES-422 gives a hit rate of 35.62%, however a large amount of material that did not map was included in the area examined. The mineral layer coating the shell did not map along with epoxy that the shell was imbedded in which was included in the map due to the field of view and in order to map a larger portion of the eggshell. EDX mapping of the shell (Fig. 36) concurrent with the EBSD reveals that the areas that did not map are also high in magnesium and phosphorus similar to the eggshell of MOR 11881. These poorly mapping areas were primarily comprised of the radiating crystals surrounding the lobes. The crystals show no preferred orientation and there are few low angle grain boundaries between the individual grains. Phase mapping of the eggshell reveals that several of the crystals are partially replaced with dolomite.

With the eggshell mapping so poorly in EBSD it is likely that the Egg Mountain eggs represent a slightly more severe case of the same alteration seen in the MOR 11881 clutch.

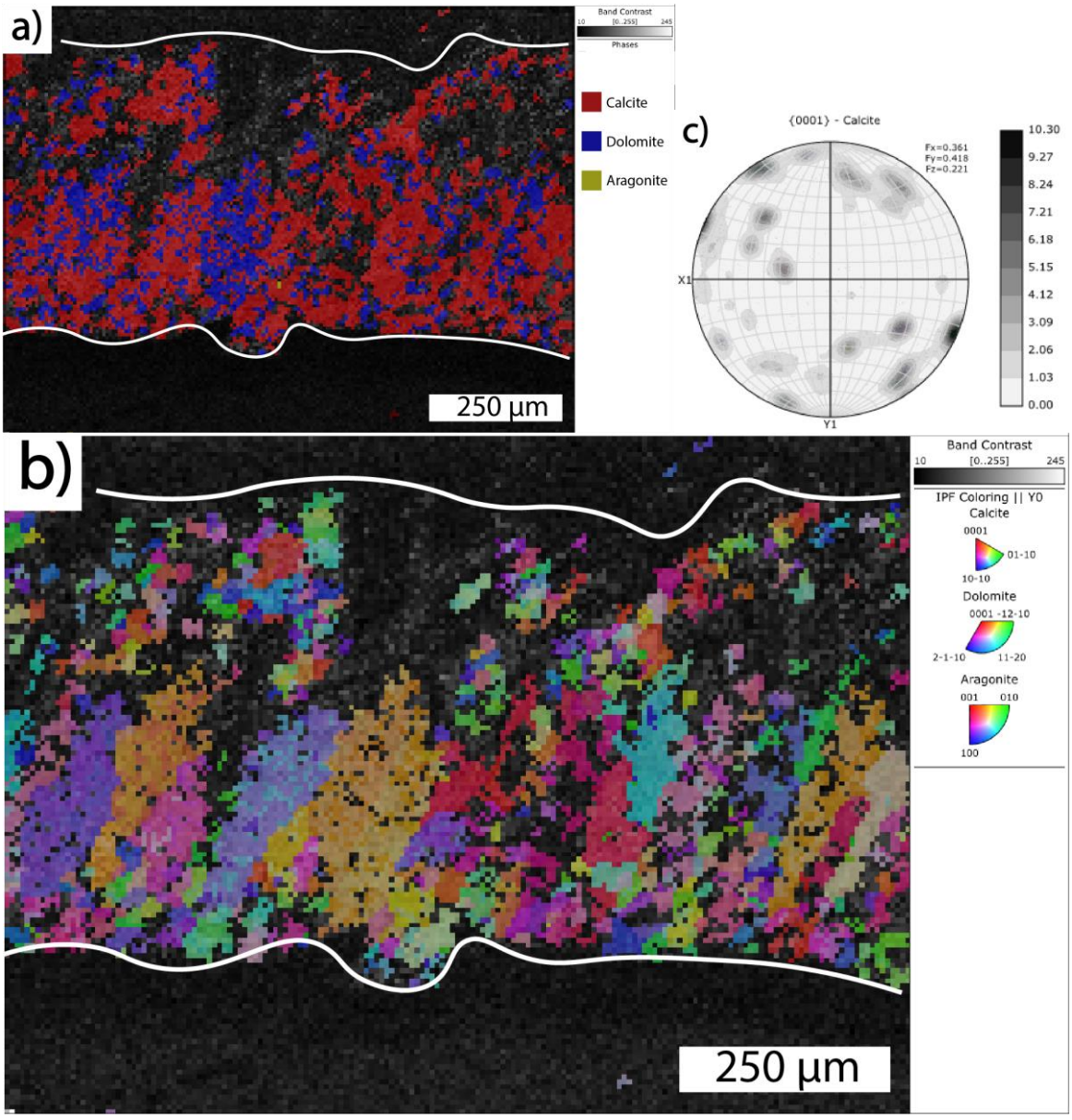

Figure 35: EBSD maps of ES-422. White line indicates the edges of the eggshell and the top of the eggshell is at the top of the image based off of the orientation of the lobes. Scale bars for a) and b) are 250µm. a) Phase map with band contrast image as background. b) IPF Y map with SEM image as background. c) Pole figure of the eggshell.

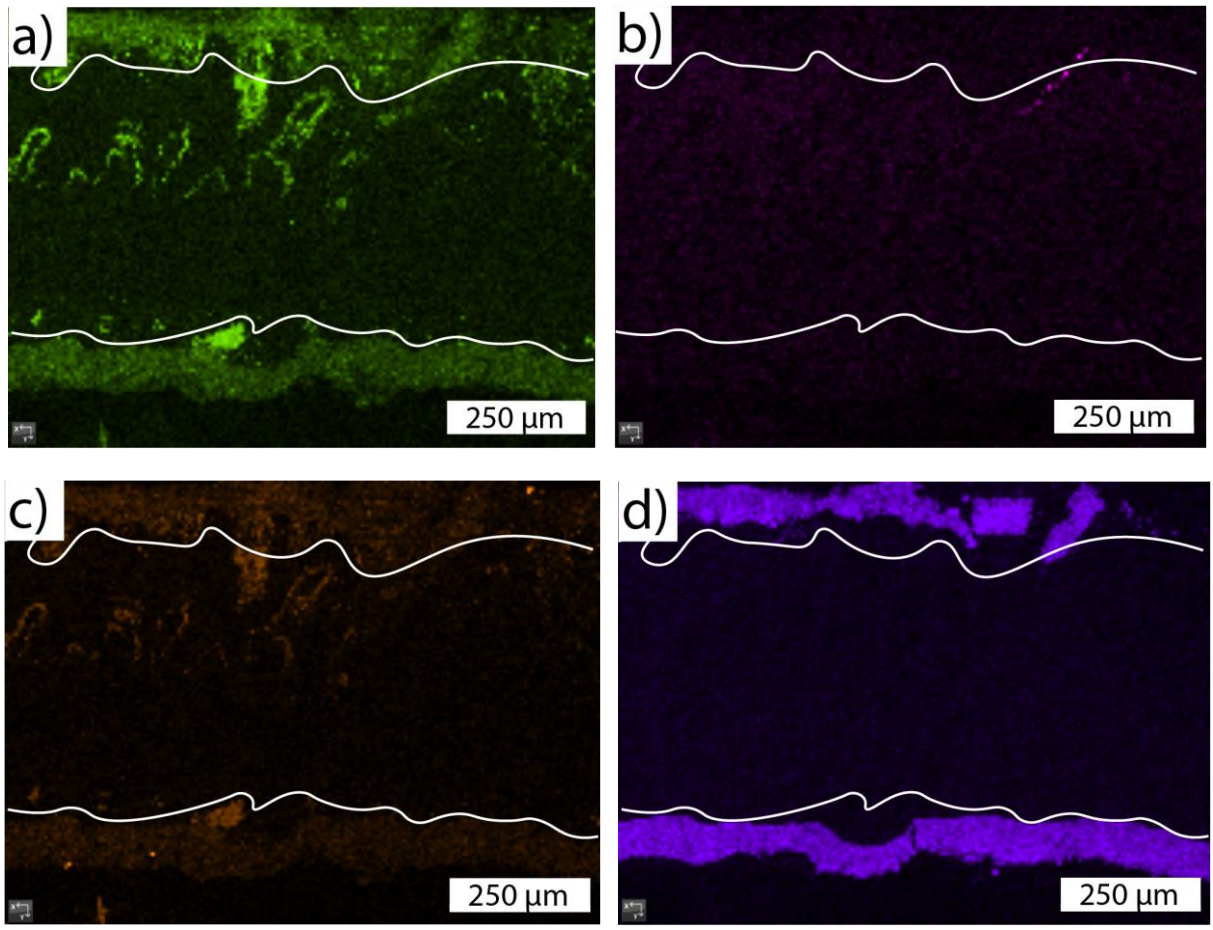

Figure 36: EDX maps of the ES-422 with the edges of the shell marked by the white lines. All scale bars are 250µm. a) Magnesium, b)Manganese, c) Iron, d) Phosphorous.

CHAPTER FOUR

DISCUSSION AND CONCLUSIONS

Egg Identification

It is impossible to rule out alteration as the cause of the unusual eggshell structure seen in MOR 11881 making it impossible to identify the eggs precisely or assign them to an ootaxon. However, some animals can be eliminated as the producers of these eggs. Poorly crystalline eggshells of both squamates and testudines can be ruled out as they lack large crystals or have individual crystals suspended in the proteinaceous portion of the shell (Kusuda et al., 2013; Legendre et al., 2022). Similarly both modern and fossil testudines with highly crystalline eggshell construct the eggshell out of aragonite that is organized into shell units (Kusuda et al., 2013; Choi et al., 2021). Additionally modern testudines eggshell membrane is known to be perforated with straight canals (Kusuda et al., 2013). MOR 11881 both possesses a layer of blocky calcite crystals and lacks canals through its membrane.

In highly crystalline squamate eggs the crystals grow inward toward the eggshell membrane (Choi et al., 2018; Legendre et al., 2022). Some of the eggshell found in MOR 11881 has regions of eggshell with inward growing crystal, however this could also be the result of alteration. Further the inward growing crystals in this eggshell are also accompanied by upward growing crystals, a feature not seen in squamate eggshell. The only pterosaur eggs found so far have been poorly mineralized with a very thin (30μm) crystalline layer (Li et al., 2022). Pterosaur eggs are also elongate in shape (Wang et al., 2017; Li et al., 2022). The shape and thickness of these eggs do not match the clutch from MOR 11881.

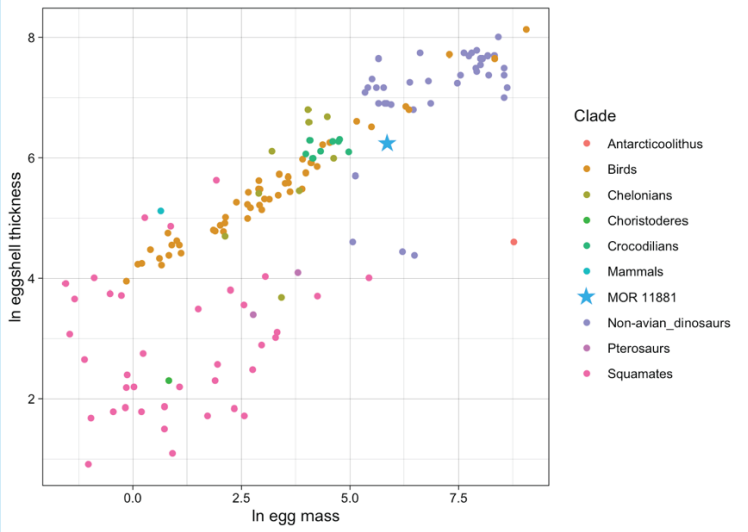

Figure 37: Eggshell thickness as measured by the thickness of the calcareous layer compared to egg mass immediately after laying. MOR 11881 is marked by the blue star, rest of the data set is from (Legendre et al., 2020).

MOR 11881's eggshell thickness when compared to its mass plots between crocodilians and non-avian dinosaurs (Fig. 37). While its eggshell is thin for its size it is not abnormally thin, and it still plots with other hard-shelled eggs. It does not plot with soft or pliable shelled eggs of squamates and pterosaurs. It's location between most of the non-avian dinosaurs and crocodilians indicates that these are the two most likely producers of the clutch in MOR 11881.

Crocodilian eggshell has been found at site TM-021 of the red rock locality of the Two Medicine Formation and in the lower Two Medicine Formation, however no whole eggs have been found (Hirsch and Quinn, 1990; Jackson and Varricchio, 2010). The membrane of the eggs of MOR 11881 are also similar to those of crocodilian eggshells, however the eggshell membranes of crocodilians and bird are very similar to each other (Mine, 2007; Lensink et al., 2023). Crocodilian eggs tend to be oval and can range greatly in size with the largest modern eggs having a length of 101mm in *Tomistoma schlegelii*, however the eggshell thickness of these eggs has not been measured (Marzola et al., 2015). The thickest modern crocodilian eggshell is

0.6mm and belongs to *Crocodylus* porosus (Marzola et al., 2015). The eggshell structure of the clutch of eggs from MOR 11881 however does not match the eggshell structure of crocodilian eggshell. These eggs lack the wedge structures and basal plates groups that are characteristic of crocodilian eggshell (Mikhailov, 1991).

Finally, these eggs could have been laid by a dinosaur. However, the eggshell of the clutch does not match that found in dinosaur eggs either. There are no structures consistent with mamillary knobs or eggshell units defined by them in these eggshells as are seen in most dinosaur eggshell (Mikhailov, 1991). The blocky and acicular crystals seen in the SEM images of broken pieces of eggshell are not consistent with the columnar or spongy layers seen in theropod or avian eggs(Mikhailov, 1991; Choi et al., 2023). Similarly the regions identified in the eggshell are also not consistent with the structural layers of most eggshell and instead show more similarities with highly altered eggshell.

If the current observed structure of the eggshell is the result of alteration, then the most likely producer of these eggs would be dinosaurs. Dinosaur eggshell is the most common type of eggshell found in the Two Medicine Formation. It should be noted however, that just because these are the most common eggs in the formation, it does not mean that eggs from MOR 118881 are dinosaur eggs. Egg identifications based off close associations, and common fossils in a formation have repeatedly been found to be incorrect such as in the case of the early misidentification of oviraptorid eggs as *Protoceratops* eggs (Norell et al., 1994).

Alteration of the Eggshell

Compared to most eggshell, eggshell of the clutch from MOR 11881 is highly unusual because it lacks many common structures found in eggshell. The structures that are found in

these eggs could be due to either an unusual starting structure or a high level of alteration. Most well mineralized eggshell from turtles, crocodilians, dinosaurs and birds exhibit pores, biologically mediated squamatic crystal texture, accretion lines, and crystals radiating from nucleation sites on the eggshell membrane (Mikhailov, 1991). While several unusual eggshell structures are known from dinosaur eggs, the eggshell of MOR 11881 does not match any of them. The eggshell associated with the clutch does, however contain several structures similar to those found in altered eggshell.

In the lobed layer of the eggshell from MOR 11881 there are Magnesium deposits that fluoresce brightly outlining the lobes. Similar magnesium deposits have been found in eggshell with false secondary shell layers (Grellet-Tinner et al., 2010). In addition to these possible dissolution fronts there are also circular formations of radiating crystals in MOR-11881 which resemble extra-spherulites as seen in Fig. 38. Extra-spherullites are associated with alteration in eggshell and growth of calcite crystals against the direction of eggshell deposition with high angle grain boundaries (Moreno-Azanza et al., 2016). Together these characteristics of the eggshell suggests that it has undergone at least some alteration. The presence of unaltered eggshell fragments in the jacket indicates that the source of alteration was not unit wide or the result of an external source to the eggs. Rather the source of the alteration seen in these eggs would be internal and driven by the decay process of the eggs themselves.

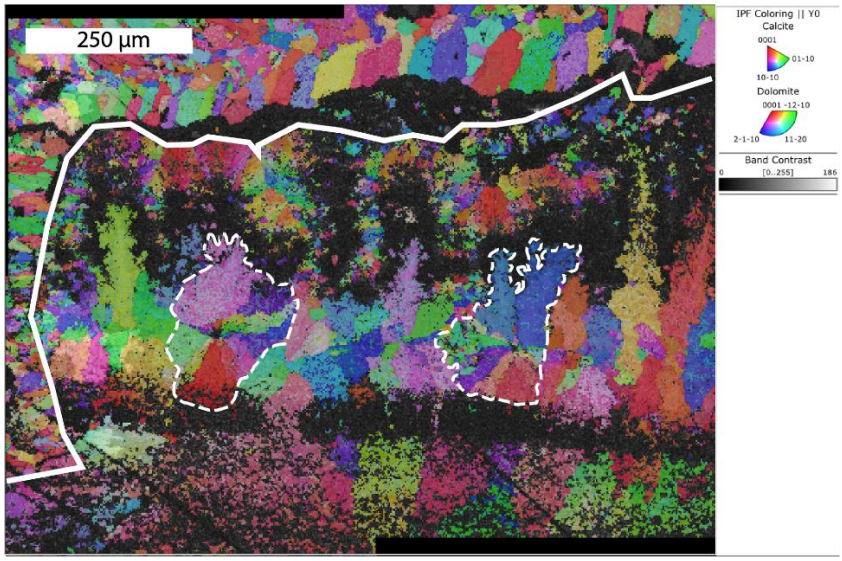

Figure 38: Extra-spherulites in the eggshell of MOR 11881 as seen in the EBSD IPF Y map of site 1 on slide KE-9. Extra-spherulites outlined in white dashed lines, solid white line indicates the surface of the eggshell.

Potential Stages of Alteration

The unusual structure of eggshell of the clutch from MOR 11881 could be explained by multiple types of alteration of the existing crystals and deposition of new crystals. These alteration events are based on the characteristics of the layers of the eggshell, and other structures found inside of the eggs. The characteristics that help differentiate the types of alteration are the chemical composition of the eggs, crystallography of the eggshell and overall structure of the eggshell layers. Between these characteristics five potential alteration stages can be determined and are listed below:

a) Partial dissolution of the eggshell and phosphate deposition

b) Secondary crystal deposition of radiating acicular crystals

c) Partial dissolution of the Secondary crystal deposition to create the surface textures

d) Tertiary calcite growth in the form of sparry calcite and isopachous fringes

e) Partial dolomitization of the calcite crystals already present

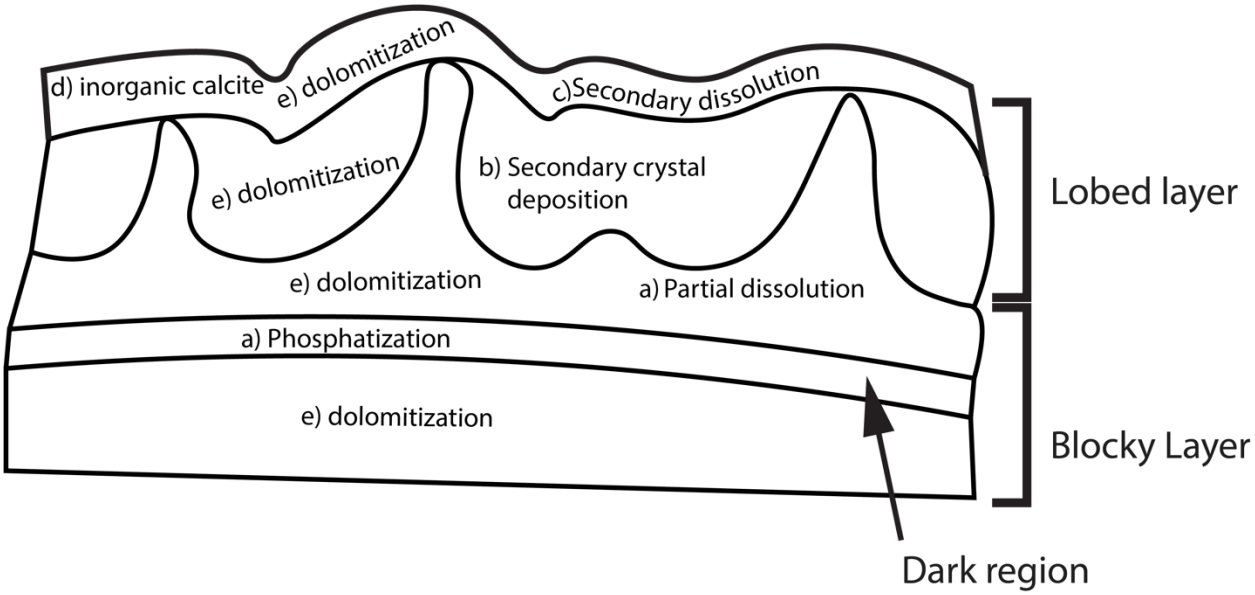

Figure 39: Schematic of the regions affected by the different alteration types. Alteration type is labeled in the region that it affects.

Stage-a Alteration: The partial dissolution of the eggshell portion of stage-a dissolved the eggshell leaving the lobes seen in the blocky layer behind and potentially reducing the thickness of the eggshell. Experimentally, eggshell that has undergone severe dissolution from exposure to slightly acidic solutions (pH 6.6) for twenty four days exhibits a rough pitted texture described as honeycombed on the outside of the eggshell (Clayburn et al., 2004). Such a texture would leave raised areas, which in cross section would appear as lobes such as those seen in the clutch. In a naturally occurring example of the same process the distinction between different layers of the shell and the shell units were lost fairly early in the process after a year with a pH of 6.4 and the entire shell gained a honeycombed texture after seven years (Hayward et al., 1991). This loss of all eggshell detail could explain the state of the bottom section of the blocky layer that does not map well in EBSD. The extreme thinness of the eggshell could also be the result of dissolution of the outer and inner layers of the eggshell along with the loss of most of the original structure. The blocky layer would thus represent what remains of the original crystal structure.

The acidic conditions that lead to eggshell dissolution can be found during the decay process as local pH around an organism decreases and has been observed to drop as low as 6.2 due to bacterial activity establishing steep concentration gradients (Sagemann et al., 1999). The decay of the eggs thus would have driven this alteration of the eggshell. The regions of sediment with similar compositions to those found inside of the eggs located beneath the eggs suggest that during the decay process the eggs broke, spilling their contents beneath them. Experimentally eggs have been seen to fracture when they rot to release gases (Bravo et al., 2003). This event caused their contents to leak into the soil beneath them, which could have helped with the dissolution of the outside of the eggshell. In addition to the decreasing pH and dissolving eggshell, bacteria and fungi also degrade eggshell. Fungal mats are known to cover eggs that decay on the surface and they invade pores (Bravo et al., 2003). Fragments of eggshell when exposed to soil bacteria lose weight and protein content (Smith and Hayward, 2010). In whole rotting turtle eggs bacteria and fungi also degrade the eggshell with fungal hyphae growing on their surfaces (Candan, 2018). If the eggs were rotting as some of the egg contents suggests, bacteria and fungi also probably contributed to the alteration and loss of eggshell thickness. These same bacteria would have also contributed to the phosphatization portion of stage-a through either bacterial mediation or the decrease in pH.

The many phosphatic structures in these eggs were produced by the phosphatization portion of stage-a. The phosphatic structures in the eggs are the dark layer of the eggshell, the eggshell membrane, larger coprolites, and collophane crystals inside of the eggs; all these structures share a similar composition of amorphous calcium phosphate also known as collophane and are rich in phosphorus in the EDX maps. The dissolution of the eggshell and

phosphatization of stage-a would have occurred concurrently and soon after the decay of the eggs began. This shared timing is based off the shared conditions required for phosphate deposition and calcite dissolution. Phosphatization usually occurs under slightly acidic conditions with pH ranging from 6.7 to 6. 2 which in otherwise neutral environments can be caused by the decay of the organism itself (Briggs et al., 1993; Briggs and Wilby, 1996; Sagemann et al., 1999; Skawina, 2010). Similarly the decay also provides a source of phosphorus for the phosphate deposition in environments that do not have high phosphate concentrations (Briggs et al., 1993; Sagemann et al., 1999; Skawina, 2010). In this way the bacteria and fungi invading the eggs would have caused both the dissolution of the eggshell and the deposition of phosphate.

Phosphatization is known for preserving soft tissues at different scales with small scale fine details being preserved like muscle fibers and at large scales the preservation of entire organs (McNamara et al., 2009; Qvarnström et al., 2016). In eggs, phosphates have been found in the eggshell several times and occasionally preserve the eggshell membrane. Phosphate is found in the exterior layer of the soft-shelled egg from Antarctica which is a soft tissue structure (Legendre et al., 2020). However, the phosphorus in the Antarctic egg could be part of the original structure. Some poorly mineralized eggshells of turtles are high in phosphorus (Kusuda et al., 2013). There is also a phosphatized eggshell membrane in a Miocene bird egg from the Czech Republic (Kohring, 1999). This indicates that the membrane can be phosphatized while still retaining recognizable eggshell unlike that seen in MOR 11881. In the Holocene, phosphatization of the eggshell itself has been seen in proto-fossil Adéle penguin eggshells found in sediments enriched in phosphate due to penguin droppings (Cavallerano, 2005). In this

example the phosphatization started along the edges of the eggshell in younger specimens and eventually permeated the entire eggshell in older specimens (Cavallerano, 2005). This pattern of phosphatization in the penguin eggs is different from the one found in MOR 11881 as the phosphatic layer is in the middle of the shell layer in the MOR 11881 eggs. However, some modern avian eggshells do exhibit a porous or granular layer in the middle of the eggshell (Choi et al., 2023). The existence of a porous layer in the original eggshell could have facilitated the deposition of phosphate in the middle of the shell to create the dark region seen in MOR 11881.

Beyond eggs, similar fine detail preservation of soft tissues in phosphate can be found in other enclosed environments. Articulated specimens of Jurassic bivalves from Dorset commonly preserve gill filaments, muscle tissue, and mantle (Wilby and Whyte, 1995). In experiments similar phosphatized soft tissues have been produced with the source of the phosphate being the organisms own tissues (Briggs et al., 1993; Skawina, 2010). Phosphate preservation of soft tissues are also often associated with coprolites and a wide range of phosphatized structures have been found in them including muscle tissues and microorganisms (Qvarnström et al., 2016). Similarly in the egg contents of MOR 11881 there are fragments of eggshell membrane in a small number of the coprolites. With both the coprolites and the membrane preserved in phosphate, it is possible that the larger phosphate crystals preserved in the egg also represent an originally organic structure such as albumin or yolk. Yolk is known to mummify under acidic conditions in addition to xeric conditions (Bravo et al., 2003). However, the yolk has few identifiable structures that could be used to differentiate it after it has been replaced.

Finally, stage-a is the most likely time for the production of the hematite crystals seen inside of the eggs. These crystals form rinds around the phosphatic type 1 pellets and collophane crystals.

Their presence primarily along the outside of stage-a structures does indicate that they were forming somewhat later in stage-a. They can also be found inside some of the type 1 pellets. They are not found in the middle of later forming structures such as the radiating crystals or sparry calcite, suggesting that they did not form later.

Stage-b Alteration: The growth of the radiating crystals that form the lobes in stage-b resulted in calcite deposition along the outside of the eggshell. The crystals deposited during this stage are small acicular crystals radiating from the lobes and forming the new exterior of the shell. The calcite of these crystals chemically resembles the calcite of the blocky layer more than the inorganic calcite surrounding the eggshell. These crystals are higher in manganese and magnesium than the inorganic calcite. Some of the lobes have magnesium deposits along their outside borders that the radiating crystals would have grown over. Secondary crystal growth of calcite that resembles the eggshell is relatively common and false shell layers have been observed separated from the original eggshell by magnesium deposits (Grellet-Tinner et al., 2010). The stage b crystal growth occurred after stage a as pH increased again allowing for the deposition of calcite. Experiments have shown that during the decay process the pH does not stay depressed and it eventually increases again and calcite is deposited (Briggs and Wilby, 1996).

Stage-c Alteration: After their deposition these radiating crystals then underwent dissolution in stage-c resulting in the unusual surface texture. This texture is comprised of rosettes of radiating crystals surrounding blocky crystals. The blocky crystals that comprise the center of the lobes are identical to the ones found in the center of the rosettes along with the radiating crystals around them. In all the thin sections at least some of the lobes are truncated by

the surface of the eggshell as seen in Fig. 40. Thus, the surface texture of the eggs is the result of the truncation of the lobed layer.

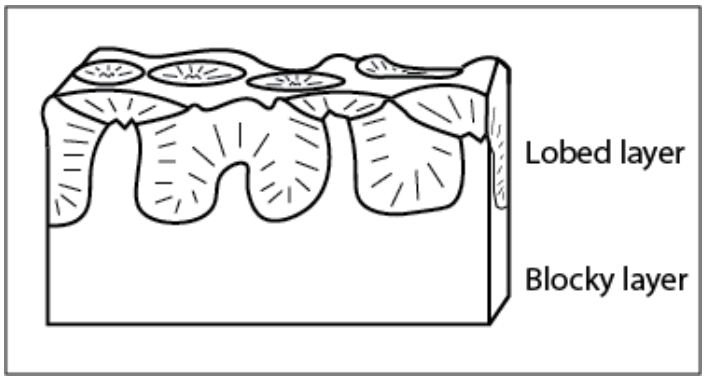

Figure 40: Schematic of surface texture with the blocky and lobed layers labeled.

Stage-d Alteration: The inorganic calcite coating the surface of the eggshell and filling the voids inside of the eggs is the product of stage-d calcite deposition. These crystals, where present, cover the surface of the eggshell and the truncated lobes indicating that they formed after stage-c. Additionally, the crystals of stage-d deposition are chemically distinct from those formed during stage-c deposition and have a different crystal texture. Crystals formed by stage-d deposition are either equant sparry calcite or isopachous fringes along the eggshell compared to the acicular crystals that were the result of stage-c.

Stage-d deposition resulted in calcite crystals that have lower levels of magnesium and manganese compared to the calcite the eggshell is comprised of. This phase of deposition is also responsible for filling the branching structures found in the collophane crystals and the preservation of the smaller pellets in calcite. The difference in composition of the two pellet types could be due to them being produced at different times or due to their producers having different diets. The calcite deposited during this stage coats the outside of the eggshell in equant to elongate crystals in isopachous fringes or fills the insides of the eggs with sparry calcite with

equant crystals. Based off the elongate crystals of isopachous fringes, these calcite crystals were formed under shallow meteoric conditions (James and Jones, 2016). The multiple different directions and layers of crystals above the isopachous fringes suggests several periods of deposition under different conditions and flow regimes.

Stage-e Alteration: Stage-e alteration is the partial dolomitization of the eggshell and inorganic calcite coating it. The partially dolomitized crystals are indistinguishable from the rest of the calcite crystals. This characteristic is visible in both the eggshell and the stage-d derived calcite under normal and cross polarized light microscopy. The retention of the original calcite or aragonite crystal fabrics despite their replacement with dolomite is known as fabric retentive dolomitization and usually occurs under more shallow burial settings (Cai et al., 2021). The site was buried under approximately 1400m based off of the thicknesses of the younger units in the cordilleran foreland basin system that overly it (Fuentes et al., 2011). The overlying unit above the Two Medicine Formation near Choteau are claystones and shales containing brackish water faunas that transition into the Horsethief sandstone (Lorenz and Gavin, 1984). Both conditions are known to contribute to dolomitization with shallow burial around 1000m is associated with fabric retentive dolomite formation along with manganese rich pore water circulation (Ehrenberg et al., 2006; Jiang et al., 2016).

Comparison to Egg Mountain Eggshell

The eggs from Egg Mountain underwent alteration events similar to stages-a dissolution and phosphatization, stage- b secondary calcite deposition, stage-c secondary calcite deposition, and stage-e dolomitization from the MOR 11881 clutch. Stage-a dissolution along with stage-b and stage-c resulted in the same pattern of lobes and radiating crystals while the phosphatization

of stage-a only resulted in the deposition of collophane inside the eggs and coating of the eggshell rather than a separate phosphatic layer in the eggshell. The presence of dolomite in egg mountain eggshell along with MOR 118881 eggshell and inorganic calcite suggests that the partial dolomitization may be widespread within the formation, however more samples should be examined to confirm this. This slight partial dolomitization has not been reported in the formation before.

Pellet Identification

Type 1 pellets found inside and around the eggs are similar to the *Edaphichnium* isp. found at egg mountain. The Egg Mountain coprolites are 1.5mm to 1.8mm in diameter, show no preferred grain orientation inside of them and contain around twice the phosphate compared to the surrounding sediments (Freimuth and Varricchio, 2019; Freimuth et al., 2021). The type 1 pellets found in and around the eggs of MOR 11881 are similar to the ones found at the Egg Mountain Quarry but do have a few differences. The type 1 pellets are a third the size of those found at egg mountain at an average diameter of 0.6mm. Their average length to width ratio is 1.84 while the length to width ratio of the coprolites found at egg mountain is 1.57 (Freimuth et al., 2021). It should be noted that the sample size for the MOR 11881 coprolites is only six and that only one of the measured coprolites is from the inside of an egg. The *Edaphichnium* found at the Egg Mountain quarry were enriched in both carbon and phosphorus compared to their host rock (Freimuth et al., 2021). The larger coprolites from MOR 11881 are also more phosphatic than their sparry calcite surroundings.

The coprolites from the egg mountain quarry were found in multiple different arrangements with some arranged linearly, constrained horizontally to single horizons and found

in dispersed clusters (Oser, 2014; Freimuth et al., 2021). Type 1 pellets from MOR 11881 are arranged most similarly to the dispersed clusters, however the rarity of coprolites oriented with their long axis parallel to the cut of the slides could indicate that inside of the eggs they are arranged linearly, however no lines of coprolites are observable in any of the slides or fragments of egg contents. While not identical to the previously found *Edaphichnium* isp. found at the egg mountain quarry these coprolites could represent another variety of *Edaphichnium*.

The type 2 pellets found in the eggs are unlike any other pellets previously reported from the Two Medicine Formation. Most microscopic pellets also sometimes called microcoprolites described are found in marine, or freshwater environments and are difficult to compare to the smaller coprolites found in MOR 11881. The extreme difference in size and morphology between these pellets and the larger type 1 pellets found in the egg however do indicate that at least two different organisms were living inside of these eggs after they died.

Identification of the Hyphae Like Structures

The branching structures found inside of the eggs represent molds and casts of either fungal hyphae or bacterial structures based off their size and branching structure. There is a single example of fungal structures being found in eggs before. Fungal hyphae were found in a turtle egg from the lower cretaceous of China which contained hyphae 1.5-3μm wide that showed signs of replacement with hematite and calcite (Jackson et al., 2009). The structures found in MOR 11881 are considerably larger than these hyphae at an average of 8μm based on all measurements. However, since the structures observed in this study are molds it is possible that the thickness recorded in the collophane crystals is an exaggeration of the true thickness of the hyphae themselves.

In fossil wood with traces of both rootlets and fungal hyphae, the hyphae were an order of magnitude smaller than the rootlets but showed considerable variation in thickness between different structural groups ranging between 1μm and 10.8μm in diameter (Vera and Perez Loinaze, 2022). Beyond fungal hyphae, multiple other organisms can also leave branching filamentous trace fossils. Rootlets can also leave branching traces however, they are around 400μm in diameter and are therefore considerably larger than hyphae (Vera and Perez Loinaze, 2022). The difference in size between rootlets and the traces from MOR 11881 make it unlikely that they are the product of rootlets.

Closer in size to the egg traces are branching filaments found in amber which are 4μm to 10μm in diameter that were made by sheathed bacteria similar to the modern taxa *Leptothrix* (Saint Martin and Saint Martin, 2018). These traces differ from the egg traces in that they are comprised of two layers with a hollow space in the middle termed a lumen (Saint Martin and Saint Martin, 2018). This lack of internal structure in the MOR 11881 is not surprising due to their nature as molds and casts which do not preserve internal structure. The lack of any internal structure and fruiting bodies makes it impossible to determine the exact identity of these structures. Regardless, these structures represent another decay process that was occurring in the eggs.

Conclusion

The clutch of eggs found in MOR 11881 has highly altered eggshell making them impossible to identify to any meaningful taxonomic level. However, they provide a rare glimpse into the decay of eggs during the Cretaceous, preserving several unusual structures within them.

Seemingly paradoxically both exceptional preservation and highly replaced mineral components exist in these eggs due to their taphonomic history.

The exceptional preservation within these eggs is found in the hyphae like structures and eggshell membrane. There is only one other report of fossil hyphae from an egg, despite the commonness of fungal attack on eggs and the role of fungi in the decay process (Jackson et al., 2009). While the hyphae like structures in MOR 11881 are not preserved as well as those described in Jackson et al. (2009), they still represent an unusual find in the fossil record of a microscopic organism associated with decay.

In addition to the hyphae like structures, the eggshell membrane is also exceptionally preserved in these eggs. The structure of the membrane is discernible with individual collagen fibers being replaced with calcium phosphate. The orientations of these fibers are visible in both broken sections under SEM and backscatter images of the membrane. The only other preserved membrane from the Two Medicine Formation is a few fibers and fiber impressions on the mammillary cones of *Troodon* eggs (Varricchio et al., 1999). The detail of MOR 11881's membrane allows it to be compared to modern eggshell membrane. The fossil membrane is similar to both crocodilian and avian eggshell membranes. The decay of these eggs facilitated both the exceptional preservation of the eggs and the destruction of the original crystal structure of the eggshell.

The discernable taphonomic history of MOR 11881 begins with either the failure of the nest or its burial. Due to the lack of sedimentary structures and pores in the eggshell, it is impossible to tell if these eggs were originally in a buried nest such as those seen in modern crocodilians and turtles, or an open nest as seen in modern birds. It is also impossible to tell

exactly what caused the death of the eggs. Drowning, fungal attack, weather events, and initial non-viability are all possible reasons why the nest failed to hatch. Prolonged submersion in water can drown eggs, although shorter periods are survivable (Gjerdrum et al., 2008). Similarly, any short weather event or genetic problems with the eggs would be unlikely to leave any evidence. Fungi that attack nests often first infect non-viable eggs before spreading to the rest of the nest (Phillott and Parmenter, 2001). Thus, the presence of the hyphae like structures in MOR 11881 could be associated with either the death of the eggs or their decay. However, the relative timing of these structures' places them as a later event in the taphonomic history of the clutch. It is impossible to know what exactly happened to the eggs that resulted in them not hatching but there is evidence of the next steps in their taphonomic history.

While not all the processes that contributed to the decay of MOR 11881 are easy to place temporally, on a geologic time scale they happened rapidly. Many of the steps in their taphonomic history had to have happened soon after the eggs' deaths and some of them would have occurred at the same time. The soil beneath the eggs has been altered to also contain hematite, coprolites, and fragments of collophane. This alteration of the soil is the result of the breakage of the eggs, resulting in them spilling their contents into the soil beneath them. The egg contents may have already started to decay at this point. The breakage of the eggs allowed the invertebrates that produced the coprolites to enter the inside of the eggs.

The type 1 pellets sometimes contain recognizable fragments of eggshell membrane which suggests that the membrane was not fully mineralized at this point. The deposition of phosphate would have been simultaneous with the dissolution of the shell since they were the

result of the same decay process. Thus, the coprolites were deposited before the dissolution of the eggshell and the preservation of the membrane.

The deposition of the stage-b radiating acicular calcite would have occurred as the rate of decay decreased due to most of the organic matter being consumed or mineralized. The presence of these crystal on only the outside of the shell may indicate that the inside of the eggs was still too acidic for calcite deposition. This event would have occurred after or at the end of the dissolution of the eggshell and mineralization of the membrane.

The hematite was being deposited throughout the decay process, with some of the coprolites containing hematite inside of them and others only having hematite rinds. The hematite inside of the coprolites could have either been from consumption of sediments already containing the crystals or the infiltration of the coprolites by the bacteria that produced the crystals. The hematite crystals can also be found around and in cracks through collophane masses indicating that they were probably formed after the collophane masses. These collophane masses would have been formed around the same time that the membrane was mineralized. Thus, the hematite was deposited after the deposition of the coprolites, dissolution of the eggshell and mineralization of the membrane.

After decay ceased the last two steps in the taphonomic history of MOR 11881 occurred. First further calcite was deposited to fill the open space inside of the eggs and coat the eggshell. The shape of these crystals of calcite suggests that they formed under shallow burial conditions. Second, deep burial of the nest caused some of the calcite crystals in both the coating calcite and what remains of the eggshell to start to be replaced with dolomite.

This complicated taphonomic history is not an isolated occurrence in the Two Medicine formation. Two clusters of eggs found at the Egg Mountain Quarry also show similar alteration and it is possible that there are other examples that have been overlooked due to the poor preservation of the eggshell. Such eggs may give further insights into ecological interactions in the form of the invertebrates that eat eggs. They may also give insight into soft tissue structures that are uncommon in eggs showing more common preservation types. Studying eggs such as those found in MOR 11881 is complicated by the lack of acutalistic studies on decaying eggs to compare them with. Specifically, there is need to examine the eggshell structure of decayed eggs to better quantify and constrain the environmental factors that lead to such preservation and alteration.

REFERENCES CITED

Bravo, A.M., Buscalioni, Á.D., Merino, L., and Muller, G.B., 2003, Experiemntal taphonomy of avian eggs and eggshells: effects on early diagenesis: Palaeovertebrata, v. 32, p. 77–95.

Briggs, D.E.G., Kear, A.J., Martill, D.M., and Wilby, P.R., 1993, Phosphatization of soft tissue in experiments and fossils: Journal of the Geological Society, v. 150, p. 1035–1038.

Briggs, D.E.G., and Wilby, P.R., 1996, The role of the calcium carbonate-calcium phosphate switch in the mineralization of soft-bodied fossils: Journal of the Geological Society, v. 153, p. 665–668, doi:10.1144/gsjgs.153.5.0665.

Cai, W.K., Liu, J.H., Zhou, C.H., Keeling, J., and Glasmacher, U.A., 2021, Structure, genesis and resources efficiency of dolomite: New insights and remaining enigmas: Chemical Geology, v. 573, p. 120191, doi:10.1016/j.chemgeo.2021.120191.

Candan, E.D., 2018, Molecular identification of fungal isolates and hatching success of green turtle (Chelonia mydas) nests: Archives of Microbiology, v. 200, p. 911–919, doi:10.1007/s00203-018-1496-0.

Carpenter, K., 1999, Eggs, Nests, and Baby Dinosaurs: a look at dinosaur reproduction (J. O. Farlow, Ed.): Bloomington, Indiana University Press, 336 p.

Cavallerano, E.J., 2005, Temporal diagenetic alterations in adélie penguin eggshells throughout the late Holocene of Antarctica [M.S. thesis]: University of North Carolina Wilmington, 39 p.

Cazenave, S., Chapoulie, R., and Villeneuve, G., 2003, Cathodoluminescence of synthetic and natural calcite: The effects of manganese and iron on orange emission: Mineralogy and Petrology, v. 78, p. 243–253, doi:10.1007/s00710-002-0227-y.

Chin, K., 2007, The paleobiological implications of herbivorous dinosaur coprolites from the Upper Cretaeous Two Medicine Foramtion of Montana: why eat wood? Palaios, v. 22, p. 554–556, doi:10.2110/palo.2006.p06-087r.

Choi, S., Han, S., Kim, N.H., and Lee, Y.N., 2018, A comparative study of eggshells of gekkota with morphological, chemical compositional and crystallographic approaches and its evolutionary implications: v. 13, 1–31 p., doi:10.1371/journal.pone.0199496.

Choi, S., Hauber, M.E., Legendre, L.J., Kim, N.H., Lee, Y.N., and Varricchio, D.J., 2023, Microstructural and crystallographic evolution of palaeognath (Aves) eggshells: eLife, v. 12, doi:10.7554/eLife.81092.

Choi, S., Kim, N.-H., Kim, H.-I., Kweon, J.J., Lee, S.K., Zhang, S., and Varricchio, D.J., 2021, Preservation of aragonite in Late Cretaceous (Campanian) turtle eggshell: Palaeogeography, Palaeoclimatology, Palaeoecology, v. 585, p. 110741, doi:10.1016/j.palaeo.2021.110741.

Clayburn, J.K., Smith, D.L., and Hayward, J.L., 2004, Taphonomic effects of pH and temperature on extant avian dinosaur eggshell: Palaios, v. 19, p. 170–177, doi:10.1669/0883-1351(2004)019<0170:TEOPAT>2.0.CO;2.

Dalman, S.G., Lucas, S.G., and Malinzak, D.E., 2018, Tyrannosaurid teeth from the Upper Cretaceous (Campanian) Two Medicine Formation of Montana: Bulletin- New Mexico Museum of Natural History and Science, v. 79, p. 125–139.

DeMar, D.G., Conrad, J.L., Dead, J.J., Wilson, G.P., Varricchio, D.J., and Anonymous, 2014, Two nearly complete lizard skeletons from the Upper Cretaceous (Campanian) Two Medicine Formation, Montana, USA, offer novel insights into the morphology and evolution of Squamata: Abstracts with programs- Geological Society of America, v. 46, p. 99.

Douglas, R.M., 1990, Volume determination of reptilian and avian eggs with practical applications: South African Journal of Wildlife Research, v. 20, p. 111–117.

Ehrenberg, S.N., Eberli, G.P., Keramati, M., and Moallemi, S.A., 2006, Porosity-permeability relationships in interlayered limestone-dolostone reservoirs: American Association of Petroleum Geologists Bulletin, v. 90, p. 91–114, doi:10.1306/08100505087.

Falcon-Lang, H.J., 2003, Growth interruptions in silicified conifer woods from the Upper Cretaceous Two Medicine Formation, Montana, USA: Implications for palaeoclimate and dinosaur palaeoecology: Palaeogeography, Palaeoclimatology, Palaeoecology, v. 199, p. 299–314, doi:10.1016/S0031-0182(03)00539-X.

Ferguson, A.L., 2016, Nest site taphonomy of modern archosaurs: 135 p.

Ferguson, A.L., Varricchio, D.J., and Ferguson, A.J., 2020, Nest site taphonomy of colonial ground-nesting birds at Bowdoin National Wildlife Refuge, Montana: Historical Biology, v. 32, p. 902–916, doi:10.1080/08912963.2018.1546699.

Foreman, B.Z., Fricke, H.C., Lohmann, K.C., and Rogers, R.R., 2011, Reconstructing paleocatchments by integrating stable isotope records, sedimentology, and taphonomy: A Late Cretaceous case study (Montana, United States): PALAIOS, v. 26, p. 545–554.

Francischini, H., Paes Neto, V.D., Martinelli, A.G., Pereira, V.P., Marinho, T.S., Teixeira, V.P.A., Ferraz, M.L.F., Soares, M.B., and Schultz, C.L., 2016, Invertebrate traces in pseudo-coprolites from the upper Cretaceous Marília Formation (Bauru Group), Minas Gerais State, Brazil: Cretaceous Research, v. 57, p. 29–39, doi:10.1016/j.cretres.2015.07.016.

Freimuth, W.J., 2020, Paleoecological utility of feeding traces at egg mountain, a rich terrestrial vertevrate locality of the upper cretaceous Two Medicine Formation, Montana, U.S.A.[Ph.D. thesis]: Montana State University, p. 219.

Freimuth, W.J., and Varricchio, D.J., 2019, Insect trace fossils elucidate depositional environments and sedimentation at a dinosaur nesting site from the Cretaceous (Campanian) Two Medicine Formation of Montana: Palaeogeography, Palaeoclimatology, Palaeoecology, v. 534, p. 109262, doi:10.1016/j.palaeo.2019.109262.

Freimuth, W.J., Varricchio, D.J., and Chin, K., 2021, Paleoenvironmental implications of invertebrate fecal pellets (Edaphichnium ISP.) at an ichnofossil-rich dinosaur nesting locality, upper cretaceous two medicine formation, Montana, USA: Palaios, v. 36, p. 283–300, doi:10.2110/PALO.2021.003.

Fuentes, F., DeCelles, P.G., Constenius, K.N., and Gehrels, G.E., 2011, Evolution of the cordilleran foreland basin system in northwestern montana, U.S.A.: Bulletin of the Geological Society of America, v. 123, p. 507–533, doi:10.1130/B30204.1.

Gjerdrum, C., Sullivan-Wiley, K., King, E., Rubega, M.A., and Elphick, C.S., 2008, Egg and chick fates during tidal flooding of saltmarsh sharp-tailed sparrow nests: Condor, v. 110, p. 579–584, doi:10.1525/cond.2008.8559.

Graf, J., Tabor, N.J., Ferguson, K., Winkler, D.A., Lee, Y.N., May, S., and Jacobs, L.L., 2018, Diagenesis of dinosaur eggshell from the Gobi Desert, Mongolia: Palaeogeography, Palaeoclimatology, Palaeoecology, v. 494, p. 65–74, doi:10.1016/j.palaeo.2017.11.011.

Grellet-Tinner, G., Corsetti, F., and Buscalioni, A.D., 2010, The importance of microscopic examinations of eggshells: discrimination of bioalteration and diagenetic overprints from biological features: Journal of Iberian Geology, v. 36, p. 181–192.

Hayward, J.L., Amlaner, C.J., and Young, K.A., 1989, Turning eggs to fossils: a natural experiment in taphonomy: Journal of Vertebrate Paleontology, v. 9, p. 196–200.

Hayward, J.L., Folsom, S.D., Elmendorf, D.L., Tambrini, A.A., Cowles, D.L., 1997, Experiments on the taphonomy of amniote eggs in marine environments: Palaios, v. 12, p. 482–488.

Hayward, J.L., Hirsch, K.F., and Robertson, T.C., 1991a, Rapid dissolution of avian eggshells buried by Mount St. Helens ash: PALAIOS, v. 6, p. 174–178.

Hayward, J.L., Zelenitsky, D.K., Smith, D.L., Zaft, D.M., and Clayburn, J.K., 2000, Eggshell taphonomy at modern gull colonies and a dinosaur clutch site: Palaios, v. 15, p. 343–355, doi:10.1669/0883-1351(2000)015<0343:ETAMGC>2.0.CO;2.

He, Q., Gui, Z., Mao, L., Huang, J., Xing, L., Chen, Y., and Zhang, W., 2021, Element and isotope compositions of newly discovered dinosaur eggs and geochemical environmental instructions from the early Late Cretaceous of Xiuning Basin, China: Historical Biology, v. 00, p. 1–10, doi:10.1080/08912963.2021.1952195.

Hirsch, K.F., and Quinn, B., 1990, Eggs and eggshell fragments from the upper cretaceous two medicine formation of Montana: Journal of Vertebrate Paleontology, v. 10, p. 491–511, doi:10.1080/02724634.1990.10011832.

Horner, J., 1999, Egg cluches and embryos of two hadrosaurian dinosaurs: Journal of Vertebrate Paleontology, v. 19, p. 607–611.

Horner, J.R., 1982, Evidnece of colonial nesting and "site fidelity" among ornithischian dinosaurs: Nature, v. 297, p. 675–676.

Horner, J.R. and Weishampel, D.B., 1996,Horner and Weishampel 1988 (correction): Nature, v. 383, p. 103.

Horner, J.R., and Makela, R., 1979, Nest of juveniles provides evidence of family structure among dinosaurs: Nature, v. 282, p. 296–298, doi:10.1038/282296a0.

Horner, J.R., and Weishampel, D.B., 1988, A comparative embryological study of two ornithischian dinosaurs: Nature, v. 332, p. 256–257, doi:10.1038/332256a0.

Hoyt, D.F., 1979, Practical methods of estimating volume and fresh weight of bird eggs: Auk, v. 96, p. 73–77.

Imai, T., Varricchio, D.J., Cahoon, J., and Plymesser, K., 2015, Sedimentological analyses of eggshell transport and deposition: Implication and application to eggshell taphonomy: Palaios, v. 30, p. 435–445, doi:10.2110/palo.2013.116.

Jackson, F.D., Jin, X., and Schmitt, J.G., 2009, Fungi in a lower cretaceous turtle egg from china: Evidence of ecological interactions: Palaios, v. 24, p. 840–845, doi:10.2110/palo.2009.p09-053r.

Jackson, F.D., Schaff, R.J., Varricchio, D.J., and Schmitt, J.G., 2015a, A theropod nesting trace with eggs from the upper cretaceous (Campanian) two medicine formation of Montana: Palaios, v. 30, p. 362–372, doi:10.2110/palo.2014.052.

Jackson, F.D., and Schmitt, J.G., 2008, Recognition of vertebrate egg abnormalities in the Upper Cretaceous fossil record: Cretaceous Research, v. 29, p. 27–39, doi:10.1016/j.cretres.2007.02.004.

Jackson, F.D., and Varricchio, D.J., 2010, Fossil eggs and eggshell from the lowermost Two Medicine Formation of Western Montana, Sevenmile Hill locality: Journal of Vertebrate Paleontology, v. 30, p. 1142–1156, doi:10.1080/02724634.2010.483537.

Jackson, F.D., Varricchio, D.J., Jackson, R.A., Walde, D., and Bishop, G.A., 2015b, Taphonomy of Extant Desert Tortoise (Gopherus agassizii) and Loggerhead Sea Turtle (Caretta caretta) Nesting sites: Implications for Interpreting the Fossil Record: Palaios, v. 30, p. 207–233.

James, N.P., and Jones, B., 2016, Origin of Carbonate Sedimentary Rocks: Chichester, Wiley.

Janssen, J.D., Mutch, G.W., Hayward, J.L., 2011, Taphonomic effects of high temperature on avian eggshell: Palaios, v. 26, p. 658–664.

Jiang, L., Cai, C., Worden, R.H., Crowley, S.F., Jia, L., Zhang, K., and Duncan, I.J., 2016, Multiphase dolomitization of deeply buried Cambrian petroleum reservoirs, Tarim Basin, north-west China: Sedimentology, v. 63, p. 2130–2157, doi:10.1111/sed.12300.

Knaust, D., 2020, Invertebrate coprolites and cololites revised: Papers in Palaeontology, v. 6, p. 385–423, doi:10.1002/spp2.1297.

Kohring, R.R., 1999, Calcified shell membranes in fossil vertebrate eggshell: evidence for preburial diagenesis: Journal of Vertebrate Paleontology, v. 19, p. 723–727.

Kusuda, S., Yasukawa, Y., Shibata, H., Saito, T., Doi, O., Ohya, Y., and Yoshizaki, N., 2013, Diversity in the matrix structure of eggshells in the testudines (reptilia): Zoological Science, v. 30, p. 366–374, doi:10.2108/zsj.30.366.

Legendre, L.J., Choi, S., and Clarke, J.A., 2022, The diverse terminology of reptile eggshell microstructure and its effect on phylogenetic comparative analyses: Journal of Anatomy, v. 241, p. 641–666, doi:10.1111/joa.13723.

Legendre, L.J., Rubilar-Rogers, D., Musser, G.M., Davis, S.N., Otero, R.A., Vargas, A.O., and Clarke, J.A., 2020, A giant soft-shelled egg from the Late Cretaceous of Antarctica: Nature, v. 583, p. 411–414, doi:10.1038/s41586-020-2377-7.

Lensink, A. V., Swan, G.E., and Myburg, J.G., 2023, The structure of the eggshell and eggshell membranes of Crocodylus niloticus: Journal of Microscopy, p. 23–39, doi:10.1111/jmi.13173.

Li, Y., Zhu, X., Wang, Q., Jiang, S., Yang, Y., Luo, W., and Wang, X., 2022, Apatite in Hamipterus tianshanensis eggshell: advances in understanding the structure of pterosaur eggs by Raman spectroscopy: Heritage Science, v. 10, p. 1–14, doi:10.1186/s40494-022-00720-7.

Liong, J.W.W., Frank, J.F., and Bailey, S., 1997, Visualization of eggshell membranes and their interaction with Salmonella enteritidis using confocal scanning laser microscopy: Journal of Food Protection, v. 60, p. 1022–1028, doi:10.4315/0362-028x-60.9.1022.

Lorenz, J.C., 1981, Sedimentary and tectonic history of the two Medicine Formation, Late Cretaceous (Campanian), Northwestern Montana [Ph.D. thesis]: Princeton University, 251 p., https://remote-lib.ui.ac.id:6066/docview/303325315?accountid=17242.

Lorenz, J.C., and Gavin, W., 1984, Geology of the Two Medicne Formation and the sedimentology of a dinosaur nesting ground: Montana Geological Society Feild Guide, p. 175–186.

Lourembam, R.S., Dhiman, H., and Prasad, G.V.R., 2023, Preservation of membrana testacea in titanosaurid dinosaur eggshells from the Upper Cretaceous Deccan volcano-sedimentary strata of Central India: Geological Magazine, v. 160, p. 361–371, doi:10.1017/S0016756822000978.

Saint Martin, J.P., and Saint Martin, S., 2018, Exquisite preservation of a widespread filamentous microorganism in French Cretaceous ambers: Crucial for revising a controversial fossil: Comptes Rendus - Palevol, v. 17, p. 415–434, doi:10.1016/j.crpv.2017.05.003.

Marzola, M., Russo, J., and Mateus, O., 2015, Identification and comparison of modern and fossil crocodilian eggs and eggshell structures: Historical Biology, v. 27, p. 115–133, doi:10.1080/08912963.2013.871009.

McNamara, M.E., Orr, P.J., Kearns, S.L., Alcalá, L., Anadón, P., and Molla, E.P., 2009, Soft-tissue preservation in miocene frogs from Libros, Spain: Insights into the genesis of decay microenvironments: Palaios, v. 24, p. 104–117, doi:10.2110/palo.2008.p08-017r.

Mikhailov, K., 1991, Classification of fossil eggshells of amniotic vertebrates: Acta Palaeontologica Polonica, v. 36, p. 193–238, https://app.pan.pl/archive/published/app36/app36-193.pdf.

Mikhailov, K.E., 1997, Fossil and Recent Eggshell in Amniotic Vertebrates:Fine Structure, comparative Morphology and Classification: Special Papers in Palaeontology, p. 83.

Mine, Y., 2007, Egg Bioscience and Biotechnology: Hoboken, New Jersey, Johy Wiley & Sons, Inc., 1–362 p., doi:10.1002/9780470181249.

Montellano, M., Weil, A., and Clemens, W.A., 2000, An exceptional specimen of cimexomys judithae (mammalia: Multituberculata) from the campanian two medicine formation of montana, and the phylogenetic status of cimexomys: Journal of Vertebrate Paleontology, v. 20, p. 333–340, doi:10.1671/0272-4634(2000)020[0333:AESOCJ]2.0.CO;2.

Moreno-Azana, M., Mariani, E., Bauluz, B., and Canudo, J.I., 2013, Growth mechanisms in dinosaur eggshells: an insight from electron backscatter diffraction: Journal of Vertebrate Paleontology, v. 33, p. 121–130, https://www.jstor.org/stable/23361076.

Moreno-Azanza, M., Bauluz, B., Canudo, J.I., Gasca, J.M., and Fernández-Baldor, F.T., 2016, Combined use of electron and light microscopy techniques reveals false secondary shell units in Megaloolithidae eggshells: PLoS ONE, v. 11, p. 1–17, doi:10.1371/journal.pone.0153026.

Nadon, G.C., 1993, The association of anastomosed fluvial deposits and dinosaur tracks, eggs, and nests: implications for the interpretation of floodplain environments and a possible survival strategy for ornithopods: Palaios, v. 8, p. 31–44, doi:10.2307/3515220.

Norell, M.A., Clark, J.M., Demberelyin, D., Rhinchen, B., Chiappe, L.M., Davidson, A.R., Mckenna, M.C., Altangerel, P., and Novacek, M.J., 1994, A theropod dinosaur embryo and the affinities of the Flaming Cliffs dinosaur eggs: Science, v. 266, p. 779–782.

Oser, S.E., 2014, Fossil eggs and perinatal remains from the Upper Cretaceous Two Medicine Formation of Montana: Description and Implications[M.S. thesis]: Montana State University, 135 p.

Oser, S.E., and Jackson, F.D., 2014, Sediment and eggshell interactions: using abrasion to assess transport in fossil eggshell accumulations: Historical Biology, v. 26, p. 165–172, doi:10.1080/08912963.2013.814650.

Padian, K., and Smith, M., 1992, New light on late cretaceous pterosaur material from Montana: Journal of Vertebrate Paleontology, v. 12, p. 87–92.

Phillott, A.D., and Parmenter, C.J., 2001, The distribution of failed eggs and the appearance of fungi in artificial nests of green (Chelonia mydas) and loggerhead (caretta caretta) sea turtles: Australian Journal of Zoology, v. 49, p. 713–718, doi:10.1071/ZO9730435.

Qvarnström, M., Niedźwiedzki, G., and Žigaitė, Ž., 2016, Vertebrate coprolites (fossil faeces): An underexplored konservat-lagerstätte: Earth-Science Reviews, v. 162, p. 44–57, doi:10.1016/j.earscirev.2016.08.014.

Ramezani, J., Beveridge, T.L., Rogers, R.R., Eberth, D.A., and Roberts, E.M., 2022, Calibrating the zenith of dinosaur diversity in the Campanian of the Western Interior Basin by CA-ID-TIMS U–Pb geochronology: Scientific Reports, v. 12, p. 1–20, doi:10.1038/s41598-022-19896-w.

Rogers, R.R., Fricke, H.C., Addona, V., Canavan, R.R., Dwyer, C.N., Harwood, C.L., Koenig, A.E., Murray, R., Thole, J.T., and Williams, J., 2010, Using laser ablation-inductively coupled plasma-mass spectrometry (LA-ICP-MS) to explore geochemical taphonomy of vertebrate fossils in the upper cretaceous two medicine and Judith River formations of Montana: Palaios, v. 25, p. 183–195, doi:10.2110/palo.2009.p09-084r.

Rogers, R., Horner, J., Ramezani, J., Robersts, E., and Varricchio, D., In Press, Updating the Upper Cretaceous (Campanian) Two Medicine Formation of Montana : Lithostratigraphic revisions, new CA-ID-TIMS U-Pb ages, and a calibrated framework of dinosaur occurrences: Geological Society of America Bulletin,.

Sagemann, J., Bale, S.J., Briggs, D.E.G., and Parkes, R.J., 1999, Controls on the formation of authigenic minerals in association with decaying organic matter : An experimental approach: Geochimica et Cosmochimica Acta, v. 63, p. 1083–1095.

Shelton, J.A., 2007, Application of Sequence Stratigraphy To the Nonmarine Upper Cretaceous Two Medicine Formation, Willow Creek Anticline, Northwestern Montana [M.S. theiss]: Montana State University, 221 p.

Skawina, A., 2010, Experiemental decay of gills in freshwater bivalves as a key to understanding their preservation in upper Triassic lacustrine deposits: Palaios, v. 25, p. 215–220.

Smith, D.L., and Hayward, J.L., 2010, Bacterial decomposition of avian eggshell: A taphonomic experiment: Palaios, v. 25, p. 318–326, doi:10.2110/palo.2009.p09-115r.

Varricchio, D.J., Horner, J.R., and Jackson, F.D., 2002, Embryos and eggs for the cretaceous theropod dinosaur Troodon formosus: Journal of Vertebrate Paleontology, v. 22, p. 564–576, doi:10.1671/0272-4634(2002)022[0564:EAEFTC]2.0.CO;2.

Varricchio, D.J., Jackson, F., Borkowski, J.J., and Horner, J.R., 1997, Nest and egg clutches of the dinosaur Troodon formosus and the evolution of avian reproductive traits: Nature, v. 385, p. 247–250, doi:10.1038/385247a0.

Varricchio, D.J., Jackson, F., and Trueman, C.N., 1999, A nesting trace with eggs for the Cretaceous theropod dinosaur Troodon formosus: Journal of Vertebrate Paleontology, v. 19, p. 91–100, doi:10.1080/02724634.1999.10011125.

Vera, E.I., and Perez Loinaze, V.S., 2022, Ecological interactions in conifers (Agathoxylon and Protocupressinoxylon) from the Punta del Barco Formation (Baqueró Group, upper Aptian), Patagonia, Argentina: Cretaceous Research, v. 129, p. 105035, doi:10.1016/j.cretres.2021.105035.

Wang, X. et al., 2017, Egg accumulation with 3D embryos provides insight into the life history of a pterosaur: v. 1201, p. 1197–1201.

Weaver, L.N., Varricchio, D.J., Sargis, E.J., Chen, M., Freimuth, W.J., and Wilson Mantilla, G.P., 2021, Early mammalian social behaviour revealed by multituberculates from a dinosaur nesting site: Nature Ecology and Evolution, v. 5, p. 32–37, doi:10.1038/s41559-020-01325-8.

Wilby, P.R., and Whyte, M.A., 1995, Phosphatized soft tissues in bivalves from the Portland Roach of Dorset (Upper Jurassic): Geological Magazine, v. 132, p. 117–120, doi:10.1017/S001675680001147X.

Zelenitsky, D.K., and Therrien, F., 2008, Unique maniraptoran egg clutch from the upper cretaceous two medicine formation of montana reveals theropod nesting behaviour: Palaeontology, v. 51, p. 1253–1259, doi:10.1111/j.1475-4983.2008.00815.x.

APPENDICES

APPENDIX A

COMPLETE TABLE OF SLIDES

Table 1A: Complete list of slides made for this thesis.

Slide	Preparation	Location	Egg Number	Structures Present	Techniques Preformed
KE -1	Polished thin section	2020 float	NA	Eggshell, dark region, membrane, type 1 pellets,	Light microscopy
KE-2	Polished EBSD thick section	2020 float	NA	Eggshell, dark region, membrane, type 1 pellets,	SEM, backscatter images, CL, EDX
KE-3	Polished thin section	Brown material from sieve	NA	Eggshell	Light microscopy
KE-4	Polished thin section	Black material from sieve	NA	Type-a and type-b sieve eggshell	Light microscopy
KE-5	Polished EBSD thin section	Black material from sieve	NA	Type-a and type-b sieve eggshell	
KE-6	Polished thin section	Top of egg 1	Egg 1	Eggshell, membrane	Light microscopy,
KE-7	Polished EBSD thin section	Top of egg 1	Egg 1	Eggshell, membrane	Light microscopy, SEM, backscatter images, EBSD
ES-579	Polished thin section	Soft sediment	NA	Sediment	Light microscopy
ES-580	Polished thin section	Hard sediment	NA	Sediment	Light microscopy
ES-581	Polished EBSD thin section	upper float bag	NA	Eggshell, membrane	Light microscopy, CL

Table 1A Continued:

Slide	Preparation	Location	Egg Number	Structures Present	Techniques Preformed
ES-583	Polished EBSD thin section	upper float bag	NA	Inorganic Calcite, Eggshell, membrane, Type 2 pellets	Light microscopy, SEM, EDX,
ES-584	Polished thin section	Sediment near egg	NA	Sediment	Light microscopy
KE-8	Polished EBSD thin section	Side of egg	Egg 5	Eggshell	Light microscopy
KE-9	Polished EBSD thin section	Bottom edge of egg	Egg 6	Inorganic calcite, Eggshell, dark region, membrane	Light microscopy, CL, SEM, backscatter images, EDX, EBSD
KE-10	Polished EBSD thin section	Bottom middle of egg	Egg 8	Eggshell, dark region	Light microscopy, CL, SEM, Backscatter images, EDX
KE-11	Polished EBSD thin section	Bottom edge of egg	Egg 9	Eggshell, dark region, membrane	Light microscopy, CL, SEM, Backscatter images, EDX
KE-12	Tangential Polished thin section	Bottom middle of egg	Egg 8	Eggshell	Light microscopy

APPENDIX B

SYMBOL KEY FOR NEST IN THE WALL BENTONITE STRATIGRAPHIC COLUMN

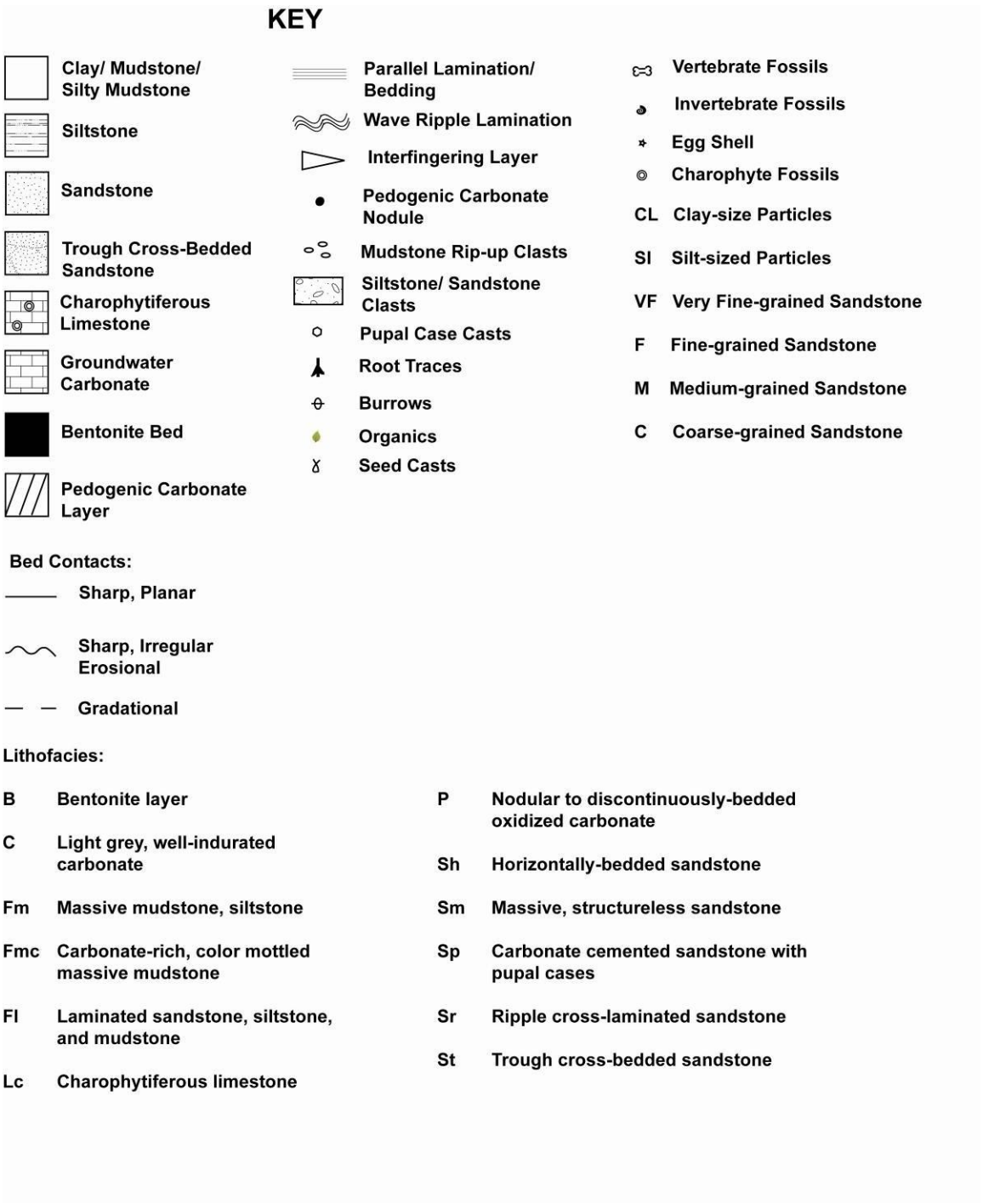

Figure 1B: Full key for stratigraphic columns from Shelton (2007).

APPENDIX C

ADDITIONAL EBSD AND EDX MAPS

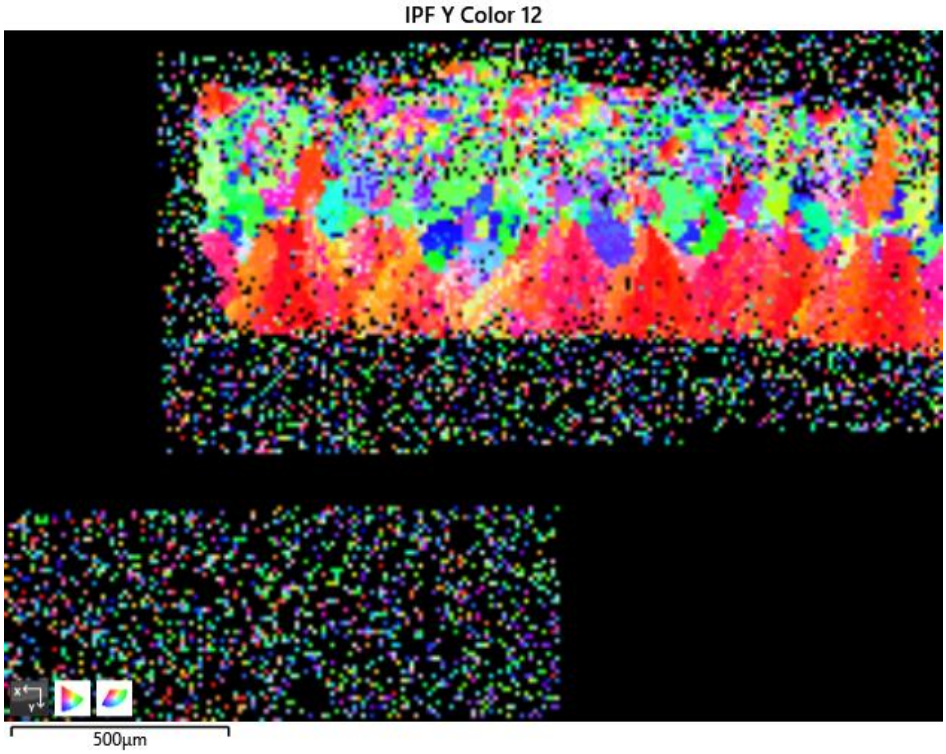

Figure 1C: Raw EBSD map of Slide KE-7 from egg-1. Surface of the eggshell is up.

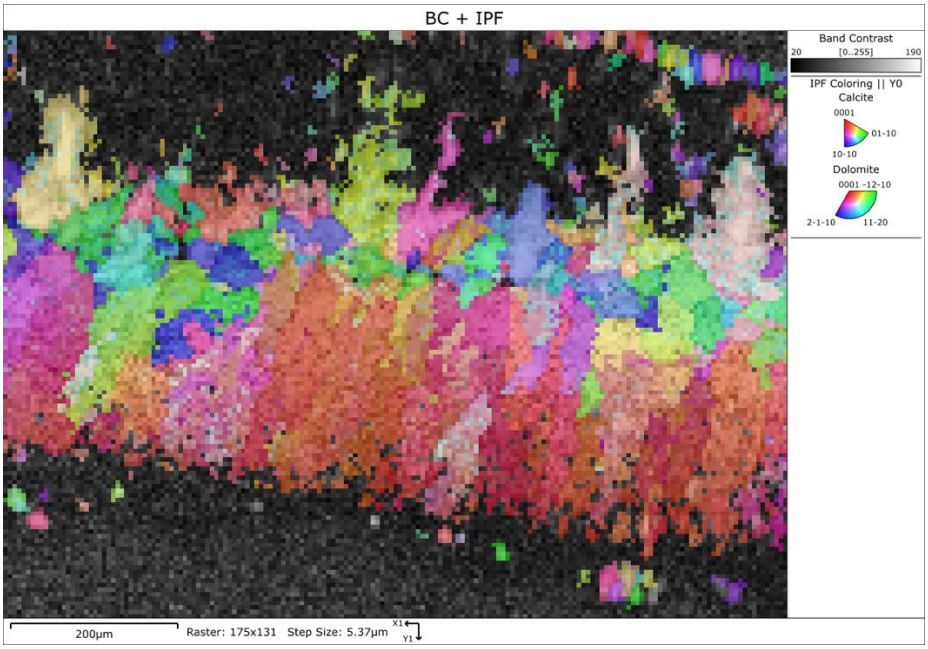

Figure 2C: Higher resolution, processed EBSD map of KE-7 from egg-1. Surface of the eggshell is up.

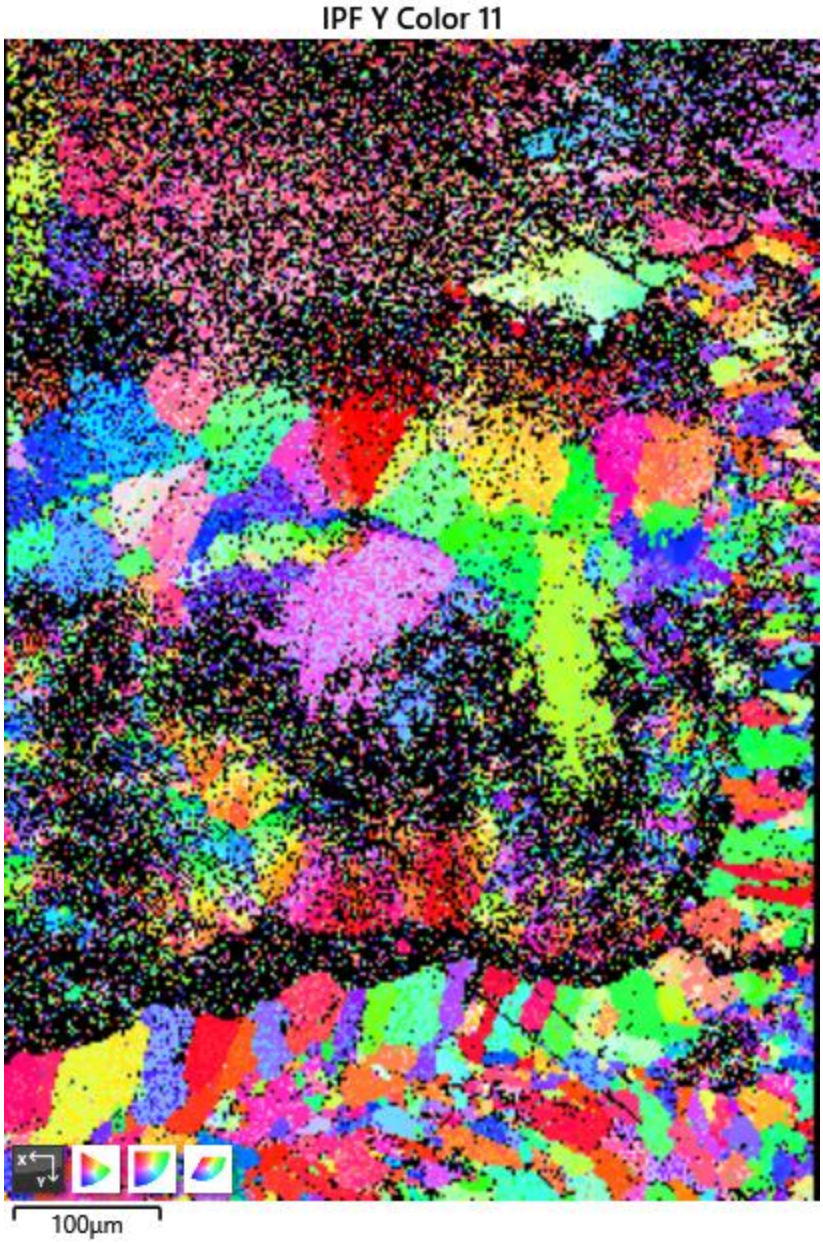

Figure 3C: Raw higher resolution test EBSD map of KE-9. Surface of the eggshell is at the bottom of the image.

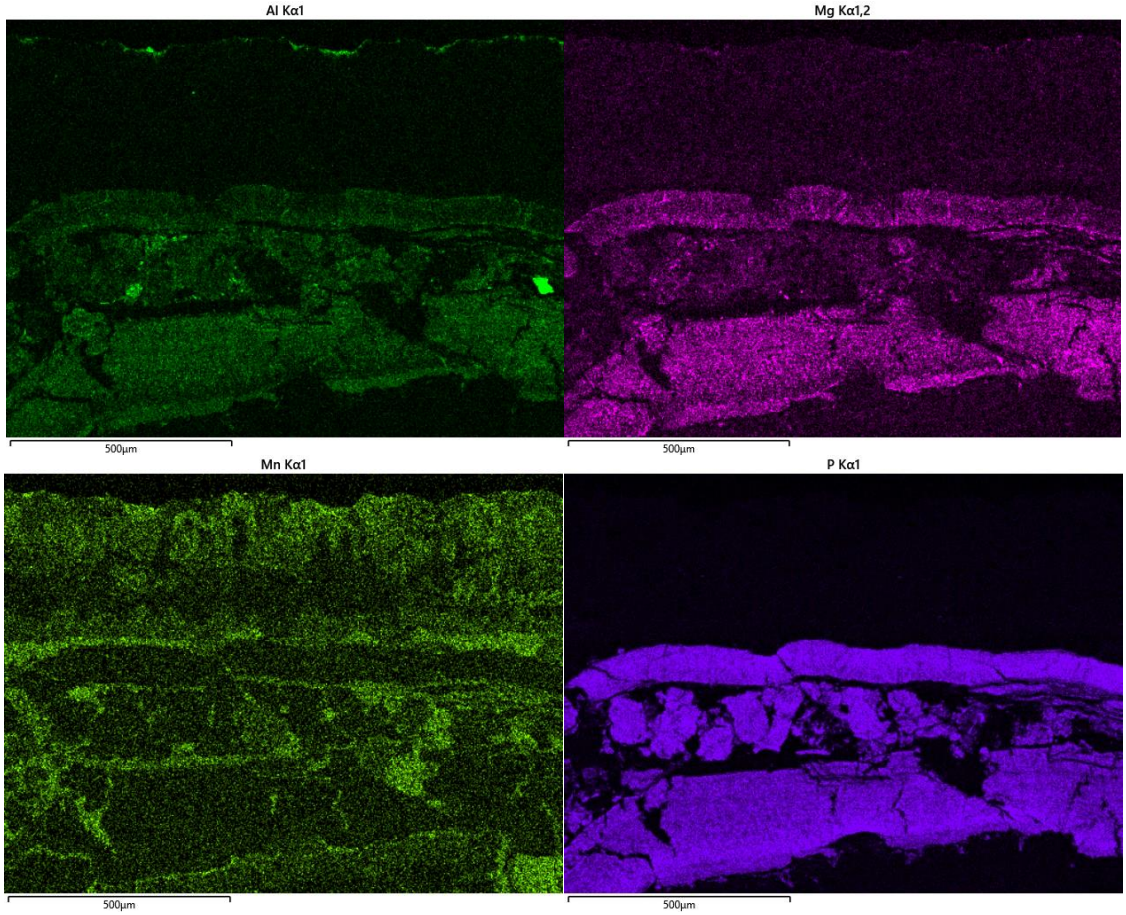

Figure 3D: Slide KE-11 EDX maps of aluminum in the top left, magnesium in the top right, manganese in the lower left, and phosphorous in the lower right. Eggshell surface is at the top of the image.